

*SELF-ASSEMBLY OF POLYMER COATED
NANOPARTICLES ON WATER-OIL INTERFACES*



PHILIPP FABIAN

INSTITUTE FOR BIOLOGICALLY INSPIRED MATERIALS

DEPARTMENT OF NANOTECHNOLOGY

UNIVERSITY OF NATURAL RESOURCES AND LIFE SCIENCES, VIENNA

THIS THESIS IS SUBMITTED FOR THE DEGREE OF MASTER OF SCIENCE

FEBRUARY 25, 2019

Kurzfassung

Kürzlich wurde ein erneutes Interesse an Pickering-Emulsionen festgestellt. Diese Emulsionstypen verwenden feste Kolloide, die an der Öl-Wasser-Grenzfläche adsorbiert sind, um die dispergierte Phase einzugrenzen und die Anordnung zu stabilisieren. Die Anwendung von rezeptiven Nanopartikeln als Stabilisatoren ermöglicht eine externe Kontrolle des Emulsionszustands.

Superparamagnetische Eisenoxid-Nanopartikel (SPION), die mit temperaturempfindlichen Polymerschalen gefropft wurden, wurden als Bausteine für die Untersuchung der Selbstorganisation von Trägern im Nanomaßstab für hydrophobe Verbindungen ausgewählt, da die Partikellöslichkeitsübergänge dieser biokompatiblen Nanopartikel magnetisch und thermisch ausgelöst werden können. Mehrere thermosensitive Polymertypen wurden synthetisiert und auf SPIONs gefropft. Die resultierenden Core-Shell-Nanopartikel (CSNPs) wurden dann verwendet, um Öl-in-Wasser-Emulsionen zu erzeugen, die durch Adsorption von Nanopartikeln an der Grenzfläche stabilisiert wurden und über mehrere Wochen beobachtet wurden.

Der erste Teil dieser Arbeit widmet sich der erfolgreichen Synthese von Poly-(N-isopropylacrylamid) und diversen Poly-2-alkyloxazolinen unter lebenden Bedingungen mittels Atomtransfer-Radikalpolymerisation bzw. Kationenringöffnungs-Polymerisation. CSNPs wurden unter Verwendung des "grafting-to" Ansatz erhalten.

Der zweite Teil konzentriert sich auf die Bildung stabiler CSNP-vermittelter Emulsionen nach Einführung einer hydrophoben Substanz als dispergierte Phase in unsere Systeme. Die resultierenden Öl-in-Wasser-Emulsionen wurden daher durch dynamische Lichtstreuung beobachtet. Wir haben die Eigenschaften mehrerer Anordnungen anhand verschiedener Parameter wie CSNP-Konzentration, Dispersionsphase und Zusammensetzung der Polymerhülle untersucht. Wir fanden, dass unsere Proben normalerweise eine Stabilisierungsphase von etwa einer Woche durchliefen, bevor stabile Tropfengrößen erreicht wurden.

Abstract

Recently a rekindled interest in Pickering emulsions was noticed. These emulsion types use solid colloids adsorbed to the oil-water interface in order to arrest the dispersed phase and stabilize the assembly. Applying responsive nanoparticles as stabilizers allows external control over the state of the emulsion.

Superparamagnetic iron oxide nanoparticles (SPION) grafted with temperature responsive polymer shells were chosen as building blocks to investigate the self-assembly of nanosized carriers for hydrophobic compounds due to the possibility to magnetically and thermally trigger the particle solubility transitions of these biocompatible nanoparticles. Multiple thermo-sensitive polymer types were synthesized and grafted onto SPIONs. The resulting core-shell nanoparticles (CSNPs) were then used to create oil-in-water emulsions stabilized by nanoparticle adsorption to the interface, which were observed over multiple weeks.

The first part of this thesis is devoted to the successful synthesis of poly-(N-isopropyl-acrylamide) and diverse poly-2-alkyl-oxazolines under living conditions via atomic transfer radical polymerization and cationic-ring opening polymerization respectively. CSNPs were obtained by using the “grafting-to” approach.

The second part focuses on the formation of stable CSNP stabilized oil-in-water emulsions. The oil-in-water emulsions were observed via dynamic light scattering. We investigated the properties of multiple assemblies by varying different parameters, such as CSNP concentration, dispersed oil phase and polymer shell composition. We found that our samples usually formed over one or more weeks, before stable droplet sizes were reached.

Acknowledgements

As my student career now closes to an end, the best time to reminisce about the past years is now. They were full of ups and downs, so I am glad to end them now with this exciting project. On my journey I was accompanied by many wonderful and interesting people, and with this I want to thank them all for being there for me in my times of need.

First of all, I want to thank my supervisor Univ. Prof. Dr. Erik Reimhult, who introduced me to the exciting world of nanotechnology and welcomed me to this working group. Without his expertise and inputs this project would not have been possible.

A big thank goes to Martina Schroffenegger, MSc for sharing her vast knowledge about chemistry, always answering my questions and teaching me how to survive in the laboratory.

For the great support in dealing with the Zetasizer instrument and the physical problems in this thesis, I want to thank DI. Iris Vonderhaid. Physics is a subject; we do not very often come across during our study, so the insights of an expert were helping a lot.

Without Tanja Zwölfer, I would not even have been aware of this fantastic project, so for that I owe her big thanks, not to mention all the great help I received from her during my writing.

Due to all the laughs and conversations we shared, during laboratory and lunch times, which made those moments so much more appealing, I want to thank all the people in the nanotechnology department, especially Max Willinger, Marlene Egelseder and Peter Bock.

And of course I have to thank my family, my girlfriend Isabella and all the people I got to meet at University. Without them, those years would have been pretty bleak and unspectacular.

Content

Kurzfassung	II
Abstract	III
Acknowledgements	IV
Content	V
1. Introduction	1
1.1. Core-shell nanoparticles	1
1.2. Surface grafting	3
1.3. Iron oxide nanoparticle cores	5
1.4. Dopamine anchor groups	6
1.5. Intelligent polymer shells	7
1.5.1. Poly(N-isopropyl-acrylamide) (PNIPAM)	8
1.5.2. Poly-2-alkyl-2-oxazolines (POXs).....	10
1.6. Analysis of Core-Shell Nanoparticles	12
1.6.1. Polymer Molecular Weight.....	12
1.6.2. Grade of Functionalization	13
1.6.3. Determination of Grafting Density.....	13
1.6.4. Analysis of particle size distribution.....	14
1.7. Pickering Emulsions	16
1.7.1. Adsorption on interfaces.....	17
1.7.2. Droplet size and stability in Emulsions	19
1.8. Drug Delivery Systems	20
2. Aim	22
3. Experimental Part	23
3.1. Material & Methods	23
3.1.1. Materials.....	23
3.1.2. Methods.....	23
3.2. 2-Isopropyl-2-oxazoline (IPOX) synthesis	25
3.3. NDA-Synthesis	25
3.4. PNIPAM-Synthesis	26
3.5. Polymerization of 2-alkyl-2-oxazolines	26

3.5.1. Carboxyl-terminated poly(2-alkyl-2-oxazoline).....	27
3.6. NDA-terminated Polymers	27
3.7. Ligand-exchange	27
3.8. Preparation of emulsions	28
4. Results and Discussion	29
4.1. Monomer Synthesis and Purification	29
4.2. Polymer Shell Synthesis and Grafting	30
4.2.1. NDA Anchor Synthesis	30
4.2.2. PNIPAM Shell Synthesis.....	31
4.2.3. Poly-2-alkyl-2-oxazoline Shell Synthesis	33
4.2.4. Functionalization and Ligand Exchange.....	35
4.2.5. Particle size distributions	39
4.3. Emulsification.....	41
4.3.1. Influence of the dispersed phase	41
4.3.2. Influence of shell size.....	49
4.3.3. Influence of core size	54
5. Conclusion.....	66
6. Outlook.....	68
7. References	69
8. Abbreviations	75

1. Introduction

Over the last decades the scientific community has shown increasing interest in the field of nanotechnology. Per definition particles in a size range of 1 and 100 nm in at least one dimension are termed nanoparticles (NPs)¹. Though “nano” is not the term for a specific size, many materials undergo changes in their properties when exceeding this threshold.

The ratio of volume to surface shifts towards the latter the smaller an object gets, hence nanoparticles, due to their small size and extremely high surface to volume ratio, are dominated by surface properties and surface forces. This means that more atoms are located on the surface of NP materials, increasing the reactivity and catalytic abilities of the particles compared to their bulkier counterparts².

Characteristics of NPs also change with their size. Whereas a small shift in the size of bulk materials does not amount to any effect in their traits, changes in the size of NPs can lead to drastic and sometimes unwanted shifts in thermal, optical, electric or magnetic properties³. This means that by controlling the size of nanoparticles, their other characteristics can also be adjusted, raising their interest for use in industrial and medical applications.

Nanoparticles, due their unique properties, already find application in e.g. medicine, electronics, energy harvesting, etc.⁴ Further investigation of the unique properties and the complex chemical and physical processes of nanoparticles are important to realise future visions like the development of drug delivery systems.

1.1. Core-shell nanoparticles

Biological fluids contain various amounts of different molecules. Due to their reactive nature, nanoparticles suspended in such fluids will automatically start

unwanted interactions in these environments and even agglomerate with other nanoparticles. This leads to loss of function⁵ but also to toxic or allergic reactions within the subject⁶.

Taking the matter into consideration, modifying the surface of nanoparticles to control their colloidal interactions is the next logical step, a feat accomplished by encapsulating them in a shell of organic material, e.g. with a polymer shell (see Fig. 1). The addition of organic matter to inorganic material can complete the list of desirable traits for nanoparticles, by adding the properties of polymers such as solubility, stability and biocompatibility^{7,8}.

Core-shell nanoparticles are divided into multiple parts. Core-shell nanoparticles (CSNPs) usually are defined as having a core surrounded by a single, well-defined shell. Mostly, an inorganic core is surrounded by an organic shell to control interactions and retain function. Anchor groups are used to attach an organic shell in a controlled way to the core. Optional, is the end group modification of the shell, adding additional properties such as selective conjugation for specific molecules⁹.

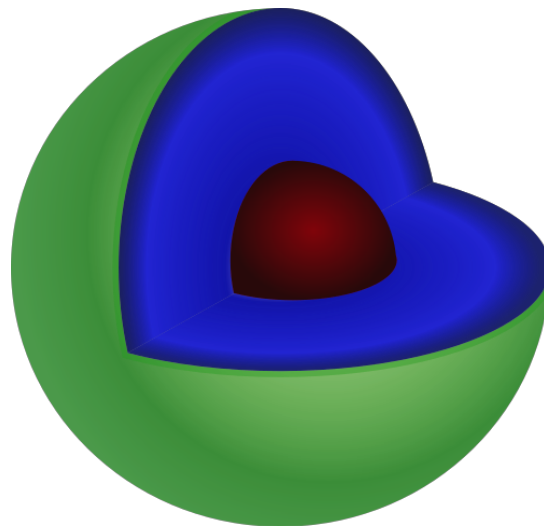


Fig. 1: A 3D-sphere model of a core-shell nanoparticle. The red interior sphere exemplifies the core, which is surrounded by the shell (blue sphere). The green enveloping sphere represents potential end group modifications on the shell, which can add new possible traits to the assembly.

The composite structure makes core-shell nanoparticles superior in many ways, when compared to their single component counterparts, which also raises further interest for different applications¹⁰. However, the accurate engineering of such materials remains a technical challenge. The requirements of enhancing colloidal stability and adding preferred surface

traits, while keeping the biocompatibility, limit the number of available materials.

1.2. Surface grafting

For proper functionality a polymer shell should be arranged in a “brush” regime, where polymer chains stand in close proximity to another. This brush regime is the result of steric repulsion between the densely grafted solvated polymer chains^{11,12}. In order to obtain a dense “brush” regime on highly curved nanoparticle surfaces, the grafting density (GD) should exceed 0.7 chains per nm². Lower GDs result in a “mushroom” regime.

Other parameters that affect polymer shells are the chain length, polymer composition and the solvent. Polymer interaction with the solvent should be higher than with the substrate, otherwise the chain will collapse to a “pancake” regime.

There are two main approaches for surface modification by a polymer brush, the “grafting-to” method and the “grafting-from” method. In the “grafting-to” method, polymers are synthesized and functionalized, before adding them onto the surface (see Fig. 2). This allows for better selection over a suitable polymerization method and a full characterization of the resulting polymer. However, during the grafting, diffusion and steric repulsion of bulky already adsorbed polymer chains can hinder the bonding of additional polymer chains at high density onto the surface. The resulting GD is thus often lower when compared to the “grafting-from” approach.

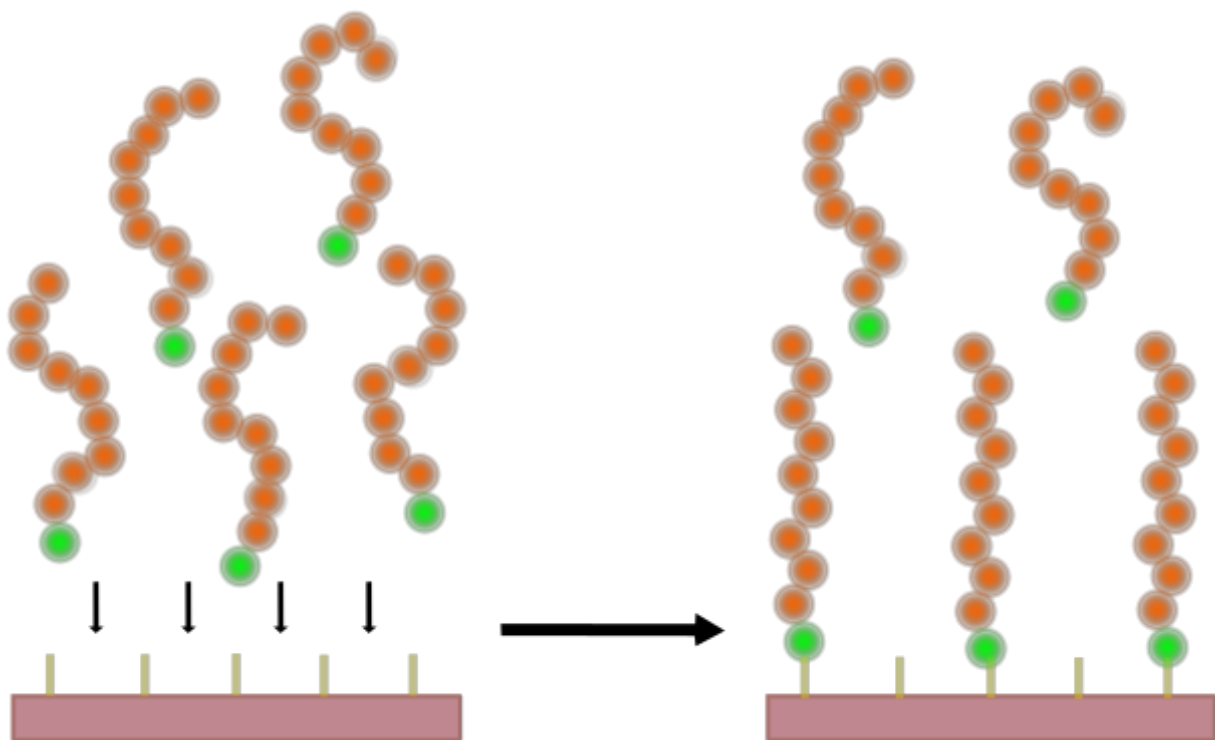


Fig. 2: Depiction of the “grafting to” approach. The already synthesized polymer chains (orange spheres) are attached to binding sites on the NP surface via anchor groups (green spheres).

For the “grafting-from” method initiator groups are immobilized on the particle surface before polymerization is started (see Fig. 3). Monomers are much smaller and can therefore pass through the growing polymer brush in contrast to larger chains and easily reach the reactive sites. Diffusion does not obstruct the assembly onto the surface as strongly and high GDs are the result^{13,14}. Disadvantageous is the increased complexity of this synthesis. First of all, the solvent must prevent the agglomeration of nanoparticles as well as avoid exerting negative influence on the polymerization. Second, growing chains attached to nanostructures are more prone to side reactions in contrast to unbound chains, for example bimolecular termination due to the dense space between the growing chains¹¹.

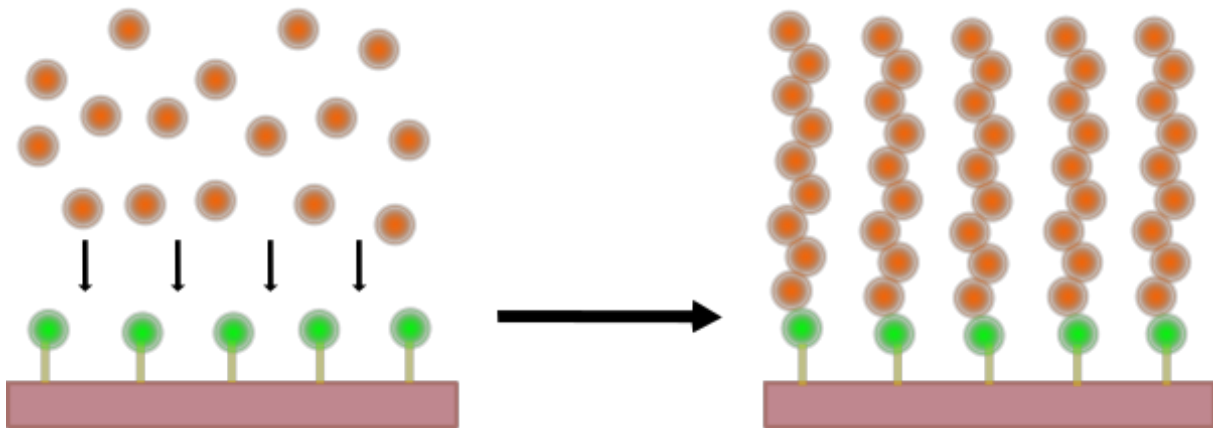


Fig. 3: Depiction of the “grafting from” approach. Anchor-initiator compounds (green spheres) are immobilized on the NP surface and trigger the polymerization of added monomers (orange spheres).

1.3. Iron oxide nanoparticle cores

Cores for CSNP can be composed out of a variety of materials. Examples include silica, ceramics, carbon, different metals (Fe, Au, Cu, ...) and metal oxides (Fe_nO_n , Al_2O_3 , TiO_2 ,...). Especially interesting are cores that add new characteristics such as superparamagnetism for magnetic oxide and metal nanocrystals¹⁵.

Superparamagnetism is a phenomenon that can only be found in adequately small, ferromagnetic, monocrystalline NPs that let them randomly flip direction of their magnetism due to thermal energy. The thermal randomization of their magnetic moments means that they will only contribute to a local directional magnetic field when an external magnetic field acts on them¹⁶. Therefore, an alternating external magnetic field will cause the flipping of the induced magnetic field as the nanoparticle magnetic dipole aligns with the redirection of the external magnetic field. As the dipole realigns frequency dependent dissipative losses occur that convert the magnetic energy to thermal energy by e.g. Néel relaxation¹⁷. Néel relaxation and losses can only be observed in sufficiently small (superparamagnetic) crystals that possess a single magnetic domain. Superparamagnetic iron oxide nanoparticles (SPIONs) are an especially interesting candidate for biomedical applications due to their biocompatibility¹⁶. Iron oxide nanoparticles (FeO-NPs) break down to Fe^{3+}

under acidic conditions, such as can be found in lysosomes. The resulting iron from use of FeO-NPs for biomedical applications is insignificant when compared to the iron storage of an adult human (3 - 5 g) and is recycled in the human body¹⁸.

1.4. Dopamine anchor groups

Polymer shells can be attached to the cores in two ways: via strong covalent bonds or via physical interactions. The latter binding type is susceptible towards environmental influences and accidental loss of the shell. While covalent binding requires the modification of the nanoparticle with a specific anchor group (see Fig. 4), in terms of long-time stability, it is the much more safer alternative¹⁹.

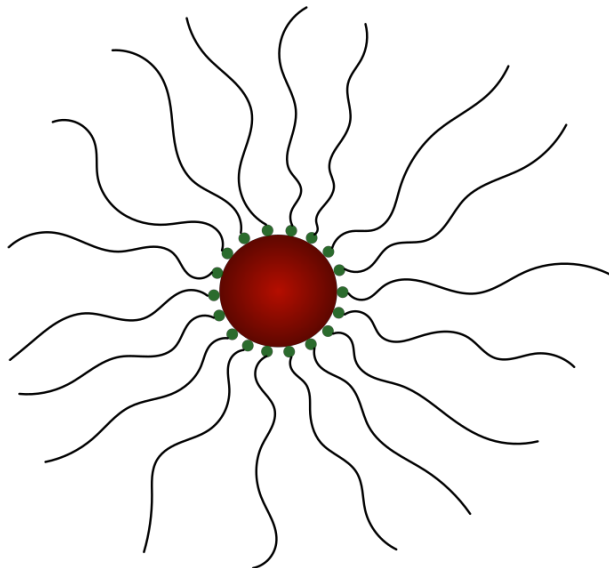


Fig. 4: This figure depicts the core-shell structure of CSNPs: Anchors (small green spheres) attach the polymer chains (black strings) to the iron core (red sphere in the center).

Catechol derivatives have proven to be an excellent choice as anchor groups for FeOx-NPs²⁰. Especially nitrodopamine (NDA) has been found as a low molecular weight dispersant, which provides high affinity towards the iron oxide surface. Moreover, the bonding maintains its stability over multiple heating and filtration steps, contrary to conventional catechol anchors²¹.

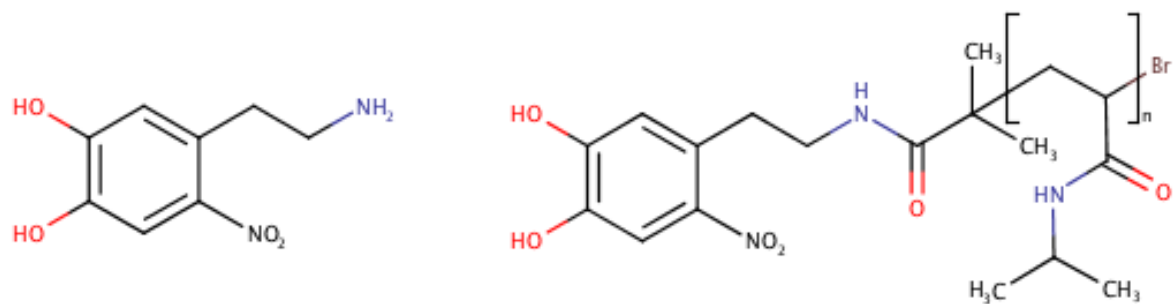


Fig. 5: Structure of NDA (left); NDA attached to PNIPAM (right). The two hydroxyl-groups on the catechol derivate ensure a stabile semi-covalent bond onto the iron particle surface.

The as-synthesized FeOx-NPs used in this thesis are have surface-bound oleic acid derivates²²; NDA anchor groups show a higher affinity towards the NP surface and replace the fatty acids as ligands.

1.5. Intelligent polymer shells

In contrast to commercial polymers, so-called intelligent polymers respond drastically to small environmental alterations²³. Little adjustments in temperature, pH or other factors can lead to abrupt, reversible changes. These transitions can come in various forms, for example charge neutralization of functional groups or conformation changes in polymer structure²⁴. The latter effect raises interest for applications of such polymers as shell on nanoparticles. The polymer shell of nanoparticles only prevents aggregation if the polymer shell is dense and thick enough to screen out the attractive interactions between the core and other colloids in the environment²⁵.

Controlling the conformation of the polymer shell allows the regulation of the state of nanoparticle through external, environmental changes. Nanoparticles will start to aggregate if an external signal causes the collapse of the polymer shell. Similarly, this collapse is reversible by returning the original environmental conditions.

In Chapter 1.3 the temperature rise in superparamagnetic nanoparticles caused by alternating magnetic fields through Néel relaxation was described. Combining these particles with temperature sensitive polymer shells, unlocks the possibility of external control over the particles.

1.5.1. Poly(N-isopropyl-acrylamide) (PNIPAM)

PNIPAM is a hydrophilic polymer, the formation of strong hydrogen bonds between water molecules and the polymer favors its solubility in water²⁶. Upon heating beyond a certain threshold, the hydrogen bonds are no longer thermodynamically favorable and thus are released from the polymer shell (see Fig. 6). A hydrophobic collapse is the result of exceeding this lower critical solution temperature (LCST)²⁷. For PNIPAM this threshold lies at around 32°C, but is adaptable by changing parameters like monomer chemistry²⁸ or salt concentration in the solvent²⁹, but also depends on the polymer molecular weight and its end groups³⁰. Its LCST behavior makes PNIPAM an interesting candidate for multiple tasks in biotech applications, such as cell sheet engineering³¹.

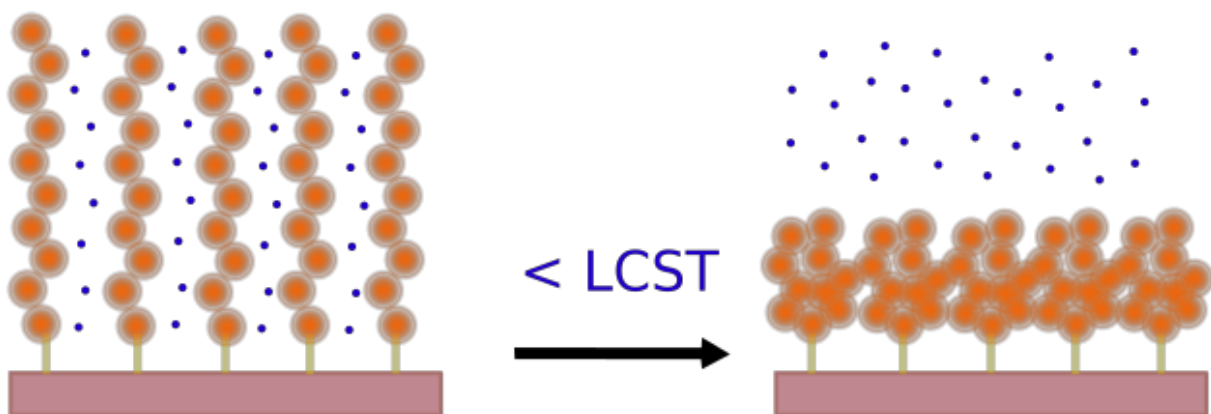


Fig. 6: A schematic drawing of the influence of temperature on polymer (built from orange spheres) conformation. On the left, below the LCST the polymers arrange in the extended brush regime, forming hydrogen bonds with water molecules (blue spheres), whereas on the right side the polymer conformation is collapsed at temperatures above the LCST.

Since a hydrated polymer shell is what keeps core-shell nanoparticles from aggregating, the collapse and partial loss of hydration of the polymer shell above the LCST leads to agglomeration of e.g. PNIPAM-grafted iron oxide. After cooling below the LCST, the polymer shell shifts back to its original conformation. Although its characteristics promise interesting results, the biocompatibility of PNIPAM is still under investigation³².

1.5.1.1. Atom transfer radical polymerization (ATRP)

Traditional polymer synthesis is known for its poor control and high polydispersity index (PDI). ATRP is a typical controlled/living free-radical polymer synthesis (CRP), which means that circumstances for accidental chain transfer and chain termination reactions are no longer available³³. Other characteristics are a faster initiation rate, when compared to the propagation, low PDI (near the optimum of 1.0) and a predictable resulting molecular weight. Living polymerization methods for different polymers have grown rapidly over the last decades³⁴.

Polymerization is triggered with an initiator; the amount of initiator used also determines the molecular weight of the polymers. In ATRP, alkyl halides with carbonyl functional groups are popular initiators, e.g. 2-bromo-2-propionic acid, which was used in this master thesis (see Fig. 7). Critical for a suitable initiator is a highly mobile halide functional group during chain growth³⁵.

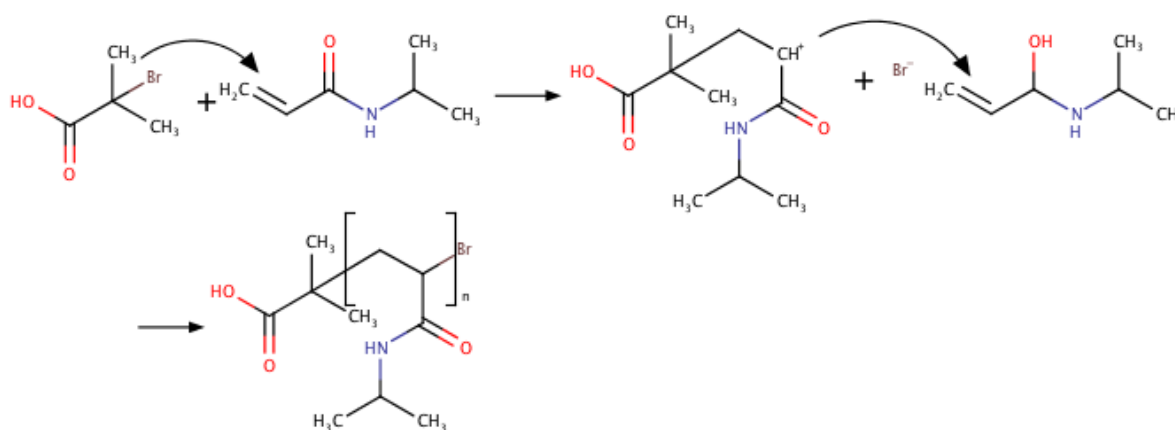


Fig. 7: Polymerization of PNIPAM with 2-bromo-2methylpropionic acid as initiator. Triggered by a nucleophile attack on the double bond located at the first C atom. The resulting molecule is positively charged and therefore attacks another monomer. Exposing the sample to air terminates the polymerization.

A metallic catalyst regulates the atom transfer equilibrium between active radicals and inactive chains. As such, a well-regulating catalyst is of critical importance for the success of an ATRP³⁵. A successful CRP requires high amounts of catalyst, which must be removed in an extra purification step before a pure final product can be obtained. The required amount of catalyst

can be reduced by the use of strongly active ligands, e.g. tris[2-(dimethylamino)ethyl]amine (Me₆TREN)³⁶.

Solvent should be chosen to minimize chain transfer and catalyst inhibition. Reaction temperature and time also contribute to a successful CRP.

1.5.2. Poly-2-alkyl-2-oxazolines (POXs)

Despite its advantages PNIPAM is subject to a lot of skepticism. With a LCST below body temperature, its use in the biomedical field is associated with a lot of difficulties. Poly-2-alkyl-2-oxazolines offer similar properties to PEG, but also an easily tunable LCST, which in contrast to PNIPAM can be tailored to be at or above body temperature³⁷.

The first synthesis of POXs via cationic-ring opening polymerization was reported in the 1960s³⁸⁻⁴¹. Improved synthesis protocols for living polymerization were established over the next decades, reporting of excellent control over length, functionality and architecture of the products^{42,43}. Nevertheless, industry backed away from these polymers, presumably because cheaper alternatives were available⁴⁴. This resulted in a decline of interest during the 1990s.

However, with the rise of nanotechnology, interest in POXs started to develop again, mainly due to their biocompatibility and tunable characteristics. Depending on the functional group of the monomer, which is located at the second position of the oxazoline ring, the resulting polymer expresses different behaviors. A long aliphatic or aromatic side chain results in a hydrophobic residue, whereas poly-2-methyl-2-oxazoline (PMOx), the most hydrophilic example is water-soluble. Most interesting are poly-2-ethyl-2-oxazoline (PEOx) and poly-2-isopropyl-2-oxazoline (PIPOx), which show LCST behavior in water⁴⁵.

POXs are classified as “pseudo-polypeptides”, due to the similarities between their structures compared to that of a natural peptide. These polymers express excellent biocompatibility; PEOx is even FDA-approved⁴⁶. A drawback is the lack of purchasable monomers. Only the basic monomers are available,

therefore most research groups must synthesize more complex monomers themselves.

1.5.2.1. Cationic-ring opening polymerization (CROP)

This type of polymerization is declared as living, which is described in Chapter 1.5.1.1. An anhydrous atmosphere is required for polymerization, since water acts as a terminating agent; usually polymerization is performed in an inert gas atmosphere. Depending on the choice of initiator and monomer, polymerization can last several hours to days, but can be accelerated by heating the synthesis to up to 200 °C⁴⁷. Aprotic-polar reaction solvents, such as acetonitrile, are frequently used, however recent dimethylacetamide⁴⁸ (DMA) and chlorobenzene⁴⁹ were used successfully.

For inducing CROP, the initiator requires an electrophile group. Commonly used, due to their rapid initiation rates, are Lewis-acids and their esters (e.g. p-toluenesulfonic acid); as well as alkylhalogenides and arylhalogenides (e.g. benzyl bromid), depending on desired end group functionalization⁵⁰. Using halogenic initiators, the resulting polymerization mechanism is covalent, whereas a Lewis-acid leads to an ionic mechanism.

As example, the polymerization mechanism with methyl tosylate (MetTos) as initiator is described. The free electron pair on the endocyclic nitrogen atom in the oxazoline ring start a nucleophile attack on the sulfonic group of the initiator, causing a separation of the methyl end group, which attaches to a now cationic oxazolium ion. This positively charged moiety is prone to be attacked by another nitrogen of a fresh oxazoline. As a result, the oxazoline ring opens at C5-O1 and the newly attached oxazoline obtains a positive charge, repeating the process with the next monomer. Nucleophilic agents terminate the reaction. A schematic replica of the progress can be seen in Fig. 8.

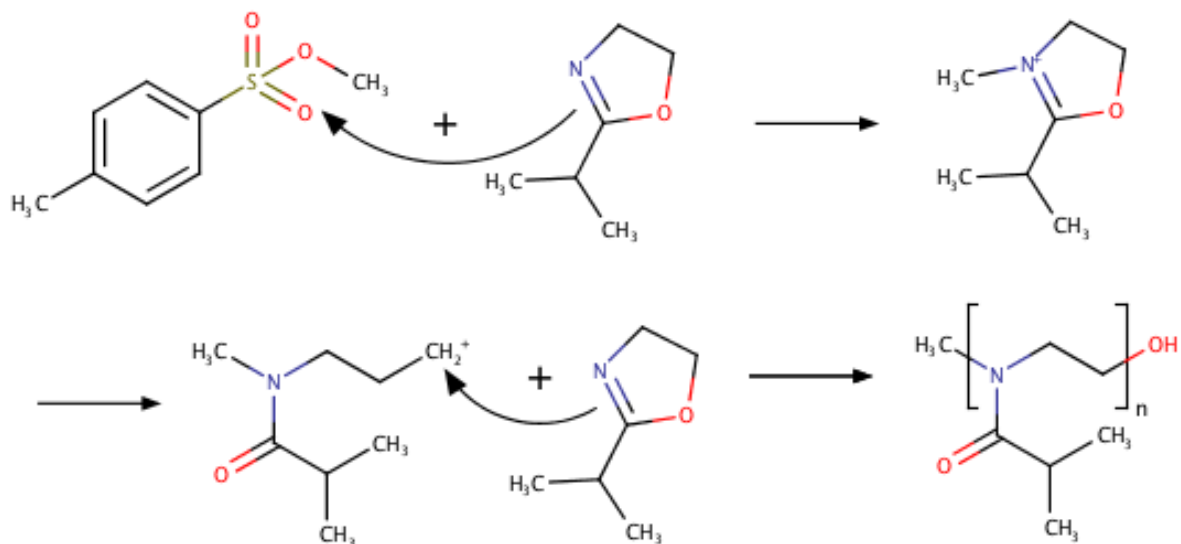


Fig. 8: Synthesis of PIPOx with Methyl-tosylate as initiator. A nucleophilic attack on the sulfonic group triggers the polymerization. Attachment of the methyl group on the N atom causes a ring opening; the oxazoline cation is then attacked by another monomer. The reaction is repeated until a terminating agent is introduced, in this case it is water.

1.6. Analysis of Core-Shell Nanoparticles

1.6.1. Polymer Molecular Weight

To determine the size and weight of polymers gel permeation chromatography (GPC) is a common tool. This method belongs to the size exclusion chromatographies, where the separation principle is based on the size or hydrodynamic diameter of the sample molecules. The analytes are moved by an eluent (the mobile phase) through a column, which is packed with a gel containing porous beads (the stationary phase). Smaller molecules are trapped more easily inside these pores and therefore their residence time inside the column (retention time) is elongated. The composition of stationary and mobile phase is chosen depending on the analytes; the mobile phase is commonly an organic solvent, whereas the stationary phase consists of a commercial gel like Sephadex or PLgel. A pump speeds up the separation process, by supplying fresh eluent into the column. After the separation, a detector monitors the bypassing molecules. Commonly, UV photometer and differential refractometers are used as detectors; it is also possible to combine

multiple detectors for better characterization. Through this method the number average molecular weight (M_n) and weight average molecular weight (M_w) can be obtained. These two factors are necessary to evaluate the PDI of a polymer:

$$PDI = \frac{M_w}{M_n} \quad (1)$$

The PDI determines the uniformity of all molecules in a sample; a PDI near 1.0 means, that the polymer chains are similar in shape and size.

1.6.2. Grade of Functionalization

Nuclear magnetic resonance spectroscopy (NMR) is a non-invasive, spectroscopic method to identify the structure of organic compounds. The sample is surrounded by a strong static magnetic field. If the nuclei of certain isotopes possess a magnetic spin (such is the case in ^1H , ^{13}C , ^{15}N , etc.) this magnetic spin aligns with the magnetic field. Strong magnetic radiation excites the nucleus and its magnetic spin changes direction, so its spin opposes the magnetic field now. This high-energy condition is unstable, so the excited nucleus returns to its original state, by emitting excess energy. Since the local environment around the isotope influences the emitted signal, the received spectra of very similar compounds are still distinguishable. Therefore, NMR has become the explicit method for molecule identification and verification of purity.

1.6.3. Determination of Grafting Density

Since colloidal stability of SPIONs is only given if a certain dense brush regime is present, the GD of nanoparticles has to be evaluated. In thermogravimetric analysis (TGA) the change of sample mass induced by the change of temperature over time is evaluated. The sample is exposed to increasing temperature in an inert atmosphere and is under constant observation by a microbalance over the entire process. Pressure and atmospheric composition

can be adjusted according to the sample; examples for such atmospheres include synthetic air, vacuum and nitrogen. An oven increases the temperature with a regulated heating rate until a certain endpoint is reached. Under the rising temperature the sample mass will rise due to induced oxidation processes or decrease on account of substance, decomposition, combustion and evaporation. In our example the organic polymer shell will decompose and evaporate during the process and the metal oxide core will remain as a leftover. This way the masses of both the inorganic and the polymer contents can be evaluated. If the core surface area and polymer molecular weight are taken into account, the information obtained can be used to calculate the GD of nanoparticles.

1.6.4. Analysis of particle size distribution

Dynamic light scattering (DLS) is a non-invasive method for measuring the movement pattern of small particles in solution and relating this to evaluate their size. When a laser illuminates a sample, sufficiently small particles contained within this sample will cause the light to scatter in all directions (Rayleigh scattering). This scattered light can illuminate a nearby screen. If the laser illuminated thousands of such particles at the same time, the screen would show a speckle pattern of bright and dark areas by their combined scattered light. Bright areas would be caused by scattered light hitting the screen; whereas dark areas are results of the absence of light, due to destructive interference from other surrounding particles. However, particles in a solution are not stationary, but constantly moving due to random collisions with other fast-moving molecules (Brownian motion). This in term means that the resulting speckle pattern is also never constant but always fluctuating. According to Stokes-Einstein equation the diffusion constant (D) of spherical particles in a liquid is size-dependent (R):

$$D = \frac{k_B T}{6\pi\eta R} \quad (2)$$

This means smaller particles move quicker through liquids than larger ones. When dynamic viscosity (η), Boltzmann constant (k_B) and temperature (T) are taken into consideration, the fluctuation of the speckle pattern can be used to calculate the particle size distribution via correlation function. A correlator measures the intensity signal of an area in the speckle pattern at a given moment in time (t) and then again a very short time later (Δt) and compares the two results. If the two signals are very similar, a high correlation is given. As time passes by, the correlation between those two signals decays exponentially. Consequently, since large particles display slower Brownian motion, the correlation time is longer for the scattering signal. The information given by the correlation function can then be used to calculate the diffusion coefficients for each particle. Applying the Stokes-Einstein equation results in a size distribution histogram, where the x-axis shows the distribution of size classes and the y-axis the relative intensity of the signal for each size. However, the different volumes of particles will influence the received signals. The volume of spheres can be calculated as such:

$$V = \frac{4}{3}\pi(R^3) \quad (3)$$

Therefore a particle with 10 times the radius of a smaller one will end up with 1000 times the volume and will be hit by 1000 times more light. To compensate for this geometric factor, the intensity distribution can be converted into a volume distribution using Mie theory. In addition, according to Rayleigh's approximation, larger particles scatter much more light (proportional to R^6). Therefore, taking only the raw intensity signal into account, the signal of smaller particles can be overshadowed. As a counteraction, the distribution can be reweighted based on the number of particles; a number-weighted distribution is the result. Number, volume and intensity distribution are hence three representations of the same data on the sample. However, especially the number distribution is prone to errors, since small miscalculations in the correlation function can multiply to huge inaccuracies.

The setup of a DLS apparatus consists of a laser as light source, which passes through an attenuator, which adapts the intensity of the light depending

on the total scattered intensity of the sample. The sample itself is contained within a cell and illuminated by the laser. Most of the light passes through the sample, but some parts will be scattered in all directions. This means that the detector, which measures the scattered light, can be placed in any direction. In this master thesis the position of the detector was located at 175° in relative to the incoming light, for a so called “backscatter measurement”. This arrangement is very attractive, since the light now has to travel a shorter path through the sample, which allows for higher concentrations to be measured as well as greatly reduces the effect of multiple scattering (the scattered light is scattered again by another particle) and the effects of dust in the sample. The received signal is sent by the light intensity detector to the correlator, which time-correlates the scattered intensities and passes the data on to a computer.

1.7. Pickering Emulsions

Polar and apolar liquids are immiscible due to the lack of bonding forces (hydrogen bonds, van-der-Waal forces) between them. Substances favor contact with similar substances, therefore these liquids will try to minimize the surface area between the two phases. This results for example in an oil film swimming on top of a body of water.

Mixing those phases in one another will result in the oil being dispersed as small spherical droplets within the water; an emulsion is created. However, this will increase the contact area between oil and water and therefore also increase the total free energy due to high surface tension of the excess interface. Since the increase in free energy can be reduced by reducing the interfacial area between the oil droplets and water, demixing results.

As emulsions are requested for multiple products, such as food, cosmetics and pharmaceuticals, stabilizing such systems is a common task. Normally this is accomplished with the use of surfactants. However, Ramsden and Pickering found that dispersed, insoluble particles can also be used to stabilize emulsions by adsorbing onto the interface between the two phases^{51,52}. During the demixing process oil droplets will start to fuse in order to decrease the

surface area, a process, which is arrested by the steric kinetic barrier created by the particles adsorbed at the interface⁵³. These forms of emulsions are therefore called Pickering emulsions (see Fig. 9).

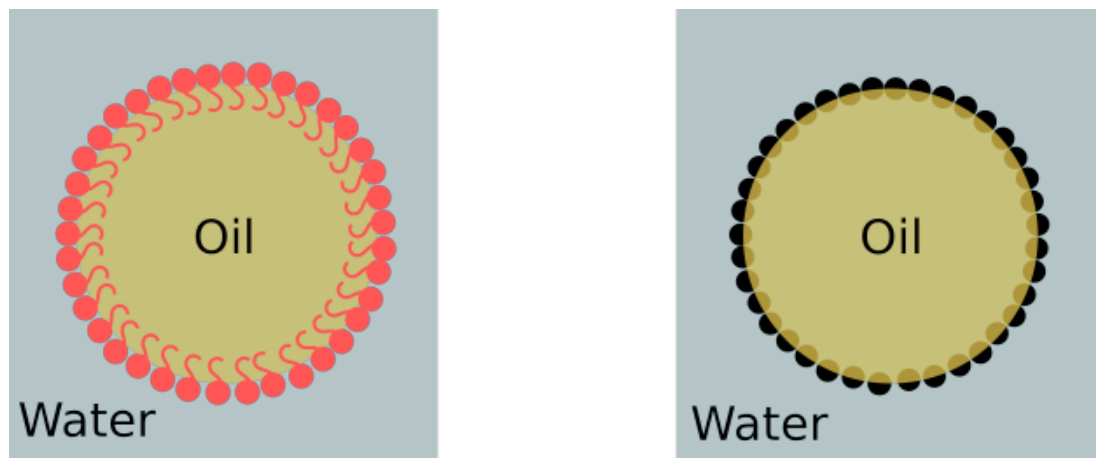


Fig. 9: Depiction of a regular emulsion with surfactants (left) and a Pickering emulsion with solid particles (right). Usually surfactants are amphiphilic entities with a hydrophilic moiety (sphere) and a hydrophobic part (string). On the other hand, solid particles in Pickering emulsions usually are uniform in their structure and better soluble in the continuous phase.

In contrast to surfactants, solid particles can add useful characteristics in addition to higher stability to emulsions⁵⁴. The rising demand of small, responsive and smart materials since the introduction of nanotechnology led to a rise of solid particles as emulsion stabilizing agents.

1.7.1. Adsorption on interfaces

As proper emulsifiers, the wettability of the particles must be given in both water and oil. Depending on the volume ratio of the two liquid phases as well as the affinity of the particles to either phase, the result will be an oil-in-water (O/W) or a water-in-oil (W/O) emulsion. The larger fractions of the particles are always exposed in the continuous phase. If the particles are totally wetted by one phase, they would remain dispersed in this phase, thus no emulsification process would occur⁵⁵. Therefore, wettability of particles in both phases must be given.

To obtain information about the wettability of particles, the three-phase contact angle θ (between the boundary of particle, oil and water) is taken into consideration (see Fig. 10). Emulsions, showing a high stability, usually

encompass a contact angle near 90° between the solid particle and the continuous phase. The contact angle θ is determined by the interfacial energies of the interfaces solid-water ($\gamma_{S/W}$), solid-oil ($\gamma_{S/O}$) and water-oil ($\gamma_{W/O}$) and can be described by Young's Law:

$$\cos(\theta_W) = \frac{\gamma_{S/O} - \gamma_{S/W}}{\gamma_{W/O}} \quad \cos(\theta_O) = \pi - \cos(\theta_W) \quad (4)$$

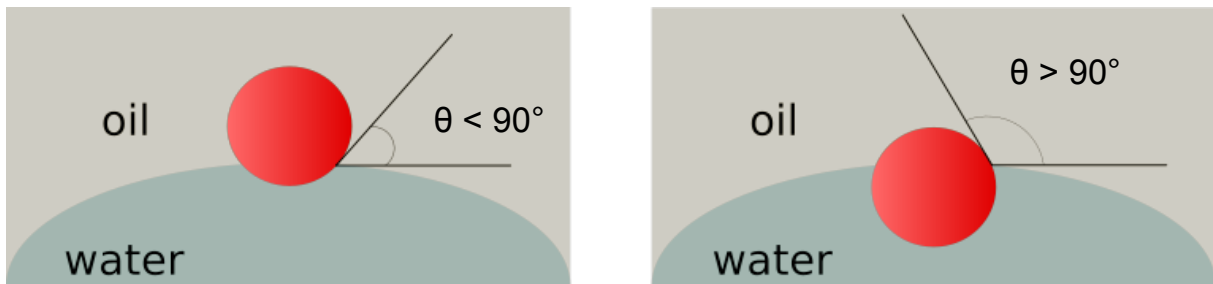


Fig. 10: Differences in contact angles dependent on wettability. On the left, the particle favors oil, whereas the right particle is better wettable in water.

As long as θ is located between 0° and 90° , the resulting emulsion will favor an oil in water (o/w) assembly; if θ is above 90° , a water in oil (w/o) emulsion will be favored. Furthermore, the contact angle gives information about the free energy of adsorption, or in other words the energy input required for desorption of one particle of given radius R ⁵⁶:

$$\Delta_{ads}F = -\pi R^2 \gamma_{\frac{O}{W}} (1 - \cos(\theta))^2 \quad \text{for } \theta < 90^\circ \quad (5)$$

$$\Delta_{ads}F = -\pi R^2 \gamma_{\frac{O}{W}} (1 + \cos(\theta))^2 \quad \text{for } \theta > 90^\circ \quad (6)$$

This means that larger nanoparticles show an increased free energy of adsorption, since a larger area per particle is removed from the oil-water interface compared to for their smaller counterparts⁵³. Thus the removal of larger particles from the interfaces is more difficult. On the opposing side, the thermal energy $k_B T$ (k_B = Boltzmann's constant and T = absolute temperature) will counteract adsorption of particles in the interfacial area and favor random distribution in the bulk phase. When comparing the decrease of total free energy to the thermal energy, the latter is negligible for particles in micrometers range. However, the two energies are comparable in size in the

case of nanoparticles. This results in a constant particle exchange at the interfacial area, depending on the particle size and wettability⁵⁷. For small particles the thermal energy overcomes the adsorption energy on a regular basis, thus increasing the particle exchange ratio at the interface.

Hydrophobicity is mainly determined by the composition and structure of the particle surface. Unmodified Fe₃O₄ particles are very hydrophilic due to an abundance of hydroxyl groups on the surface^{58,59}. A higher wettability in oil would be beneficial for emulsification. As mentioned in Chapter 1.1, a polymer shell can be used to alter nanoparticle solubility and dispersion stability. Moreover, using responsive polymers, it would be possible to control and change in situ the wettability and surface activity of the nanoparticles.

1.7.2. Droplet size and stability in Emulsions

Previously we established that volume to surface ratio rises in favor of the latter with decreasing size. This rule is also valid for emulsions, meaning that the interfacial area will increase for the same total dispersed volume with shrinking droplet size. A larger interfacial area demands more particles for stabilization, a phenomenon also observed by Arditty et al⁶⁰. This implies that limiting the amount of available particles can control droplet size. However, cases of emulsions were reported with a particle concentration that falls below the critical necessary threshold but still retain proper stability^{61,62}. Vignati et al. explained this behavior by the formation of monolayer bridges between multiple droplets, decreasing the mandatory amount of particles⁶¹.

A surplus of available solids allows the formation of very fine droplets, however the leftovers will remain as a suspension in the dispersing phase⁵⁶. Droplet size is reducible until the critical micelle concentration is reached⁶³. Excess particles will often aggregate in water due to their hydrophobicity. This in turn increases viscosity of the solution, which slows down the destabilization processes⁵⁶. On the other side, low amounts of particle require a large droplet size. If the interface is too large to cover, the oil droplets can coalesce and the emulsion will break as a result.

Usually agglomeration followed by coalescence lead to a loss of the emulsion. As is the case with ionic emulsifiers, electrostatic repulsion between particles keep the droplets at a reasonable distance⁵⁶. Transmission x-ray microscopy examinations have also shown the formation of particle bridges between oil droplets preventing agglomeration⁶⁴.

1.8. Drug Delivery Systems

In traditional medicine, drug application can only be controlled by dosage of the medication or careful monitoring. The drug itself spreads unrestricted throughout the body causing various side effects in otherwise healthy organs. Nanotechnology seeks to apply intelligent structures (e.g. liposomes and nanoparticles) to encapsulate and transport drugs in order to control distribution in tissue and cell uptake⁶⁵. Correctly realized, this means only a specific area in the organism should be exposed to the medicine. Using functional NPs for drug delivery vehicles promises some important advantages, including the possibility to improve controlled release⁶⁶.

Simplified, the drugs are encapsulated, adsorbed or otherwise attached to structures built or stabilized with the help of NPs, so that interactions between the patient and the loaded pharmaceuticals are avoided until they are released. If the nanoparticles interact strongly with e.g. optical or magnetic fields, an external electromagnetic field can be applied to the targeted body area to trigger a change in NP physical properties such as solubility or conformation, leading to a subsequent release of the drug⁶⁷. Such an intelligent release system has several advantages; it allows overcoming problematic characteristics of otherwise favorable drugs, e.g. poor solubility and stability, reducing toxicity of the drug and the dose frequency⁶⁸. However, the fact that inorganic nanoparticles could interact with biological macromolecules and agglomerate in biological systems can lead to unwanted side reactions on a cellular level⁶⁹.

With the development of Doxil®, the first FDA-approved nano-drug, NP functionalized carrier systems started to become reality. Nowadays different

concepts for drug delivery systems exist, ranging from liposome based carriers to drug loaded dendrimers and polymers⁷⁰.

A novel idea is the entrapment of the often poorly soluble pharmaceuticals in hydrophobic substances coated to disperse also in aqueous environments and injecting them into to patient. Intelligent core-shell superparamagnetic iron oxide nanoparticles should ensure stabilization of those droplets during the blood circulation time. In a nutshell, an (O/W) emulsion is established, stabilized by dispersed NPs, which attach onto the oil-water interface. An external signal (in this case an oscillating magnetic field) can cause a collapse in the polymer shell, leading to agglomeration of the NP cores and breaking the emulsion as a consequence. Thus the cargo dissolved inside the dispersed phase is released and available for cell uptake.

2. Aim

This thesis focuses on comparison of poly(N-isopropyl acrylamide) (PNIPAM) and poly-2-methyl-2-oxazoline (PMOx), poly-2-ethyl-2-oxazoline (PEOx) and poly-2-isopropyl-2-oxazoline (PIPOx) coated nanoparticles both in terms of their successful synthesis, as well as their behavior to stabilize fatty acid oils in water emulsions with low-surface tension. The aim was to combine differently sized SPION cores with PNIPAM and poly-2-alkyl-2-oxazoline chains of various molecular weights to investigate which nanoparticle architecture would be most suitable to create thermoresponsive nano-Pickering emulsions. Ideally, the emulsion should form nanoscale droplets stable over long time periods and being able to store hydrophobic cargo within the droplet lumen until an alternating external magnetic field heats up the nanoparticles, changing particle solubility, destabilizing the droplet interface to promote release of the content. We investigated influences of dispersed phase, shell size, core size and shell composition on the emulsification process.

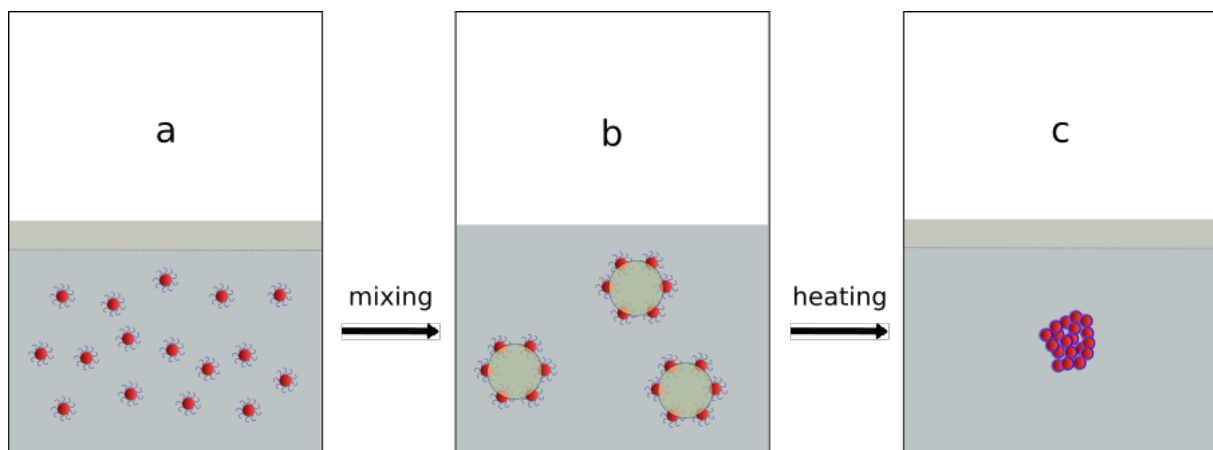


Fig. 11: a) A two-phase solution prior to mixing. The nanoparticles are all contained within the water phase of this system. b) Formation of an emulsion, the nanoparticles assemble onto the interface of the oil droplets. c) After an external trigger the polymer brush collapses and the particles agglomerate. This causes the release of the oil phase.

3. Experimental Part

3.1. Material & Methods

3.1.1. Materials

All chemicals were purchased from Sigma-Aldrich, unless otherwise stated, and were used as received, except for N-isopropylacrylamide (NIPAM), which was recrystallized once in hexane and toluene (v/v = 1:1) as well as benzyl-bromide, 2-methyl-2-oxazoline and 2-ethyl-2-oxazoline, which were redistilled to remove water residues. Oleic acid coated iron oxide nanoparticles were provided by Martina Schroffenegger MSc.; the synthesis is described in Zirbs et al.⁷¹

3.1.2. Methods

Gel Permeation Chromatography (GPC)

Polymer weights were determined via GPC measurement on an adapted Dionex HPLC with a P680 HPLC pump, an ASI-100 autosampler and STH585 column oven. For separation three MZ Gel SDPlus columns were utilized; one precolumn and two columns with separation ranges of 10-2000 and 1-40 kDa respectively. A Knauer Smartline RI Detector 2300 was used for detection. dimethyl formamide (DMF) with LiBr (5 wt %) served as eluent. Sample concentration was 3 mg/mL; measurements were carried out at 60 °C with a flow rate of 0.5 mL/min. External calibrations were carried out with polystyrene standards (1.5-651 kg/mol). Chromeleon 6.80 with the extension pack V02 was used for analytics. To obtain PNIPAM-MW, the measured molecular weight was divided by a correction factor of 2.7⁷².

NMR

¹H-NMR was carried out on a BRUKER AV III 300 spectrometer. Methanol-d₄ (MeOD) was used as a solvent for polymer functionalization grade analysis and as a reference for the chemical shifts [4.78 (1), 3.31 (5)]. Deuterated chloroform was used to verify the purity of IPOX; chemical shifts reside at 7,26 (1). Dimethyl sulfoxide-d₆ (DMSO-d₆) was used for the characterization of NDA; chemical shifts are observable at 2.50 (5). Dr. Markus Blaukopf and Ass. Prof. Andreas Hofinger-Horvath carried out the measurements.

TGA

TGA was performed on a Mettler Toledo TGA/DSC1. Synthetic air (80 ml/min) was utilized as reactive gas and nitrogen (20 mL/min) as protective gas. The heating rate was set to 10 K/min over a range from 25 to 600 °C. Weight loss was determined from 200 to 500 °C due to possible solvent leftovers, which would evaporate at < 200 °C. Residue over 500 °C was attributed to the inorganic fraction of the samples, whereas combusted matter between 200 and 500 °C was attributed to the organic polymer shell.

DLS

Hydrodynamic size distribution was determined with a 175° backscatter laser on a Malvern Zetasizer Nano-ZS. Samples were stored inside Eppendorf tubes (1.5 mL volume) and poured directly into a polystyrene cuvette (Sarstedt, semi-micro cuvette, 1.6 ml, 2 sides optical, height: 45 mm, layer thickness: 10 mm). Cuvette was put into the measurement chamber according to the manual. Measurements were conducted in backscattering mode at 22 °C after an equilibrium time of 30 sec. Three runs were conducted in order to obtain a mean value.

Core-shell nanoparticle stock solutions (5 mg/mL) for each sample were prepared and filtered with a 0.45 µm RC filter. The stock solutions were dissolved with filtered Milli-Q water to a final concentration of 1 mg/mL. For

measurements, the samples were transferred to polystyrene semi-micro cuvettes (1.6 mL volume, 10 mm layer thickness) from Sarstedt. Equilibrium time was set to 30 seconds. Three runs of 15 measurements each were conducted for each sample within each observation interval. The results of these 15 measurements were used to obtain an average plot for each run.

The handling of emulsions on this instrument is described in detail in Chapter 3.8.

3.2. 2-Isopropyl-2-oxazoline (IPOX) synthesis

A three-necked bottle was charged with 45 mL isobutyronitrile, 36 mL ethanolamine and 2,2 g ZnAc. The solution was refluxed under N₂ atmosphere at 130 °C overnight. Excess NH₃ was collected in a washing bottle filled with HCl. After cooling down to room temperature, 150 mL dichloromethane (DCM) was added and extracted against H₂O to cleanse the solution of excess NH₃. Na₂SO₄ was added to dispose of H₂O residues and the solution was subsequently filtrated. The product was distilled under N₂-atmosphere and CaH₂ was added to remove excess contaminants from the substrate. The product purity was confirmed via ¹H-NMR.

3.3. NDA-Synthesis

In a three-necked bottle 5 g dopamine HCl and 6.3 g NaNO₂ were solved in 150 mL MilliQ H₂O and cooled in an ice bath. 20 mL of an H₂SO₄ solution (25 % v/v) was added in droplets and a N₂-atmosphere was applied to the system. The solution was stirred at room temperature overnight. The product was cooled down to 4 °C, filtrated and washed with cooled water. Then the product was resuspended in ethanol and heated to 40 °C. After that the final product was precipitated with Et₂O (cooled down to -20 °C), then filtrated and air-dried.

3.4. PNIPAM-Synthesis

PNIPAM was synthesized according to previously established protocols^{26,71}. 2 g NIPAM were added to a flask alongside 26 mg CuBr and 4 mg CuBr₂ and solved in 18 mL MilliQ H₂O and 2 mL methanol. Atom-transfer radical-polymerization (ATPR) was started utilizing acid-modified initiator 2-bromo-2-methylpropanoic acid. 80 µL tris-[2-(dimethylamino)ethyl]amine (Me₆Tren) was solved in 2 mL Milli-Q H₂O and added separately after applying a N₂-atmosphere to both solutions. The sample then was stirred for 24 h at 4 °C under N₂-atmosphere. Exposing the sample to air interrupted the polymerization. Unwanted contaminants were removed via dialysis (membrane cut-off size: 3.5 kDa) and the sample was subsequently freeze-dried. Chain length and PDI were checked by separating the sample via GPC and running it past a RI-detector.

3.5. Polymerization of 2-alkyl-2-oxazolines

The steps undertaken in this synthesis can be found in the literature³⁷. Polymerization was performed in a Glovebox (GS Glovebox Systemtechnik GmbH) with oxygen-level <50 ppm and water level <1 ppm. 2 g monomer was added in a vial and suspended in 6 mL anhydrous DMA. Polymerization was initialized by addition of a Met-Tos solution (10%) and the sample was stirred at 100 °C for 19 h. Benzyl-bromide was used as initiator for PMOx and the reaction temperature was set to 70 °C. The reaction was quenched by adding 100 µL H₂O and stirring the sample at 70 °C for 5 h. To obtain hydroxyl-terminated poly(2-alkyl-2-oxazolines), the raw product was precipitated in 1:1 hexane/diethyl ether (Et₂O) and collected via centrifugation (5000 rpm, 2 min, 4 °C). The sample was resolved in 10 mL dichloromethane (DCM) and then dried by Rotavapor. The polymers were characterized as described in chapter 3.4.

3.5.1. Carboxyl-terminated poly(2-alkyl-2-oxazoline)

Succinic Anhydrite and 4-dimethylaminopyridine (DMAP) were added to hydroxy-terminated POXs, the solution was then solved in 20 mL CHCl_3 and refluxed under N_2 -atmosphere at 70 °C for 24 h. The sample was cooled down and precipitated in 1:1 (v/v) hexane/ Et_2O . The product was collected by centrifugation (5000 rpm, 2 min, 4 °C) and dried via Rotavapor.

3.6. NDA-terminated Polymers

Polymer functionalization was performed according to literature^{37,72}. Carboxyl-terminated polymer was solved alongside COMU [(1-cyano-2-ethoxy-2-oxoethylidenaminoxy) dimethylamino morpholino carbenium hexafluorophosphate] (from CarlROTH®) and DIPEA (99,5%; N,N-diisopropylethylamine) in a flask in 20 mL anhydrous DMF under N_2 -atmosphere. The solution was stirred for 15 min to activate the polymer, before NDA solved in 5 mL anhydrous DMF was added. The solution was stirred for 3 days and then dropped into 1:1 (v/v) hexane/ Et_2O to precipitate the raw product. The sample was collected via centrifugation (5000 rpm, 2 min, 4 °C) and dried *in vacuo* before resolving it in 15 mL MilliQ H_2O . Excess NDA was removed via dialysis (membrane cut-off size: 3.5 kDa) against RO- H_2O and the purified sample was freeze-dried. Grade of functionalization was determined via $^1\text{H-NMR}$ by solving 20 mg of the sample in 700 μL MeOD.

3.7. Ligand-exchange

The Fe_3O_4 particles used in this master thesis were received oleic acid capped, making them highly hydrophobic. A sufficient ligand exchange, with suitable polymers, lead to a desirable level of wettability in both water and oil. Ligand-exchange was performed according to literature with minor changes^{37,72}. Oleic acid coated SPION solved in 1 mL Toluene and NDA-terminated polymer solved in 9 mL DMF were charged in a vial and exposed

24 h to ultrasonication. The product was precipitated in 1:1 (v/v) hexane/Et₂O, collected via centrifugation and dried *in vacuo*. The sample then was solved in 10 mL of MilliQ H₂O and purified via dialysis (membrane cut-off size: 1 kDa). Water was removed by freeze-drying. The grafting density was verified via TGA.

3.8. Preparation of emulsions

Preparation of emulsions was carried out at room temperature. Nonanoic acid and rapeseed oil were stored at 4 °C and had been incubated at room temperature until thawing beforehand.

Core-shell nanoparticle stock solutions (5 mg/mL) for each sample were prepared in glass vials and filtered with a 0.45 µm RC filter. The added amounts of stock solution were diluted with prefiltered Milli-Q water to a concentration range from 0.02 to 5 mg/mL in Eppendorf cuvettes. Then 10 µL oil was added as dispersed phase and the samples were vortexed for 2 min. After that, the solutions turned cloudy. For measurements the samples were transferred to polystyrene semi-micro cuvettes (1.6 mL volume, 10 mm layer thickness) from Sarstedt. Equilibrium time before the actual measurement was set to 30 seconds. Three runs of 15 measurements each were conducted for each sample within each observation interval. The results of these 15 measurements were used to obtain an average plot for each run. For each dispersed phase a different SOP was constructed, depending on the refractive index of the dispersed oil. After each measurement the samples were returned to their original Eppendorf cuvettes and stored at room temperature.

4. Results and Discussion

4.1. Monomer Synthesis and Purification

The principle for the synthesis of IPOX were the protocols established by Witte and Seeliger in 1972⁷³ and 1974⁷⁴, where the generation of 2-oxazolines from nitriles using metallic cations as catalysts under high temperature were described. We modified their methodology, used isobutyronitrile and ethanolamine as eluents and utilized ZnAc as catalysator, since it is established that Zn^{2+} is capable to form complexes with nitrile groups⁷⁴. Reaction temperature was set to 130 °C and excess ammonia, created as by-product during the reaction, was collected in HCl (8 % (v/v)). Monnery et al. reported issues during the purification process, claiming that surplus ammonia acted as a terminating agent under influence of CaH_2 ⁴⁹. We therefore removed the contaminant via a conventional extraction process, diluting our crude product in 100 mL DCM and extracting against batches of 50 mL MilliQ- H_2O , until the collected water showed a neutral pH value. Remaining water was cleared away via water-free Na_2SO_4 .

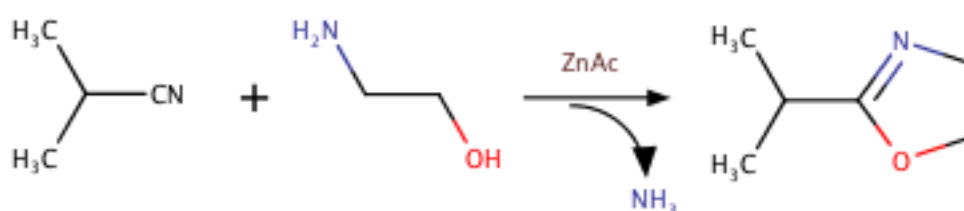


Fig. 12: Synthesis of IPOX. Metallic cations catalyze the esterification of nitriles and primary amino alcohols.

Before the distillation was started, CaH_2 was added to the mixture and stirred overnight to activate the hydrolysis process. Distillation was done under N_2 atmosphere. We utilized a distillation pig to remove the first 2 mL of the final product and then obtained 20 mL of sufficiently refined product. The purification was confirmed via 1H -NMR; deuterized chloroform was used as eluent.

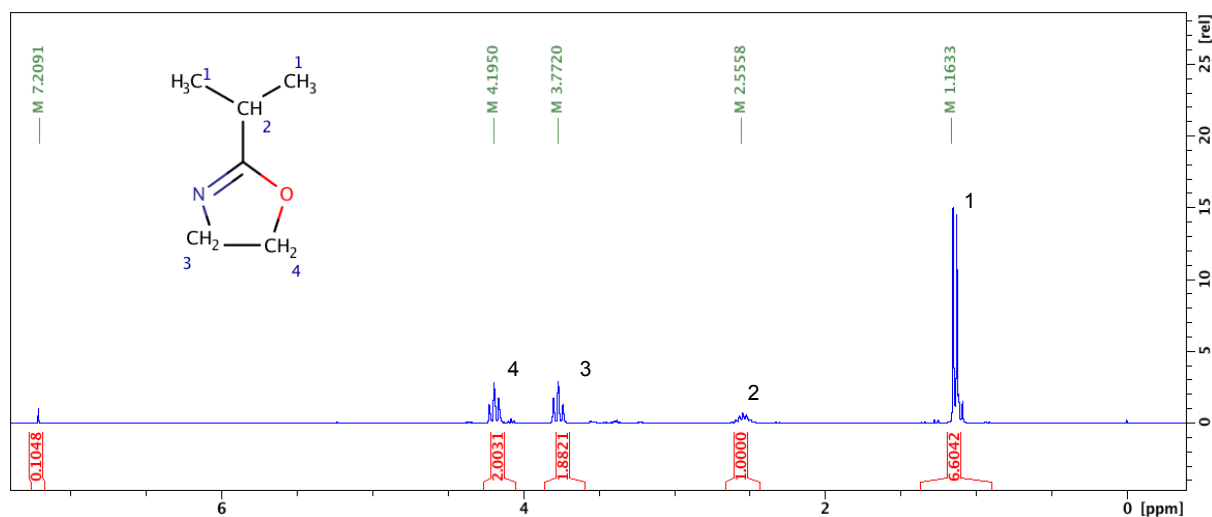


Fig. 13: ^1H -NMR spectrum of IPOX. The leftmost shift pattern belongs to leftover MeCl_3 , which was used as eluent.

4.2. Polymer Shell Synthesis and Grafting

4.2.1. NDA Anchor Synthesis

The synthesis of nitrodopamine-hemisulfate can be found in the literature⁷⁵; we used a slightly modified version established by Bixner et al.²² Acid is added dropwise under constant cooling to reduce the formation of foam. Over the course of the synthesis a color change from brown to yellow was observed, indicating the correct synthesis of the product. After filtration and washing steps the final product was covered in aluminum foil and stored at 4 °C. An aliquot of 20 mg was solved in DMSO-d_6 and examined via ^1H -NMR to verify the purity of the product. The spectra can be observed in Fig. 14. The two small leftmost peaks represent hydroxyl groups attached to the benzene ring, which can also be observed in spectra of NDA functionalized polymers (compare to Fig. 17). The peak at 2.5 ppm was assigned to leftover undeuterized DMSO.

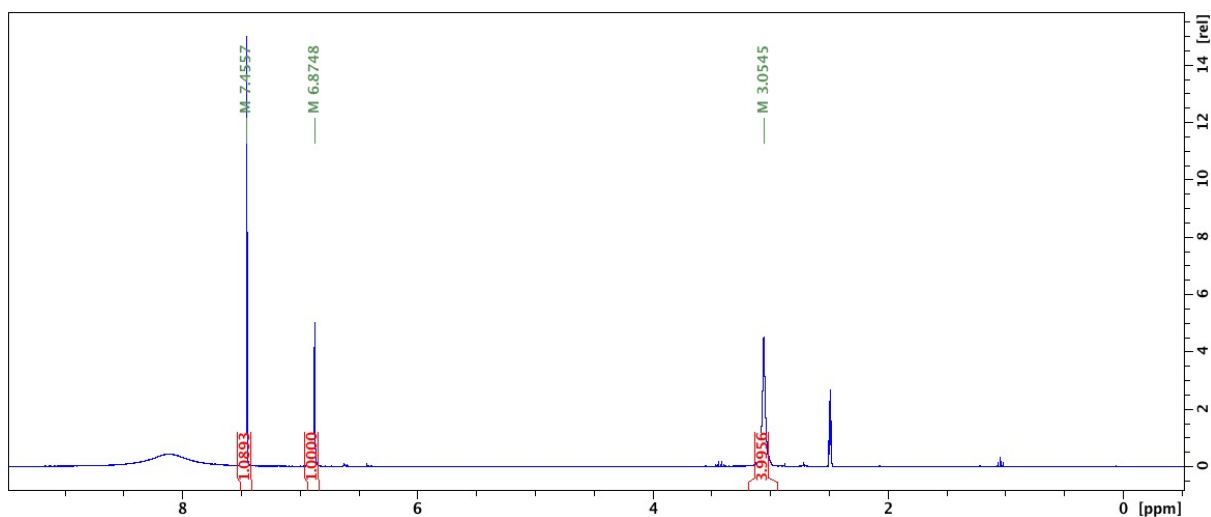


Fig. 14: ^1H NMR spectra of NDA hemisulfate.

4.2.2. PNIPAM Shell Synthesis

Preparation was done via the grafting-to approach, allowing for further investigation of the polymer characteristics prior to SPION assembly. NIPAM was polymerized via ATRP utilizing 2-bromo-2-methylpropionic acid as initiator. Adapting the amount of initiator, the chain length could be varied. We synthesized polymer chains with molecular weights of 8-40 kDa. Primarily, we applied only 6 mg CuBr_2 , however the resulting polymers showed immense PDI values. After we adapted to the protocol of Kurzhals et al. and used a higher amount of copper salts, as well as Me_6Tren , we could easily achieve the desired polymer chains⁷². Copper was removed via dialysis against $\text{RO-H}_2\text{O}$. We chose a membrane cut-off size of 3500 Da, considering the large hydrodynamic diameters of PNIPAM. However, the resulting PDI values still represented a problem, often exceeding ideal values of <1.2 . This was especially true for polymer chains larger than 20 kDa. Kurzhals et al. reported that the used method is suitable for a molecular weight range from 5-20 kDa⁷². Although not ideal, the reported PDIs were still in the acceptable range. Successful PNIPAM syntheses are summarized in Table 1. Chain length and PDI were confirmed via GPC. 3 mg sample was solved in 1 mL DMF containing 5% LiBr (w/w) to break up hydrogen bonding and then injected.

Abbreviation	M_n [Da]	M_w [Da]	PDI
PF003	29803	48601	1.63
PF005	25831	38091	1.47
PF006	8510	9470	1.11
PF008	19995	24660	1.23
PF009	37124	60531	1.63
PF012	9954	11069	1.11
PF013	15925	21087	1.32
PF016	34146	42972	1.26
PF017	22015	30561	1.39
PF040	32351	48247	1.49

Table 1: Overview of all PNIPAM syntheses.

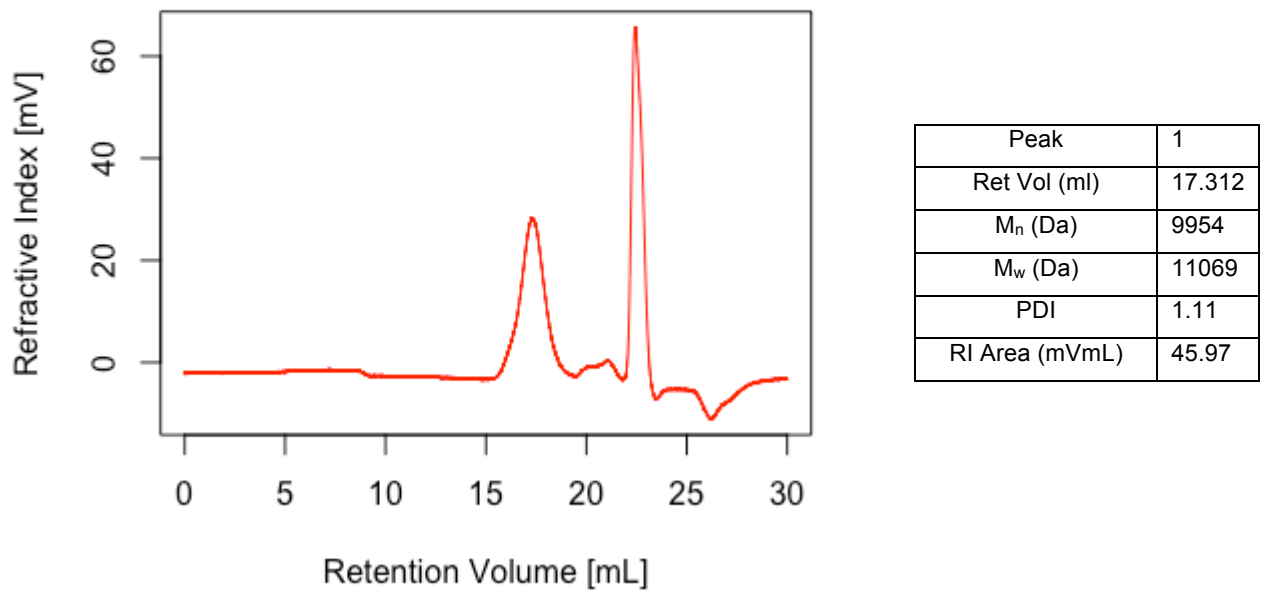


Fig. 15: GPC analysis of a PNIPAM sample. The peak between 15 and 20 mL retention signifies the sample polymer. The peaks at the right end of the spectra are system peaks signaling the end of the elution mode.

4.2.3. Poly-2-alkyl-2-oxazoline Shell Synthesis

Since water disturbs the polymerization process, poly-2-alkyl-2-oxazoline synthesis must be performed in a water-free environment, e.g. a glovebox system. Anhydrous DMA was chosen as solvent, as it was shown to minimize chain transfer reaction at a monomer concentration below 4 M⁴⁸. We utilized a varying amount of methyl-tosylate as initiator, to control the resulting polymer chain length. However, we could only achieve the requested chain length after doubling the amount of initiator that would be necessary according to our calculations. The study of Glassner et al. provides an explanation, stating that high temperatures can lead to a loss of function in thermally unstable initiators⁷⁶. Polymerization was executed at 100 °C to accelerate the reaction process. We then obtained hydroxy-terminated poly-2-alkyl-2-oxazolines. Molarity and PDI were evaluated via GPC as described in Chapter 3.2.1.

PMOx has been proven to be especially difficult to synthesize. For the first batches we used synthesis protocols similar to PEOx, but the resulting chain lengths were way larger than we expected. Since no synthesis attempts on this polymer have been done in our working group, we settled for a kinetic study prior to establish a proper synthesis protocol. We changed the reaction temperature to 80 °C to slow down the polymerization velocity, but kept the remaining parameters similar to the other poly-2-alkyl-2-oxazolines synthesis protocols, and aimed for a 21000 Da polymer chain. Four samples were taken every two hours; the fifth was measured after 24 h. The results can be seen in Fig. 16; according to the graph, the desired chain length was achieved after 8 h. After several dissatisfying unsuccessful synthesis attempts, we could improve the synthesis by implementing a reaction time of 19 h, a reaction temperature of 70 °C and benzyl-bromide as initiator.

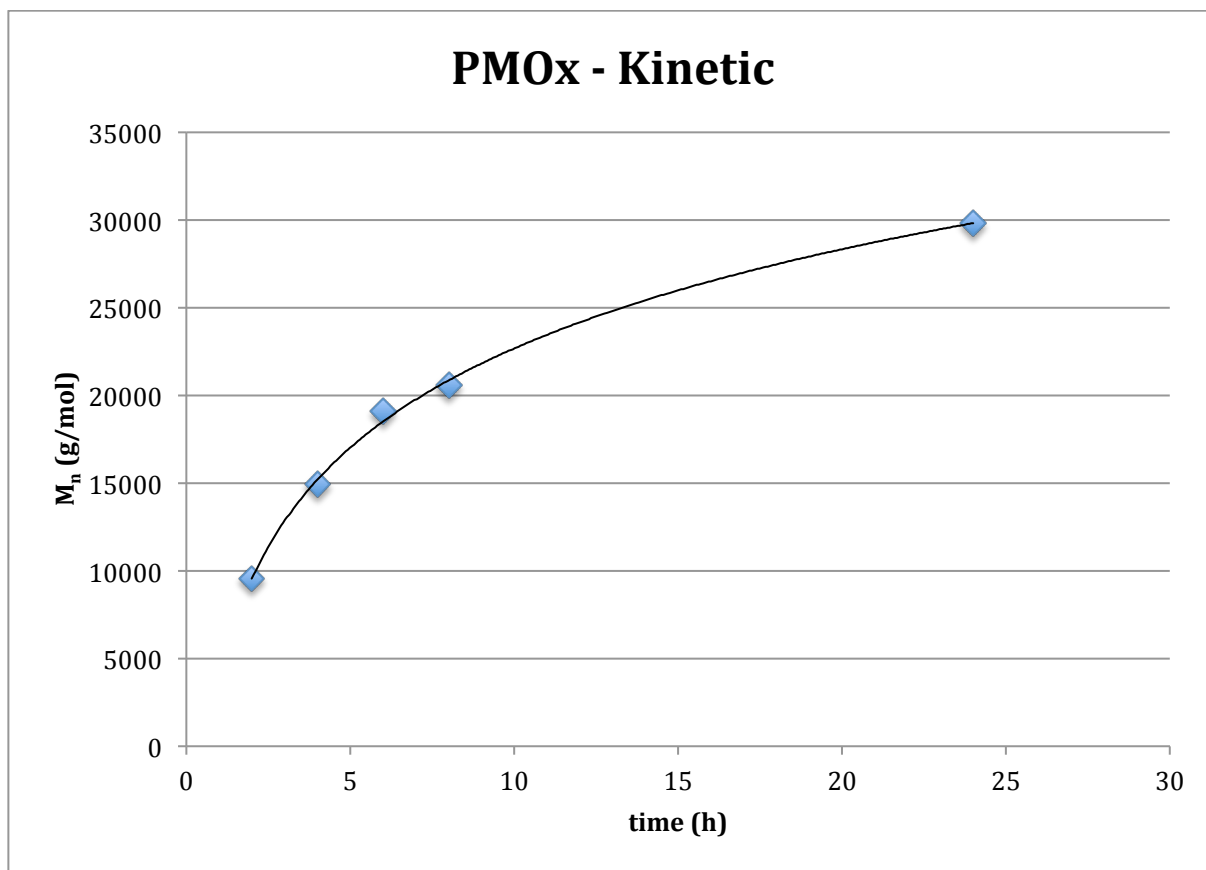


Fig. 16: Kinetic study of PMOx polymerization.

Coupling of nitrodopamine requires a carboxyl terminated end group. A modified Steglich esterification was performed with succinic anhydrite as precursor and DMAP as catalyst. A ratio of 9.6 succinic anhydrite and 3.2 DMAP equivalents respectively to the polymer amount were used to ensure total esterification. A summary of all synthesized POX samples can be found in Table 2.

Abbreviation	Polymer	M _n [Da]	M _w [Da]	PDI
PF020	PEOx	12287	13396	1.090
PF021	PEOx	19960	23721	1.188
PF022	PEOx	32605	40216	1.233
PF024	PMOx	9235	9552	1.034
PF025	PMOx	14223	14839	1.043
PF026	PMOx	24098	25819	1.071
PF027	PMOx	36206	43408	1.199
PF028	PIPOx	10507	10803	1.028
PF029	PIPOx	23046	23735	1.030
PF030	PIPOx	40059	41545	1.037
PF035	PIPOx	5557	5888	1.060
PF036	PIPOx	21524	22179	1.030

PF037	PMOx	13397	17767	1.326
PF038	PMOx	14927	18117	1.214
PF039	PMOx	12849	13880	1.080
PF041	PIPOx	8022	9067	1.130
PF042	PIPOx	16844	18442	1.095
PF043	PIPOx	26016	29330	1.127
PF044	PIPOx	5928	6271	1.058
PF045	PIPOx	12964	13357	1.030
PF046	PIPOx	29275	30038	1.026
PF050	PMOx	7831	8456	1.080
PF051	PMOx	7892	9294	1.178
PF052	PMOx	7825	9284	1.186
PF053	PMOx	17012	21241	1.249
PF054	PEOx	6681	7338	1.098
PF055	PEOx	12111	13923	1.150
PF056	PEOx	18133	23392	1.290

Table 2: Overview over all POX syntheses.

4.2.4. Functionalization and Ligand Exchange

For functionalization, the threefold excess of NDA to the molar equivalent for 100% functionalization was used to shift the reaction equilibrium towards the product. This, however, also meant that the excess of NDA had to be removed through purification after the reaction. Remaining unbound NDA would distort NMR measurements and compete with functionalized polymer for binding sites on the particle surface. For NDA removal we choose dialysis instead of extraction, since the latter resulted in higher product losses. We choose a cut-off size of 3500 Da and dialyzed against RO-H₂O. The first two water changes were performed one and two hours after preparation, respectively, and afterwards when the dialysis water retained a yellowish shade (usually after a couple of hours or overnight). Dialysis was performed until the water was clear and then one day in excess. The grade of functionalization was determined via ¹H-NMR. MeOD was chosen as solvent, since it does not disturb the measurement. Fig. 17 depicts the result of a ¹H-NMR measurement of NDA-functionalized PIPOX (13000 Da). Due to the size of the molecule and the fact, that the side-chain contains six hydrogen molecules with the same chemical

shift (represented by the large peak at 0.997 ppm), the signals contributed by NDA –groups were rather small. Due to its highly polar nature, the shifts remain at the left end of the spectra at 6.412 ppm and 7.426 ppm.

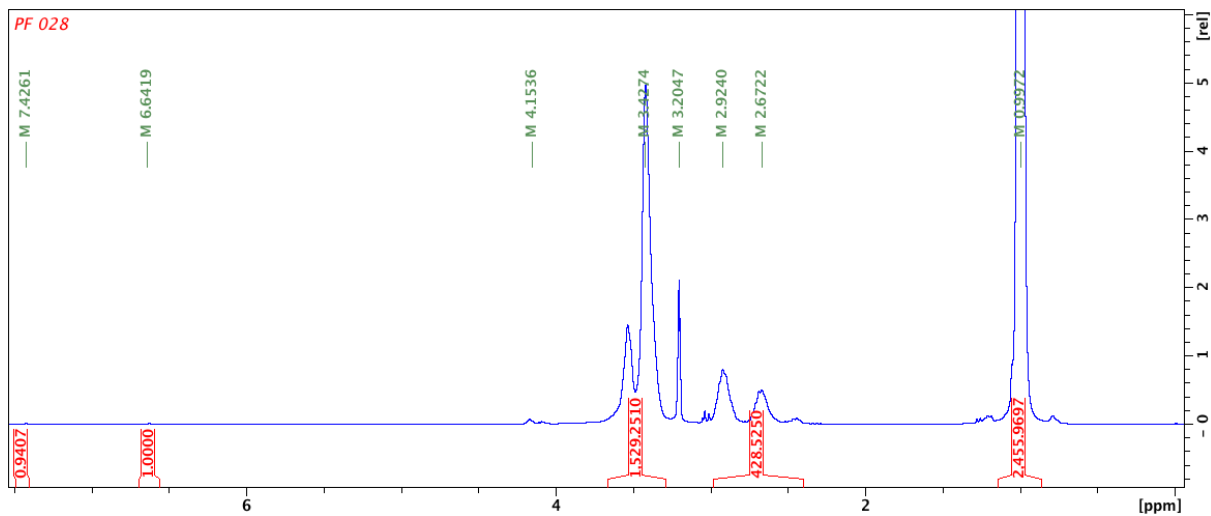


Fig. 17: ¹H-NMR spectrum of NDA functionalized PIPOx.

During the functionalization the sample solution sometimes turned cloudy after addition of NDA solution. We attributed this to undissolved NDA and tried to circumvent the problem by adding more solvent until the turbidity disappeared. However, as far as we can tell, this had no effect on the degree of functionalization of the finalized polymer. The functionalized polymers are summarized in Table 3.

Abbreviation	Polymer	Polymer size [Da]	Grade of polymer functionalization [%]
PF003	PNIPAM	29803	72,4
PF005	PNIPAM	25831	90,6
PF006	PNIPAM	8510	43,4
PF008	PNIPAM	19995	49,8
PF009	PNIPAM	37124	53,1
PF012	PNIPAM	9954	59,6
PF013	PNIPAM	15925	51,8
PF020	PEOx	12287	54
PF021	PEOx	19960	29,1
PF022	PEOx	32605	77,2
PF023	PNIPAM	34146	56,6
PF028	PIPOx	10507	24,3
PF031	PNIPAM	22015	36,7
PF036	PIPOx	21524	20,1
PF040	PNIPAM	32351	54,7

PF045a	PIPOx	12964	92,2
PF045b	PIPOx	12964	92,2
PF046	PIPOx	29275	60,8
PF050	PMOx	7831	28,8
PF053	PMOx	17012	34
PF055a	PEOx	12111	70
PF055b	PEOx	12111	70
PF056	PEOx	18133	54,6

Table 3: Summary of all polymer samples that were functionalized with NDA. For PNIPAM samples typically over 50% of polymer was successfully functionalized. While the grade of functionalization varied strongly between POX samples, in terms of functionalization, no POX was favored.

During the ligand exchange an equivalent of oleic acid capped NPs and functionalized polymer was mixed, so that 5 polymer chains would occupy 1 nm² particle surface. This procedure should ensure higher grafting densities. Usually the obtained GDs remained around 0.5 chains/nm². Only particles with a GD of 0.7 chains/nm² were retained for further characterization and assembly experiments.

Grafting densities were evaluated via TGA. An atmosphere of 80% synthetic air and 20% nitrogen should ensure total decomposition of all organic material. Weight loss was determined from 200 to 500 °C due to possible solvent leftovers, which would evaporate at < 200 °C. The residual mass over 500 °C was attributed to the inorganic fraction of the samples, whereas mass loss between 200 and 500 °C was attributed to the organic polymer shell. An example can be seen Fig. 18.

Grafting densities below 1 chain/nm² are a common characteristic of the “grafting-to” approach. Theoretically higher GDs can be obtained with the “grafting-from” method, however the oleic acid capped nature of the iron cores would complicate the synthesis route. In the case of PNIPAM coated NPs, Kurzhals et al. reported that similar grafting densities were obtained, regardless of the chosen approach⁷². For poly-2-alkyl-2-oxazoline coated NPs, the synthesis protocols of the polymers were not completely developed, so investigating their characteristics prior to the assembly was the better option.

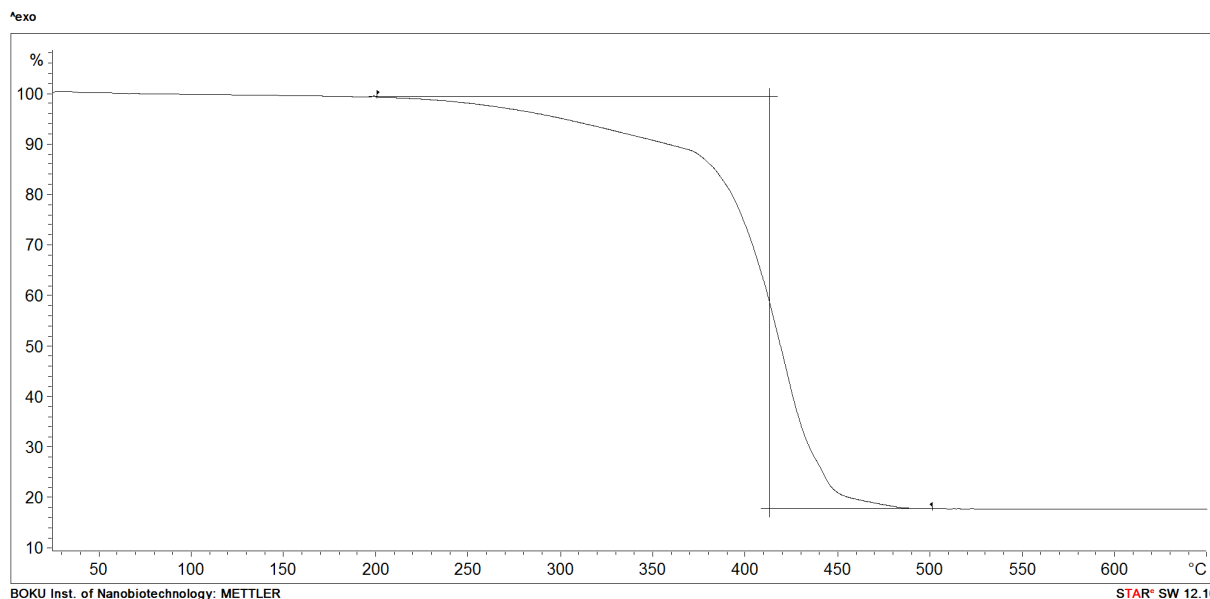


Fig. 18: Example of a TGA analysis. The x-axis shows the rising temperature, whereas the y-axis the percentage of weight loss during heating due to decomposition and evaporation. The weight-loss up to 200 °C is negligible, meaning that the solvent was removed completely during the freeze-drying process. 2.1227 mg CSNP sample (4.9 nm core with 13000 Da PIPOx shell) were inserted. 0.3783 mg of the sample remained, signifying the inorganic core, whereas 1.7444 mg evaporated, attributed to the polymer shell. From this the grafting density was calculated to be 0.9036 chains/nm².

Abbreviation	Core size [nm]	Polymer Shell	Shell size [Da]	GD [chains/nm ²]
PF007	4,9	PNIPAM	29803	0,92
PF010	4,9	PNIPAM	25831	0,45
PF011	4,9	PNIPAM	8510	1,26
PF014	4,9	PNIPAM	19995	0,58
PF015	4,9	PNIPAM	37124	0,54
PF018	9,8	PNIPAM	9954	0,44
PF019	9,8	PNIPAM	15925	0,24
PF023	9,8	PNIPAM	34146	0,15
PF031	9,8	PNIPAM	22015	0,36
PF032	4,9	PEOx	12287	0,19
PF033	4,9	PEOx	19960	0,46
PF034	4,9	PEOx	32605	0,32
PF040	9,8	PNIPAM	32351	0,74
PF057a	9,8	PIPOx	12964	0,84
PF057b	4,9	PIPOx	12964	0,90
PF058	4,9	PIPOx	29275	0,42
PF059	4,9	PMOx	17012	0,46
PF060	4,9	PMOx	7831	0,36
PF061a	4,9	PEOx	12111	0,25
PF061b	9,8	PEOx	12111	0,45
PF062	4,9	PEOx	18133	0,59

Table 4: Summary of all assembled CSNPs. As expected, GD mostly was found to be below 1 chain/nm² due to the “grafting to approach”. Especially PEOx coated CSNP showed very low GDs (mostly below 0.5 chains/nm²).

4.2.5. Particle size distributions

To evaluate the size of free, unbound NPs we prepared solutions at a concentration of 1 mg/mL CSNP for DLS measurement. Samples were diluted with additionally filtered (0.45 μm pore size) MilliQ- H_2O from dedusted stock solutions [$c(\text{CSNP}) = 5 \text{ mg/mL}$]. The results obtained in this section were used later in chapter 4.3 as control values for the particle stabilized emulsions. Since we are looking for small, dispersed particles, we used number-weighted size distribution for evaluation.

We obtained three PNIPAM grafted CSNP samples with suitable GDs exceeding 0.7 chains/nm^2 . The samples can be observed in the figures below (Fig. 19).

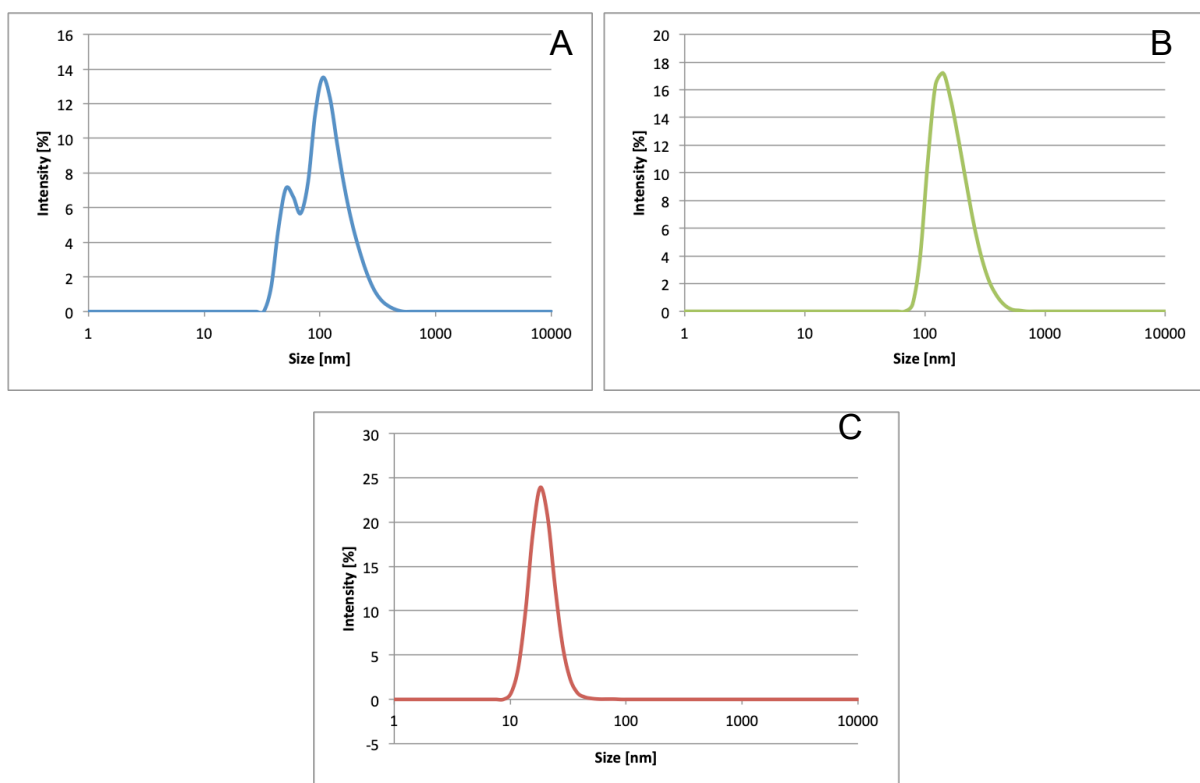


Fig. 19: PNIPAM coated CSNPs [$c = 1 \text{ mg/mL}$] evaluated by number-weighted size distribution.

A): 4.9 nm core with 30000 Da PNIPAM shell. Two local maxima are observable. The first maximum at 50 nm was attributed to free, dispersed particles; the other at 105 nm to agglomerated particles.

(B): 9.8 nm core with 32000 Da PNIPAM shell. The peak at 141 nm was attributed to agglomerated particles.

(C): 4.9 nm core with 8500 Da PNIPAM shell. The peak at 18 nm hydrodynamic diameter signifies dispersed particles.

For PNIPAM coated samples only PF011 showed dispersed particles. The sizes observed in the other two samples were too large to be attributed to dispersed particles. This was unexpected, since a polymer shell with higher MW chains is usually favorable for stabilization of nanoparticles. The more stable dispersion formed by PF011 compared to other PNIPAM-grafted core-shell nanoparticles was attributed to its higher grafting density (1.26 chains/nm²).

PF057 (13000 Da PIPOx) showed both a high yield and a high grade of functionalization; therefore, we split the sample in half and graft one part to 9.8 nm NPs (PF057a; GD: 0.84) and the other to 4.9 nm NPs (PF057b; GD: 0.90). This allowed for a better comparison of the different cores of the sample, since the polymer used to graft the shell was identical. The number-weighted size distribution of both samples can be seen in Fig. 20.

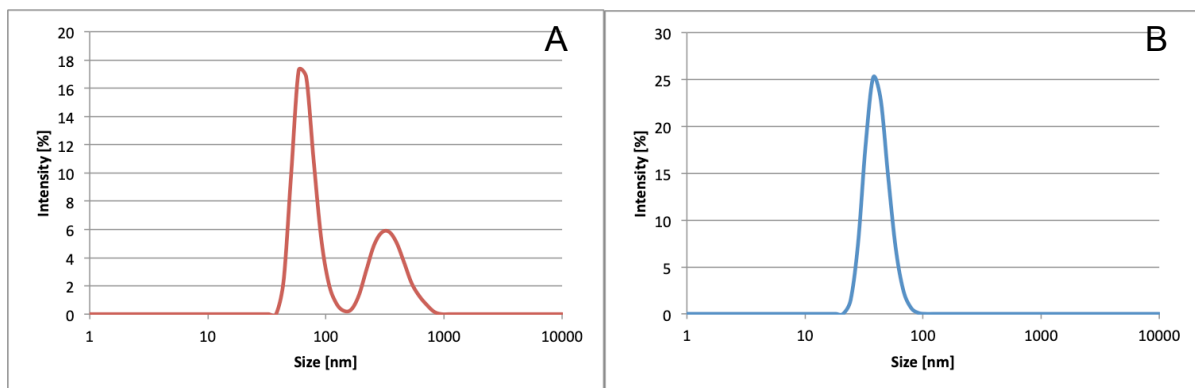


Fig. 20: PIPOx coated CSNPs [c = 1 mg/mL] calculated via number-weighted size distribution.

(A): 9.8 nm core with 13000 Da shell. Two peaks are observable; the first at 60 nm and the second at 295 nm. Both peaks are too large to indicate dispersed particles.

(B): 4.9 nm core with 13000 Da shell. The peak is located at 38 nm, which signifies free, dispersed particles.

Dispersed particles are observable in PF057b, whereas particles in PF057a are agglomerated. Considering the difference in size distributions, we assumed that a 13000 Da polymer shell is too small to prevent 9.8 nm cores from aggregating, however a similar case could not be found in the literature, so this remains purely a hypothesis.

Since a suitable grafting density for PEOx coated NP samples could not be realized through the syntheses presented above, a sample was provided by Martina Schroffenegger, MSc. 15600 Da PEOx chains were grafted onto 5.6 nm Fe₃O₄ cores (GD = 0.78 chains/nm²); the sample was synthesized by the same methods described above. A number-weighted size distribution can be seen in Fig. 21.

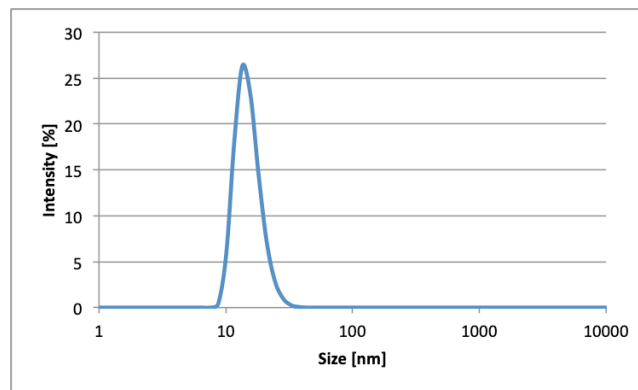


Fig. 21: 5.6 nm cores with 15600 Da PEOx chains. The peak is located at 14 nm, which is attributed to dispersed nanoparticles. The sample is well dispersed.

4.3. Emulsification

The following section contains the results of the emulsification process measured via DLS on a Malvern Zetasizer Nano-ZS. We used the size distribution to determine the emulsion quality. The volume-weighted distributions of some selected examples, as well as the dominant sizes found in each sample plotted against time, are presented to support and clarify the descriptions given for the observed samples.

4.3.1. Influence of the dispersed phase

To get an overview over different behaviors we chose three different oils to start emulsification processes:

- Novec™ 7500 technical fluid [3-Ethoxyperfluoro(2-methylhexane)] as a highly non-polar oil with high surface tension to water.

- Nonanoic acid (analytical standard) as a biocompatible oil with low surface tension to water.
- Rapeseed oil as a non-technical grade, bio-produced oil with low surface tension to water.

To optimize emulsification, the resulting oil-water interfacial tension should be kept at a minimum⁷⁷, so we expected more stable emulsions from nonanoic acid and rapeseed oil. Polarity decreases with increase in chain length of the fatty acid as well as the number of saturated links. All chosen oils remain liquid at room temperature, which simplifies the emulsification process. Novec™ 7500 was stored at room temperature, whereas nonanoic acid and rapeseed oil were stored at 4 °C and were thawed at room temperature before use.

We used nanoparticles with a core diameter of 5 nm and coated with PNIPAM (30 kDa, GD: 0.9) and PEOx (16 kDa, GD: 0.8) respectively. We created stock solutions [5 mg/mL] for both nanoparticles. Concentration values for nanoparticle content were set to 1 mg/mL and 5 mg/mL to observe influence of NP concentration on droplet pattern for the different dispersed phases. Observation dates were set to twice per week over 3 weeks and 3 repeat measurements were made for every data point.

Emulsification was initiated via vortexing the samples, after that the solution turned cloudy and phase separation was no longer visible. Quick vortexing disperses the oil phase into the water and thereby instantly increases the available surface area of the dispersed phase for NP attachment. This accelerates the formation. Between the measurements the samples were stored in Eppendorf tubes without agitation at room temperature.

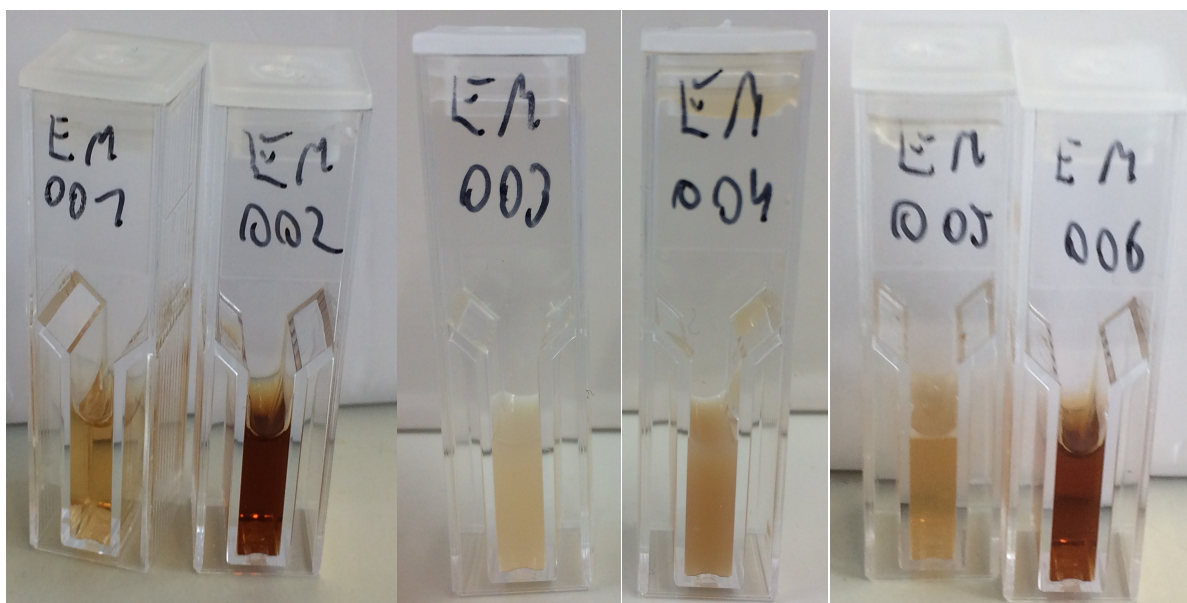


Fig. 22: 1 mg/mL (light) and 5 mg/mL (dark) PNIPAM coated NP emulsions with 10 μ L Novec™ 7500 (left), nonanoic acid (middle) and rapeseed oil (right) respectively after an incubation time of three days.

The first measurement was executed three days after emulsification. Fig. 22 depicts the first six PNIPAM-CSNP based emulsions. A successful emulsification process can be assumed by the turbidity of the sample at first glance. Following this expectation, we concluded that nonanoic acid was the most favorable dispersed phase.

We used the data from Chapter 4.2.5 as control values to compare the size distributions of emulsion droplets to pure NP solutions. The volume-weighted size distributions of pure NP solutions [1 mg/mL] are shown below. Even though a high grafting density was given for PNIPAM coated iron cores, they mainly remain as agglomerates with diameters around 100 nm, as a pure solution in MilliQ-H₂O (Fig. 23A). As can be observed in Fig. 23B, PEOx particles the signal seems to correspond to mainly free dispersed particles.

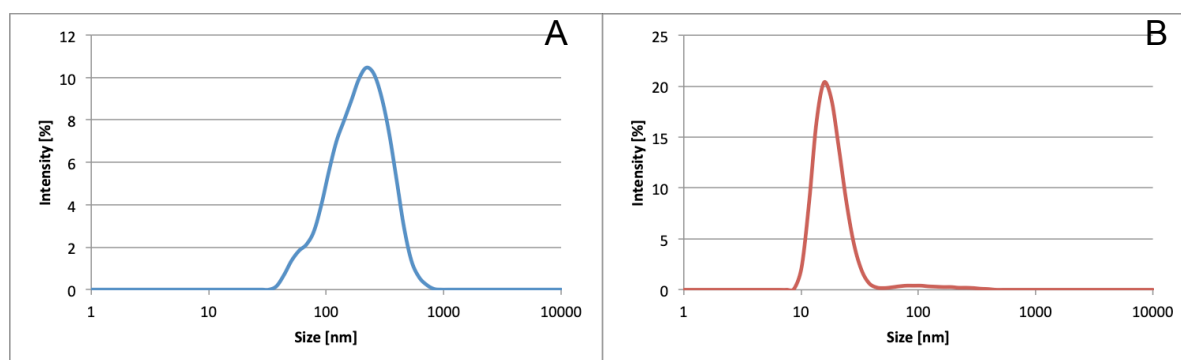


Fig. 23: (A) Control sample of 4.9 nm FeOx core with 30000 Da PNIPAM coating (GD =0.9). Concentration of the CSNP was set to 1 mg/mL. Size distribution was evaluated via volume-weighted distribution. The peak signifies colloids with a hydrodynamic diameter of 220 nm, which is attributed to agglomerated CSNPs.

(B) Control sample of 5.6 nm FeOx core with 16000 Da PEOx coating (GD=0.8). Concentration of the CSNP was set to 1 mg/mL. Size distribution was evaluated via volume-weighted distribution. The peak signifies colloids with a size of 16 nm, which is attributed to unbound CSNPs.

Evaluating the visible clues of Fig. 22, we concluded that emulsification succeeded best with nonanoic acid as apolar phase. In contrast to the control sample, the number and volume weighted size distributions of emulsified samples show the presence of smaller entities with 30 nm diameter in all samples (see Fig. 24). We concluded that this represents an excess of NPs, which are now well dispersed in the sample.

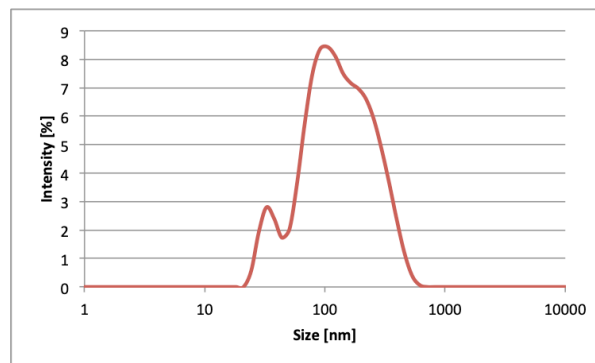


Fig. 24: Sample of 4.9 nm FeOx core with 30000 Da PNIPAM coating (GD =0.9). Nonanoic acid was used as dispersed phase. Volume-weighted size distribution is shown. The first small peak is located at 32 nm. Small peaks near this size were not visible in the control sample, but have been found throughout multiple emulsified samples and are attributed to free unbound NPs. The larger peaks at 100 nm and 200 nm are attributed to emulsion droplets.

As expected, the emulsification process worked best with oils with lower surface tension towards water. Therefore, Novec™ 7500 was a very poor choice for a dispersed phase. The resulting mixtures share many similarities with the obtained control samples and the presence of free particles was even observable in the intensity distributions. After we observed the optical indication of pure emulsification as well as the large amount of free particles in Novec™ 7500 containing samples, we stopped further investigations with Novec™ 7500 based emulsions.

Core-shell nanoparticles (4.9 nm core) grafted with 30000 Da PNIPAM chains worked exceptional well with nonanoic acid as dispersed phase. Based on the volume-weighted size distributions, the sample with 1 mg/mL NP content forms droplets with 91 nm hydrodynamic diameter throughout the 17 days of observation period. This was attributed to small emulsion droplets (see Fig. 27). In the 5 mg/mL NP sample droplet diameters at 220-255 nm were observable, which correspond to the sizes seen in the control sample. In

number and intensity distribution, the observable droplet sizes also correspond with the control sample, meaning that a surplus of particles was present in the sample. As for PEOx mediated emulsions volume-weighted size distribution of 1 mg/mL NP sample showed the presence of two peaks on the first measurement (68 and 825 nm respectively, see Fig. 25). The area of the peak at 712 nm slowly decreased over the observation period. We found droplet diameters at around 20 nm in the 5 mg/mL PEOx sample, which is a similar size found in the control sample. We attributed this to possibly slightly aggregated dispersed NP instead of droplets. Only the intensity distribution revealed objects with a hydrodynamic diameter of 255 nm.

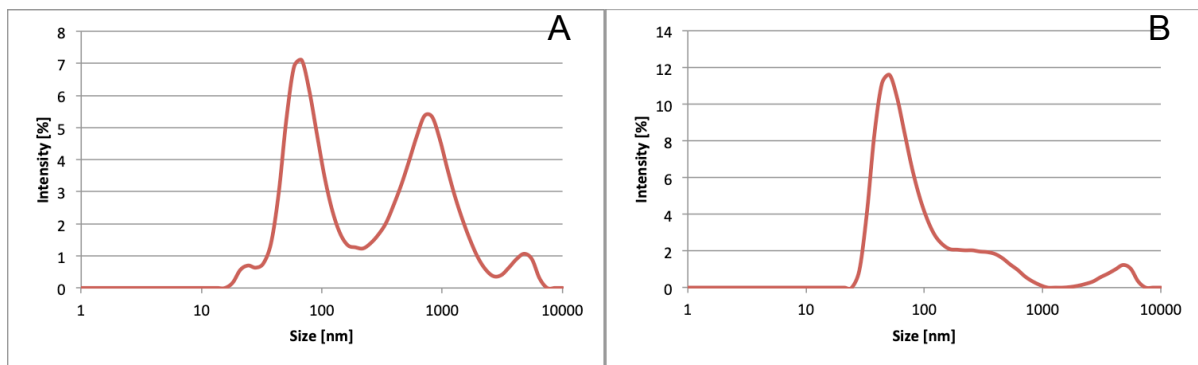


Fig. 25: Volume-weighted size distribution of 1 mg/mL NPs with PEOx shell (16000Da, GD=0.8) and nonanoic acid as dispersed phase after 3 days (A) of preparation and 10 days (B) incubation. A large peak at 712 nm is visible in the left figure, but decreases over time, as can be seen in the right figure.

Neither particle could form uniformly sized droplets with rapeseed oil. Number distributions of PNIPAM mediated emulsions displayed multiple peaks of 40 nm and 100 nm sized droplets, whereas a significant amount of PEOx coated NPs remained unbound. As can be seen in Fig. 26, volume-weighted size distributions show that a broad spectrum of droplet sizes was observed for all rapeseed oil emulsions.

Due to those observations, we decided to continue further examinations for PNIPAM mediated emulsions with nonanoic acid as dispersed phase.

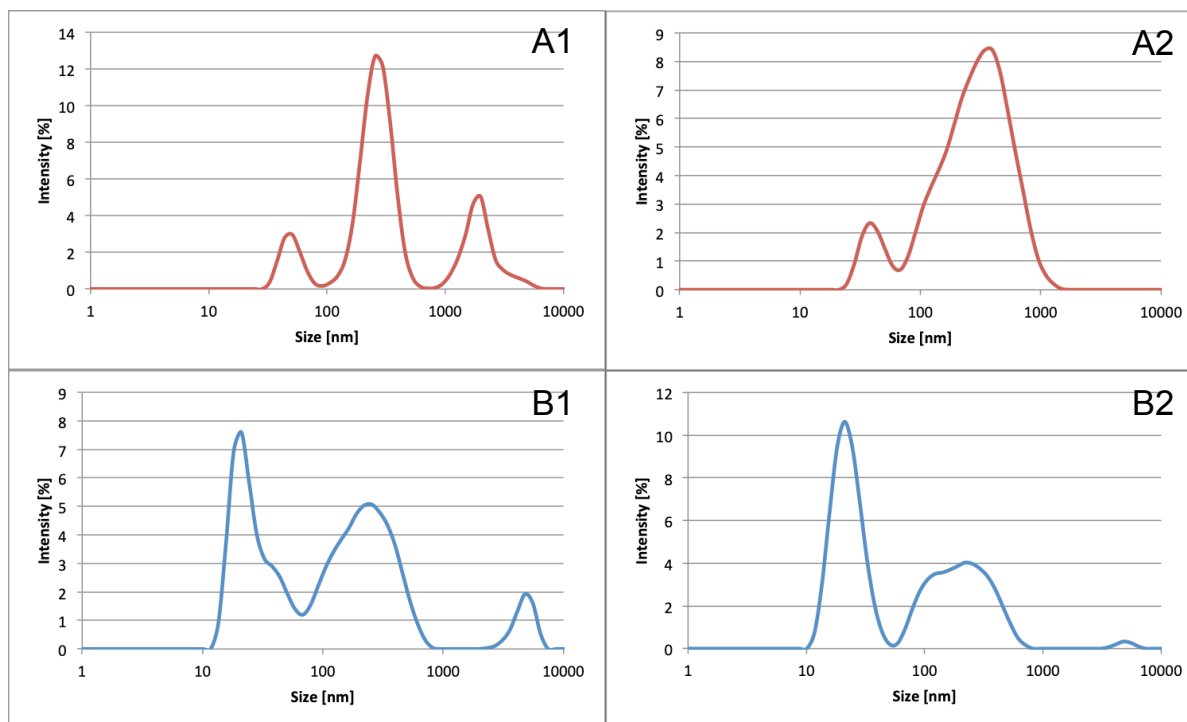


Fig. 26: Volume-weighted size distribution of two emulsions with rapeseed oil as dispersed phase. A1 and B1 were measured after 3 days of incubation; A2 and B2 after 13 days respectively.

(A): 4.9 nm FeOx core with 30000 Da PNIPAM coating (GD =0.9). (A1): after 3 days of incubation. The first peaks to the left (43nm) are attributed to unbound particles; the other peaks (maxima 255 nm and 1990 nm) are likely caused by emulsion droplets. Those two peaks merged over the course of the next two weeks to a single broad peak (A2).

(B): 5.6 nm FeOx core with 16000 Da PEOx coating (GD=0.8). Again the first peak is attributed to dispersed NPs (21nm). The second and third peaks (220 nm and 4801 nm) signify emulsion droplets. The peaks also merged together over the course of the next two weeks, resulting in a single broad peak (B2).

The dominant sizes, as determined by the approximate area under each respective peak, found in each sample by volume-weighted size distribution were plotted against time. Fig. 27 contains all PNIPAM based samples, whereas the PEOx based emulsions can be observed in Fig. 28.

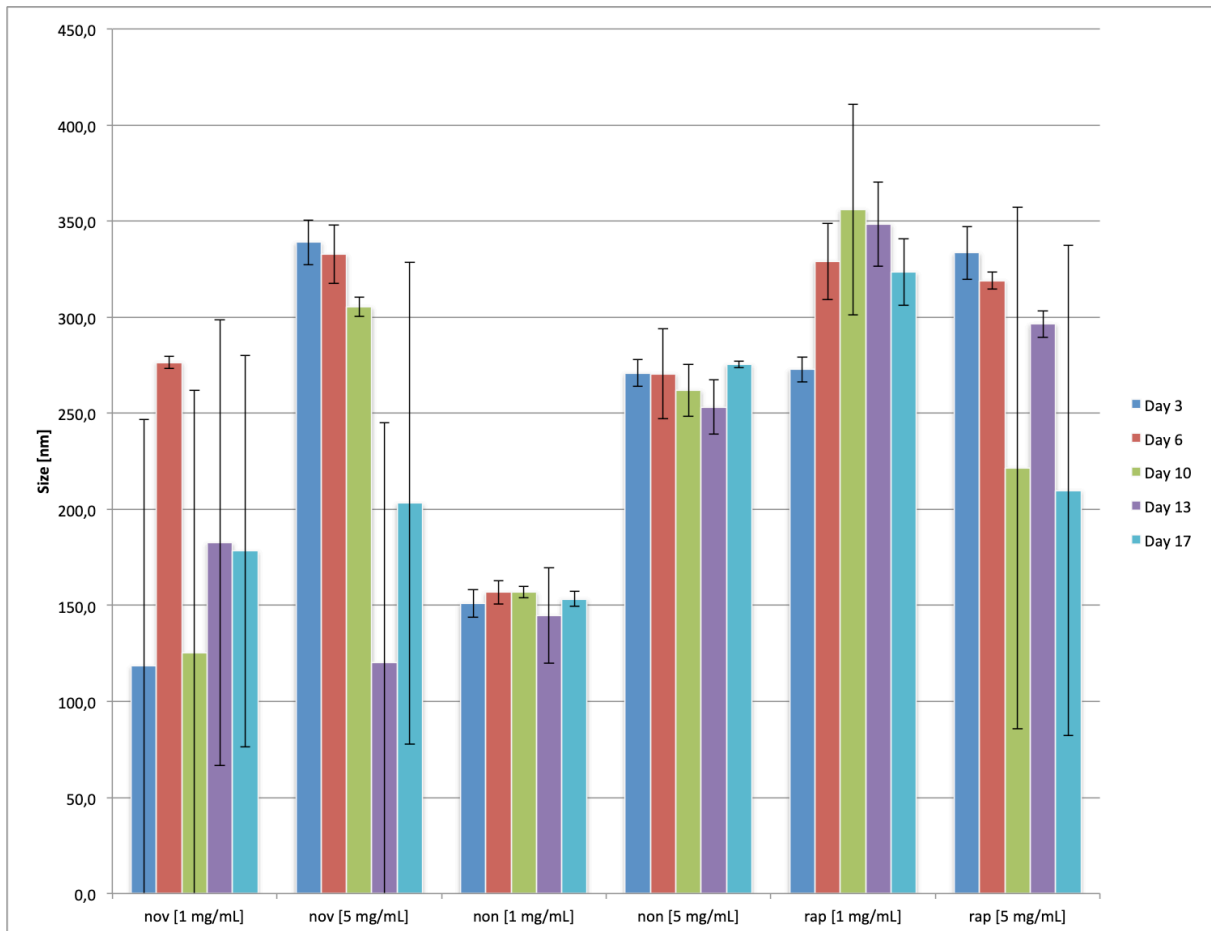


Fig. 27: Novec™ 7500 (nov), nonanoic acid (non) and rapeseed oil (rap) based emulsions with 4.9 nm FeOx core NPs with 30000 Da PNIPAM coating (GD =0.9). Size distributions were calculated using the volume-weighted distribution. Concentrations for NP were set to 1 mg/mL and 5 mg/mL for each dispersed phase respectively. With exception to the 1mg/mL NP with Novec™ 7500 based emulsions signal maxima trends remain constant over the observation period. Colloid diameters for 1mg/mL NP with nonanoic acid as dispersed phase are significantly smaller than the rest. Most particles remained at a size between 250 and 350 nm for the other emulsions.

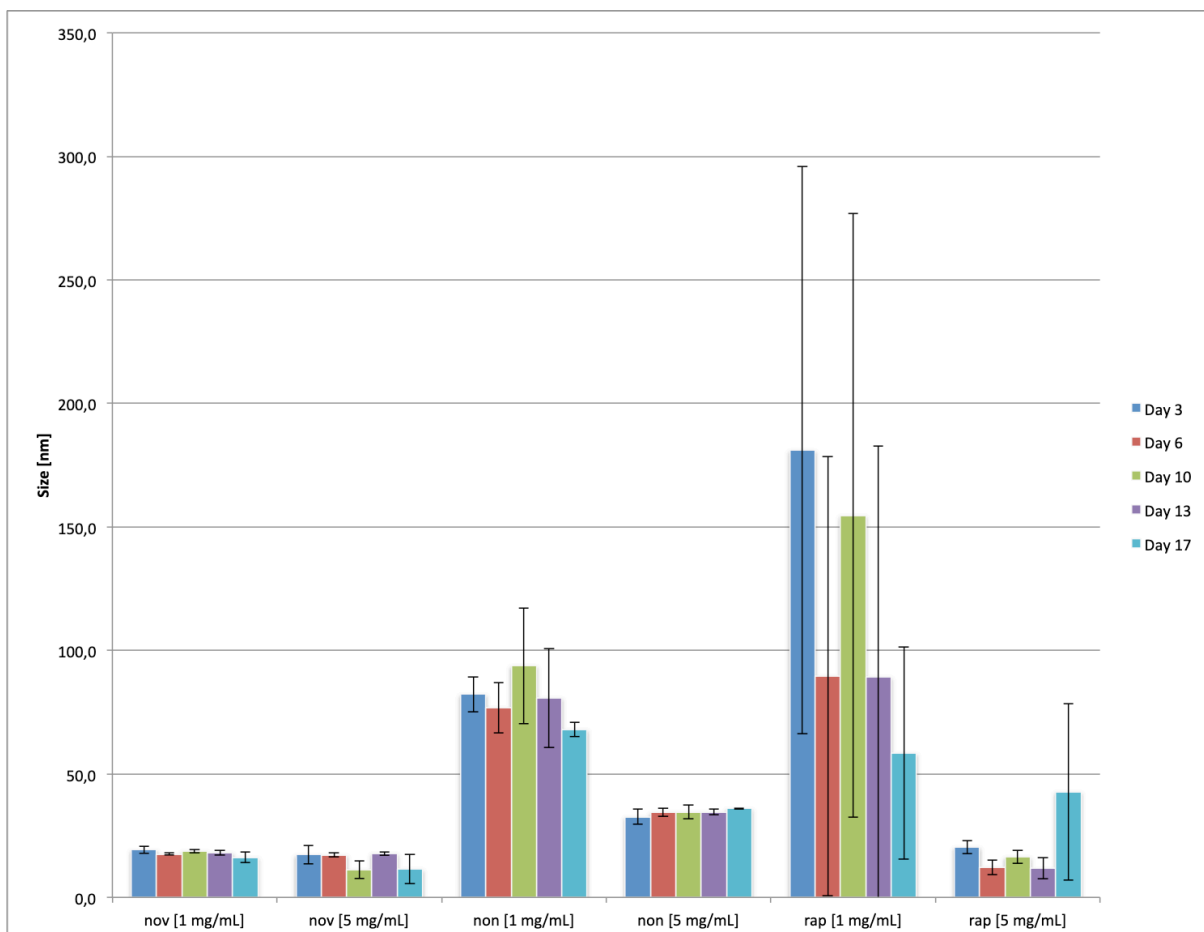


Fig. 28: Novec™ 7500 (nov), nonanoic acid (non) and rapeseed oil (rap) based emulsions with 5.6 nm FeOx core NPs with 16000 Da PEOx coating (GD =0.8) in different concentrations. Novec™ 7500 based emulsions are comparable to the obtained control values. Emulsions 5 mg/mL NP concentrations show a large surplus in dispersed NPs. For 1 mg/mL NP concentration, the dominant sizes were still dispersed nanoparticles, however we also found droplets with diameters of 600 nm in nonanoic acid based emulsions and 200 nm diameters in rapeseed oil based emulsions. Nonanoic acid however remained far more reproducible over the 3 weeks observation period.

In the initial measurements reported in Fig. 27 and Fig. 28, a large excess of nanoparticles was used compared to the estimate of the internal interfacial area in the emulsion. We therefore tested lower NP concentrations; these emulsions used concentration of NP of 0.02 mg/mL, 0.1 mg/mL, 0.5 mg/mL and 1 mg/mL to the same concentration of oil. We also tried to determine a lower threshold, where the amount of NP is not sufficient to stabilize the emulsion. Furthermore, we shifted the observation dates to each day, including the preparation date, up to day 4 and then once every week until 3 weeks after initiation for a total of eight measurements. This way, we tried to evaluate the changes in conformation until equilibrium was established, in case the equilibrium only was reached slowly.

4.3.2. Influence of shell size

We used our previously established sample of 5 nm cores and 30000 Da PNIPAM shell and compared it to a sample with the same cores, which was coated in an 8500 Da polymer shell. We compared our samples with previously established control samples with 1 mg/mL NP concentration. The control sample for 8500 Da PNIPAM coated NPs can be seen below (Fig. 29).

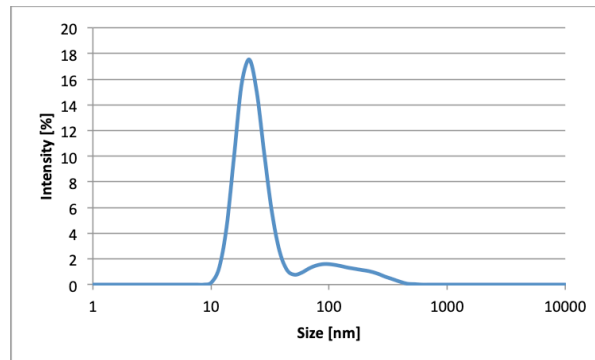


Fig. 29: Control sample of 4.9 nm FeOx core with 8500 Da PNIPAM coating (GD = 1.2). Concentration of the CSNP was set to 1 mg/mL. Size distribution was calculated using the volume-weighted distribution. The peak is located at 21 nm, which signifies the hydrodynamic diameter of dispersed NPs.

After high-speed vortexing all samples turned turbid (see Fig. 30). A brown film floating on top of the sample could be observed in some higher concentrated samples after about a week of incubation, this was probably CSNP-oil agglomerates or even larger droplets, which rose to top due to the density mismatch. This thin film could be redispersed after turning the Eppendorf cuvette gently upside-down once.

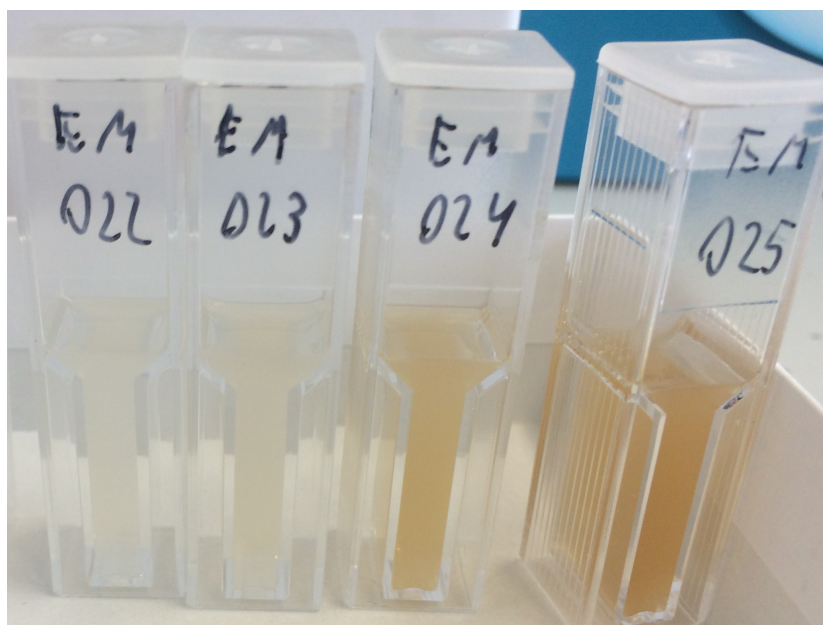


Fig. 30: Nonanoic acid mediated emulsions with 4.9 nm core / 8500 Da PNIPAM coated shell NPs on the day of preparation. CSNP concentration (from left to right): 0.02 mg/mL, 0.1 mg/mL, 0.5 mg/mL and 1.0 mg/mL.

Results of 4.9 nm cores and 30000 Da PNIPAM shell sample are described first. Nonanoic acid was used as dispersed phase. We mainly concentrated on volume-weighted distribution, since number-weighted distribution tend to overshadow the presence of larger entities in the solution by the freely dispersed nanoparticles, while the main focus of investigation is the size-evolution of emulsion droplets. The dominant size found in the volume-weighted size distribution is plotted as function of time in Fig. 31. As expected, 0.02 mg/mL NP concentration was a too low particle concentration to produce stable emulsions in all samples. A clear trend in peak shape and location was never found during the observation period. The next concentration steps were more interesting. At a NP concentration of 0.1 mg/mL we found droplets at a hydrodynamic diameter of around 70 nm continually till the end of the observation period. We found objects with larger size in samples with higher NP concentration, at 0.5 mg/mL NP the droplet diameter was around 90 nm and at 1.0 mg/mL NP 100 nm droplets were primarily found. We can therefore assume that the ideal NP concentration for these settings lies between 0.1 mg/mL and 1.0 mg/mL. However, this stands in contrast to the theory, that with more available particles, smaller droplets can be supported. Vignati and Piazza stated that the formation of monolayer bridges can lower the amount of

particles necessary to back up emulsion maintenance⁶¹, meaning that with a higher, saturated particle concentration the expected behavior would be observable. A bridging formation would not be observable in DLS methods, as it would be undistinguishable from agglomerated particles. Further examination with another method would be necessary. French et al. could observe particle bridging in Pickering emulsions based on silica particle via freeze-fracturing scanning electron microscopy^{78,79}.

We compared these findings with a sample containing the same core size, but a PNIPAM shell of 8500 Da. The dominant peak sizes found via volume weighted-size distribution plotted as a function of time can be found in Fig. 30. At 0.1 mg/mL NP concentration the volume-weighted distribution clearly showed the presence of small and large droplets at the beginning, which meld together around day 14 to droplets with 50 nm in hydrodynamic diameter. In next concentration steps, the particle diameters were found to be mainly between 40 - 80 nm in diameter, however the broad peaks also revealed the presence of larger entities. In contrast to 4.9 nm cores with 30000 Da PNIPAM shell however, CSNPs with 8500 Da shell consistently showed signals for droplet diameters around 200 nm and even higher (in the case of 0.02 and 0.1 mg/mL often exceeding 700 nm). A glimpse in these size distributions can be found in Fig. 33. The merging of these "tails" with the main peak over the 3 weeks of observation period was a visible trend. However the droplet size peaks were never as narrow as in the 30000 Da shell sample. We therefore found the assembly with a 30000 Da PNIPAM shell more favorable.

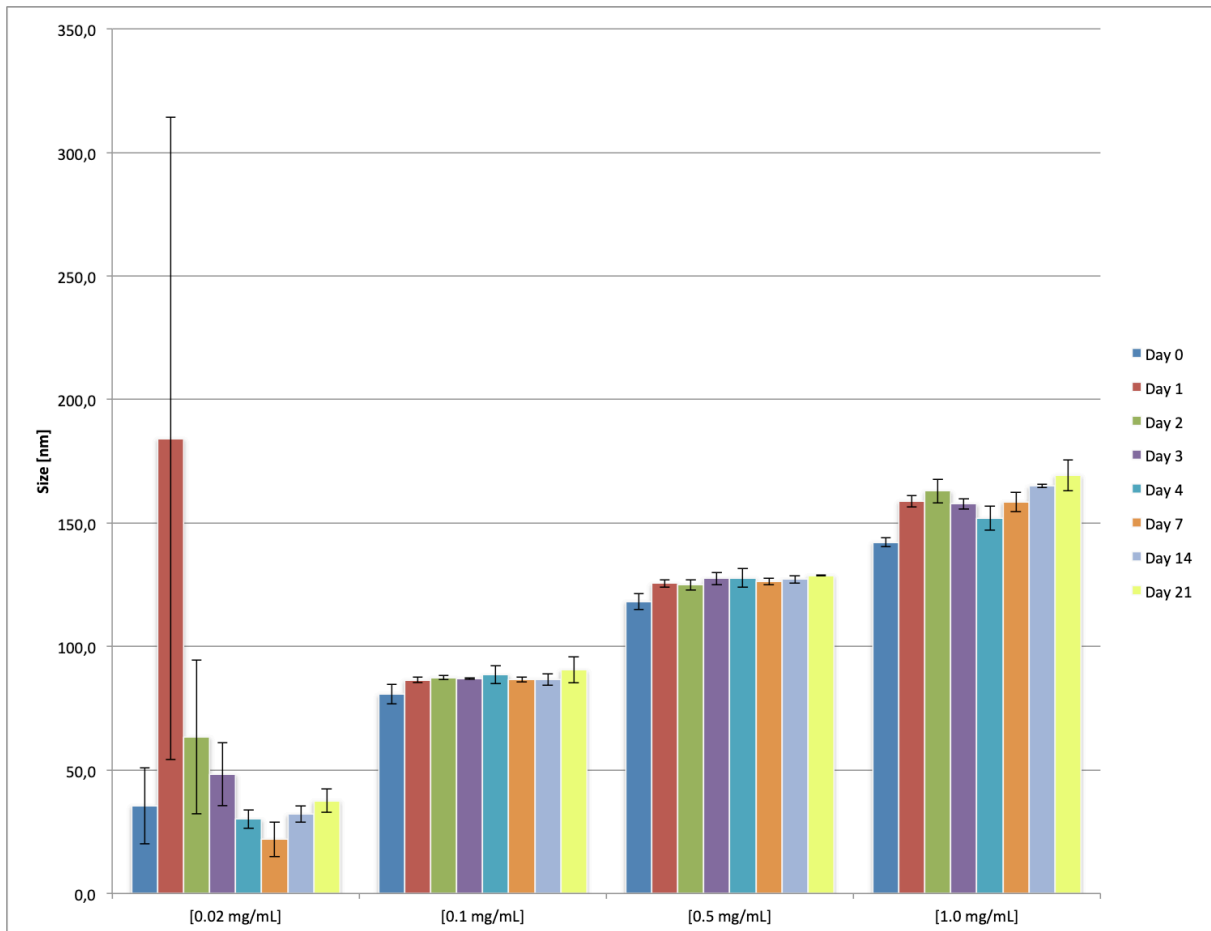


Fig. 31: Nonanoic acid based emulsion with 4.9 nm cores and 30000 Da PNIPAM shell NPs at different concentrations. Volume-weighted size distribution is shown. Interesting is the increase in droplet diameter with higher NP concentrations. A NP concentration of 0.02 mg/mL did not yield reproducible droplet diameters and was therefore deemed too low a concentration to stabilize emulsions with 1% dispersed phase.

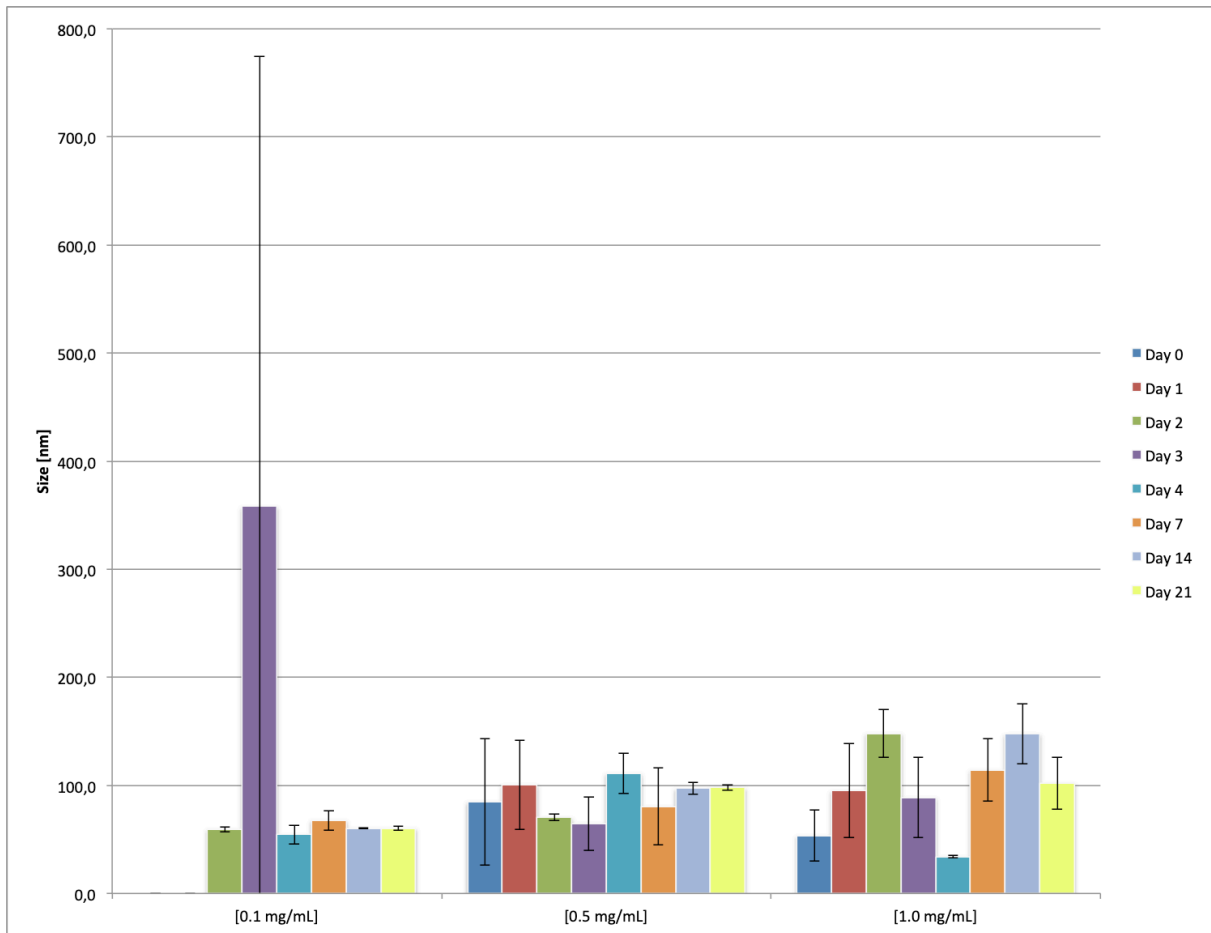


Fig. 32: Nonanoic acid based emulsion with 4.9 nm cores and 8500 Da PNIPAM shell NPs at different concentrations calculated using the volume-weighted size distribution. The values of the lowest concentration NP (0.02 mg/mL) are not shown because no consistency could be found there. Days 0 and 1 of the 0.1 mg/mL CSNP concentration are also not shown, since the respective observed diameters were too large (1162 nm and 1562 nm respectively) and would distort the rest of the figure. The observed hydrodynamic diameters on day 4 of 0.1 mg/mL CSNP concentration signifies, that the emulsion equilibrium was still not reached on that day.

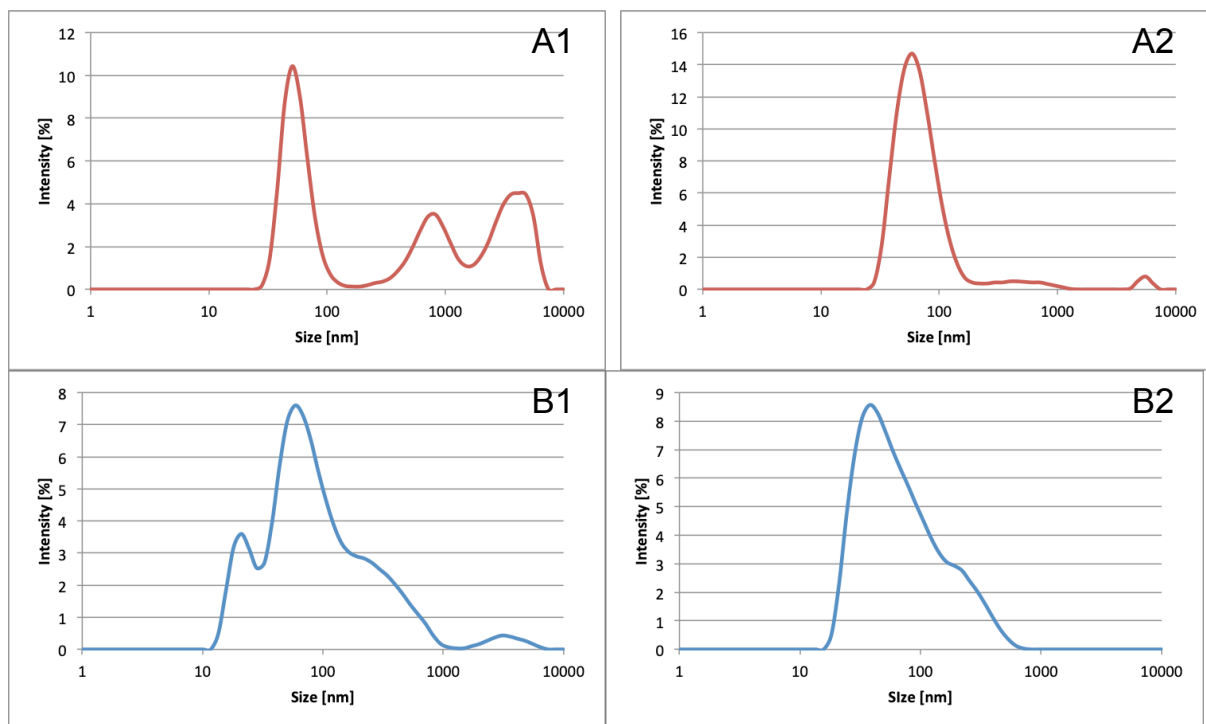


Fig. 33: Volume-weighted size distribution of 4.9 nm cores & 8500 Da PNIPAM shell (GD: 1.26 chains/nm²). CSPN concentrations were 0.1 mg/mL (A) and 0.5 mg/mL (B). Nonanoic acid was used as dispersed phase. On day of preparation (A1 and B1) droplets with large diameters were detected. A week later, these tails merged with the main peak (A2 and B2).

4.3.3. Influence of core size

We observed the effects of core size on the formation of emulsions for both PNIPAM and PIPOx grafted CSNPs. For PNIPAM coated NPs we assembled a sample with similar shell size and grafting density to our previously established sample (4.9 nm core and 30000 Da PNIPAM shell). In the case of PIPOx coated CSNPs, we managed to graft the same polymer batch onto different sized cores, both with reasonable grafting densities.

4.3.3.1. Influence of core size in PNIPAM based emulsions

We assembled 32000 Da PNIPAM chains onto 9.8 nm cores with a grafting density of 0.7 chains/nm². The particle size distribution analysis of this sample was used as a control sample; the volume-weighted size distribution is shown.

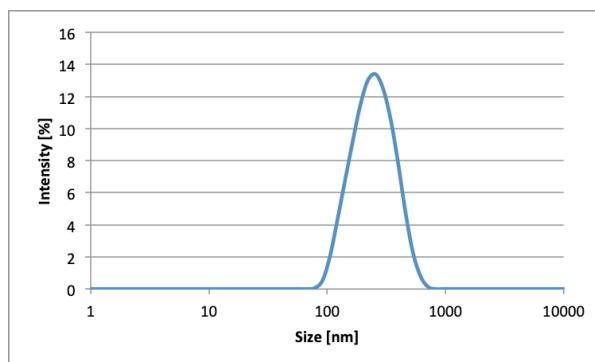


Fig. 34: Control sample of 9.8 nm FeOx core with 32000 Da PNIPAM coating (GD = 0.7). Concentration of the CSNP was set to 1 mg/mL. Size distribution was evaluated via volume-weighted distribution. The peak is located at 220 nm hydrodynamic diameter, which signifies agglomerated NPs.

As previously 10 μ L nonanoic acid was used as dispersed phase. After vortexing, the samples became turbid. After a week of incubation a thin, brown film was visible on top of the samples, which was attributed to CSNP-oil agglomerates, which rose to top due to density gradients.

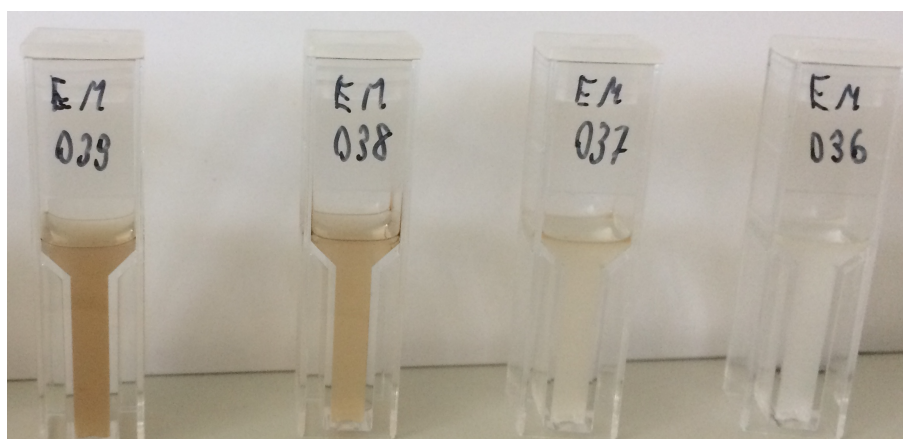


Fig. 35: Emulsion based on 9.8 nm cores & 32000 Da PNIPAM shell (GD: 0.7 chains/nm²) on day of preparation. Nonanoic acid was used as dispersed phase. Concentrations (from left to right): 1.0 mg/mL, 0.5mg/mL , 0.1 mg/mL and 0.02 mg/mL.

An evaluation of 4.9 nm PNIPAM coated cores can be found in Chapter 4.3.2. For our 9.8 nm core with 32000 Da PNIPAM shell sample, we found that after the addition of oil, the droplet size decreased when compared with its control sample (see Fig. 34). This could mean that the NPs leave their agglomerated state in favor of emulsion assembly, as described in the previous chapter. Nevertheless, despite the difference in NP concentration, the results of all samples are very reproducible. With exception of the lowest NP concentration (0.02 mg/mL), droplets with diameters around 70-120 nm were observable in all samples after at least 4 days of incubation, when weighted by volume size

distribution. Unexpectedly, the samples with higher NP concentration yielded larger objects measured by DLS (see Fig. 36).

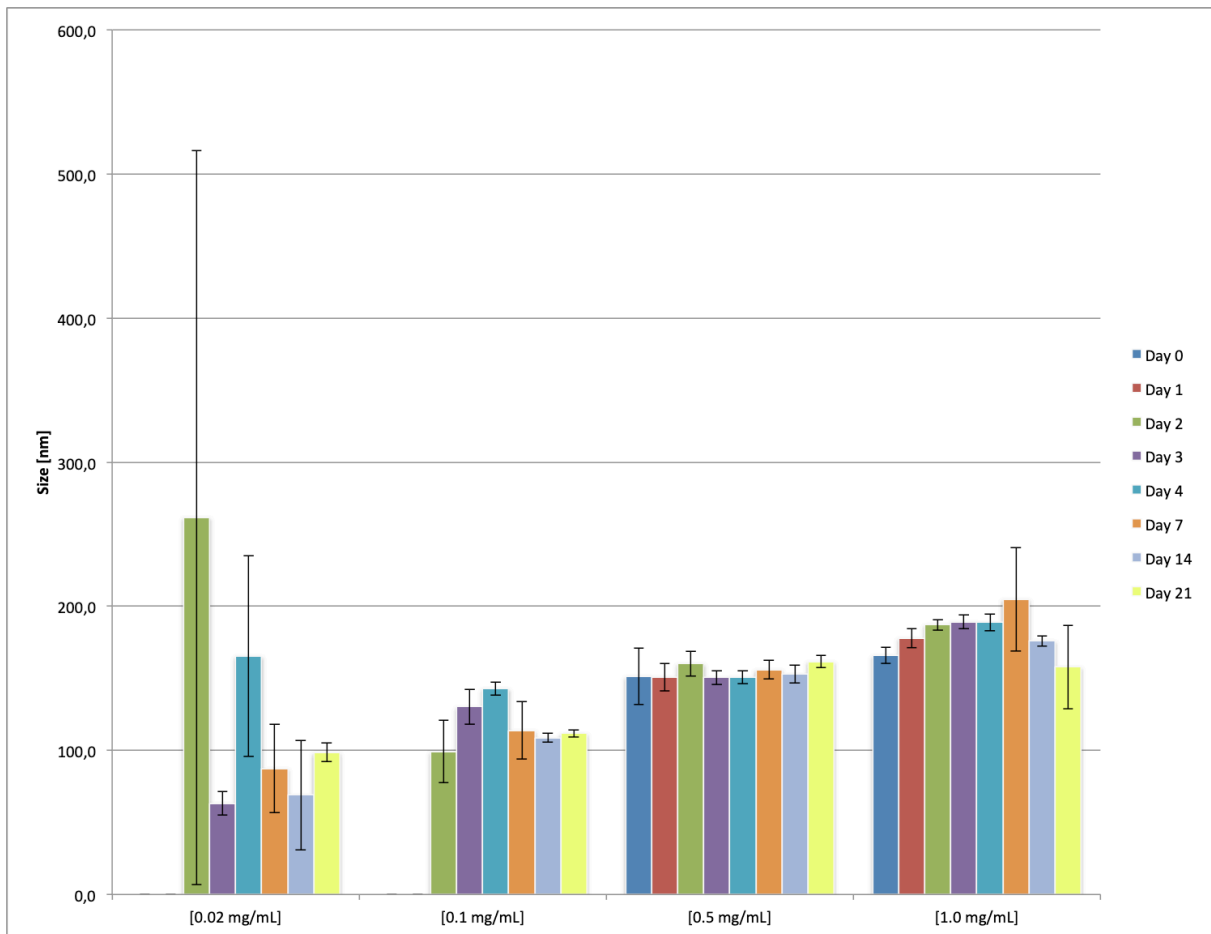


Fig. 36: Nonanoic acid based emulsion with 9.8 nm cores and 32000 Da PNIPAM shell NPs at different concentrations evaluated by volume-weighted size distribution. Values on day 0 and day 1 of 0.02 mg/mL and 0.1 mg/mL NP concentrations were considered as outliers and are therefore not shown. Again an increase in droplet diameter with rising NP concentration is observable (compare Fig. 31).

Both core sizes showed a single peak over the observation period of 3 weeks. While both core sizes yielded reproducible results, the droplet diameters in the 4.9 nm core samples were distributed narrower (compare Fig. 37). We therefore recommend this size for making emulsions with PNIPAM grafted NPs.

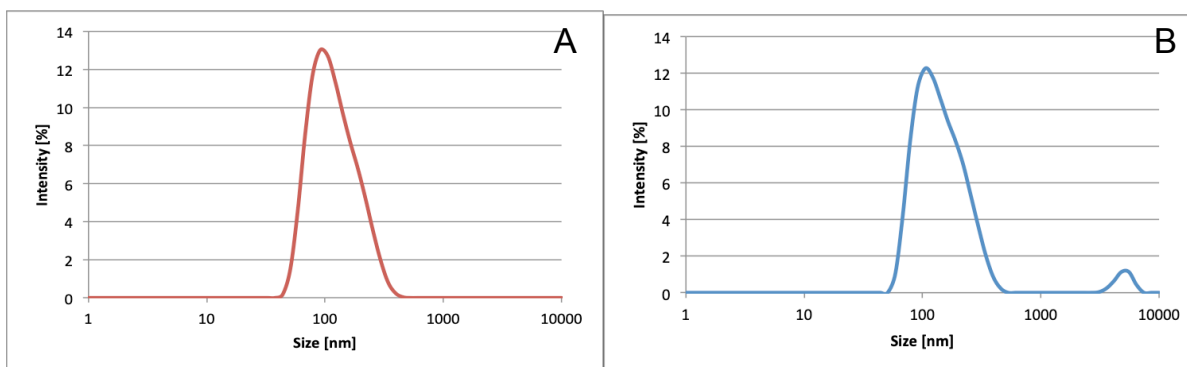


Fig. 37: Nonanoic acid based emulsions evaluated by volume-weighted size distribution. Both have 0.5 mg/mL NP concentration and were incubated 4 days after preparation. (A) 4.9 nm core with 30000 Da PNIPAM (GD = 0.9) is shown; right (B) 9.8 nm core with 32000 Da PNIPAM (GD = 0.7). The 9.8 nm showed a broader size distribution and also a small signal, signifying droplets with diameters over 6000 nm.

4.3.3.2. Influence of core size in PIPOx emulsions

The physicochemical properties of PIPOx are similar to that of PNIPAM. They are both good hydrogen bonding (hydrophilic) and flexible polymers with similar LCST, so we hypothesized similar emulsification behavior. Both nonanoic acid and rapeseed oil were tested as the dispersed oil phase using a concentration of 10 μ L in 1 mL H₂O for nanoparticle concentrations of 1 mg/mL and 5 mg/mL, respectively. We tested this first with 4.9 nm core samples. Since the polymer spacers of the two samples are identical, the effects of the core size on the emulsification process can be investigated. The results of Chapter 4.2.5 were taken as control sample, volume-weighted size distribution is shown.

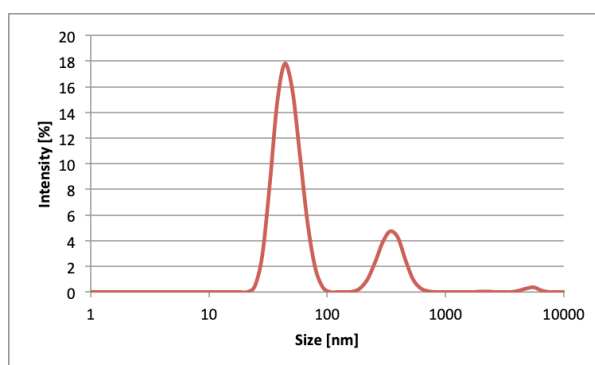


Fig. 38: Control sample of 4.9 nm FeOx core with 13000 Da PNIPAM coating (GD = 0.9). Concentration of the CSNP was set to 1 mg/mL. Size distribution was evaluated via volume-weighted distribution. The larger, first peak is located at 44 nm droplet hydrodynamic diameter and was attributed to dispersed NPs. Some agglomerates with 342 nm diameter were also detectable, as the smaller, second peak.

According to visual investigation the emulsification process seemed successful (see Fig. 39). All samples appeared turbid after preparation. No signs of phase

separation were found over the entire observation period of 3 weeks. Two weeks after preparation, a brown sediment could be found on the bottom of all samples, except for 1 mg/mL NP with nonanoic acid. This layer did not redisperse anymore, even after the container was gently shaken. However, this brownish sedimentation was only minimal.

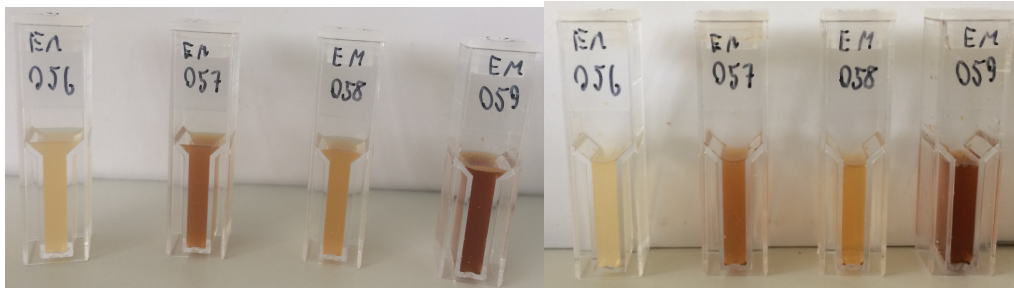


Fig. 39: (left): PIPOx-NP (5 nm core) based emulsions on the day of preparation from left to right: 1 mg/mL NP with nonanoic acid, 5 mg/mL NP with nonanoic acid, 1 mg/mL NP with rapeseed oil and 5 mg/mL NP with rapeseed oil. (right): The same emulsions after 21 days of incubation.

Volume-weighted size distributions were evaluated. In the case of nonanoic acid mediated emulsions the resulting signal peaks were located at 60 nm diameter for 1 mg/mL NP concentration and 40 nm diameter for 5 mg/mL NP concentration respectively (see Fig. 40). This was attributed to free CSNP. These maxima remained constant over the whole observation period, signifying the achievement of an equilibrium state after (or through) initial high-speed vortexing. However, those peaks were very broad (especially for 1 mg/mL NP concentration), meaning that droplets with larger diameters were contained within the samples (compare Fig. 40). The size distribution did not change significantly after 3 weeks of observation. It would be interesting to compare these results to a spontaneous emulsification approach without input of energy through convection or shearing. If the resulting signals would be comparable to our approach after reaching equilibrium, high-speed vortexing could be seen as a way to immensely accelerate the achievement of this condition.

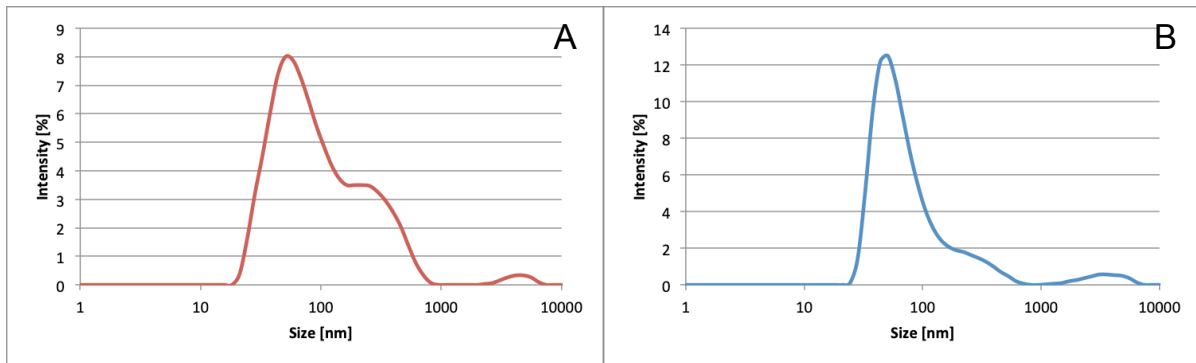


Fig. 40: Nonanoic acid based emulsions evaluated via volume-weighted size distribution 3 days after preparation. NPs 4.9 nm core & 13000 Da PIPOx coating NPs were used to stabilize the system. NP concentration was 1mg/mL (A) and 5 mg/mL (B). Both emulsions contained high amounts of free particles, since both signals peak at low droplet diameters (60 nm and 40 nm respectively). The broad peaks signify the presence of larger droplets, predominantly in the sample 1 mg/mL NP concentration.

In rapeseed oil emulsions we predominately found two peaks in both samples. The first peak represented droplet diameters of 40 nm, attributed to dispersed CSNPs. This peak was significantly larger at NP concentration of 5 mg/mL. The second peak represented emulsion droplets. Their diameter was determined to be 250 nm [c (CSNP) = 1mg/mL] and 400 nm [c (CSNP) = 5mg/mL] respectively. However the peak shape vacillated, meaning an equilibrium state was established in neither sample.

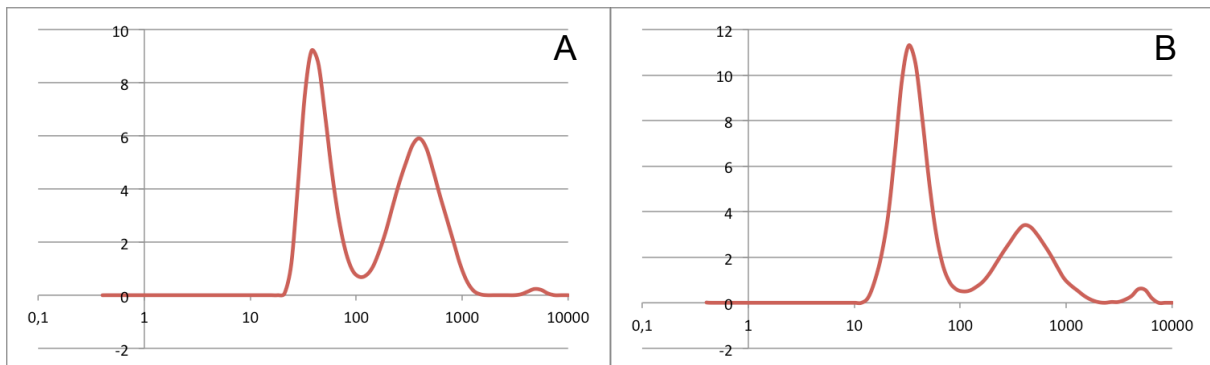


Fig. 41: Rapeseed acid based emulsions evaluated via volume-weighted size distribution 3 days after preparation. NPs 4.9 nm core & 13000 Da PIPOx coating NPs were used to stabilize the system. NP concentration was 1mg/mL (A) and 5 mg/mL (B). The first peaks in each sample were attributed to disperse particles, as it is the same diameter found in the control sample. This means a surplus of particles was contained within the sample. The other peaks signify emulsion droplets; this signal was in (A) higher than in (B).

Fig. 42 plots the predominant sizes found in each sample peaks against time for both concentrations with nonanoic acid and rapeseed oil as dispersed phase respectively.

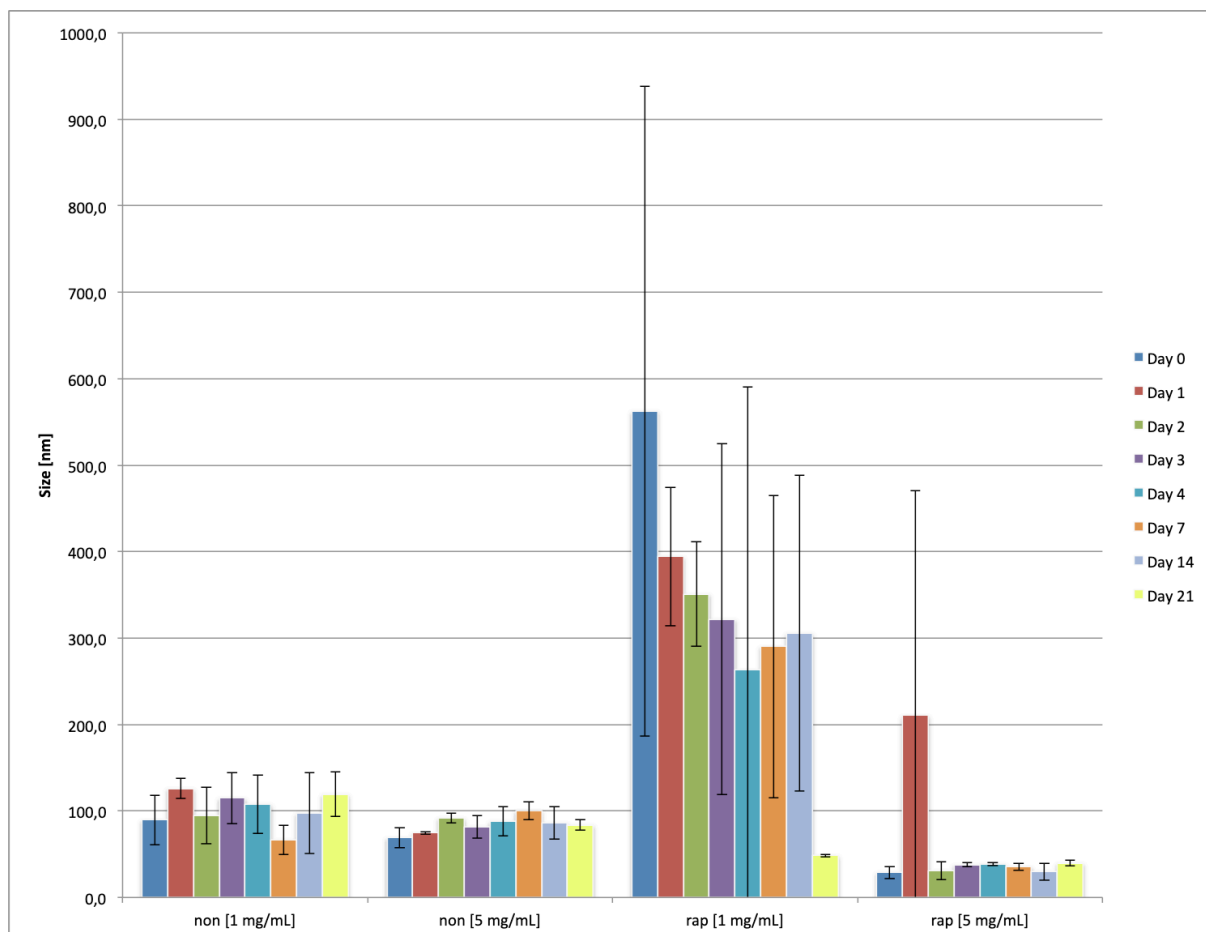


Fig. 42: Volume-weighted size distribution. Nonanoic acid (non) and rapeseed oil (rap) based emulsions were measured. 4.9 nm FeOx core NPs with 13000 Da PIPOx coatings (GD =0.9) were used as stabilizers. CSNP concentrations were 1 mg/mL and 5 mg/mL respectively. With the exception of 1 mg/mL NP with rapeseed oil, the dominant size found in each sample represented dispersed nanoparticles. The dominant size of 1 mg/mL NPs with rapeseed oil was attributed to emulsion droplets, however the average droplet diameters were widely distributed.

As the majority of objects found in the DLS histograms were below 100 nm in size we concluded that our samples contained an excess amount of particles, so a lower concentration of NPs would result in similar emulsion droplet sizes while less dispersed particles remain in solution. We could not yet decide on a single dispersed phase, so we agreed to continue with both nonanoic acid and rapeseed oil as dispersed phase in PIPOx mediated emulsions. The concentration of particles in the solutions was reduced to 0.02, 0.1 and 0.5 mg/mL respectively. We also started experimentation with 10 nm core NPs; a size distribution of pure particles (1 mg/mL) can be seen in Fig. 43. Evaluation of the volume-weighted size distribution revealed the majority of particles were present as agglomerates; a smaller peak at 50 nm hydrodynamic diameter was determined as free particles. A grafting density of 0.8 should normally be

adequate, however an insufficient spacer length to avoid interactions between particles remains a possibility.

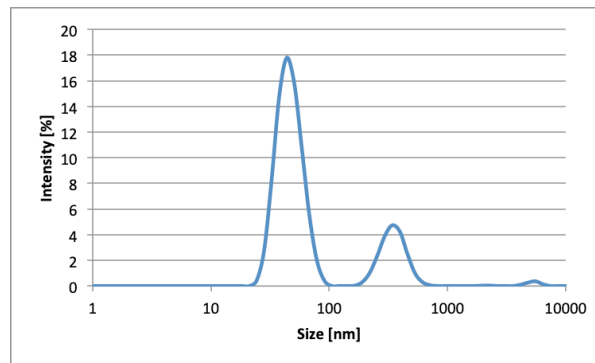


Fig. 43: The control sample of 10 nm core NP with 13000 Da PIPOx (1 mg/mL). Compared to 5 nm core particles, here the majority of particles remained as agglomerates, which is signified by the large peak at 615 nm.

We separate the results of emulsions based on the used dispersed phase, so we can better compare how each core performed with the respective phase. In case of nonanoic acid based emulsions, stabilized with 10 nm core NPs, the lowest concentration (0.02 mg/mL) did not support emulsification (Fig. 44). During the measurement the resulting peaks irreproducibly shifted in size and shape for each measurement. For the volume-weighted size distribution, we consistently found bodies at a hydrodynamic diameter range of 90 – 100 nm for 0.1 mg/mL NP concentration, as well as larger droplet diameters at around 600 nm diameters. Those peaks merged together to a diameter of 90 nm after 2 weeks of incubation. Droplet diameters of 190– 220 nm (according to signal maxima of volume-weighted size distribution) for a NP concentration of 0.5 mg/mL were found (Fig. 44). However, the respective peaks remained broadly distributed. Additionally, in 0.1 mg/ml and 05 mg/mL concentrations large entities (over 1000 nm diameter) were found in the first observation week. We attributed these to large emulsion droplets, which split up into smaller ones over the course of the first week.

We had similar trends in increasing droplet sizes with higher NP concentration samples with PNIPAM-CSNP stabilized emulsions (see Chapter 4.3.2). However, a bridging effect would mean that a saturated particle concentration was not yet reached. Considering the previous experiments, where we reached an excess amount of particles with higher NP concentrations, we have already increased the concentration beyond the particle concentration

necessary for total interfacial area coverage. This would mean that a shrinking droplet size with rising particle concentration would only be observable in a very small particle concentration frame, between 0.5 mg/mL and 1.0 mg/mL CSNPs. This does not follow the theory for monolayer bridging of emulsion droplets. Nevertheless, examination of bridging formation remains an interesting consideration.

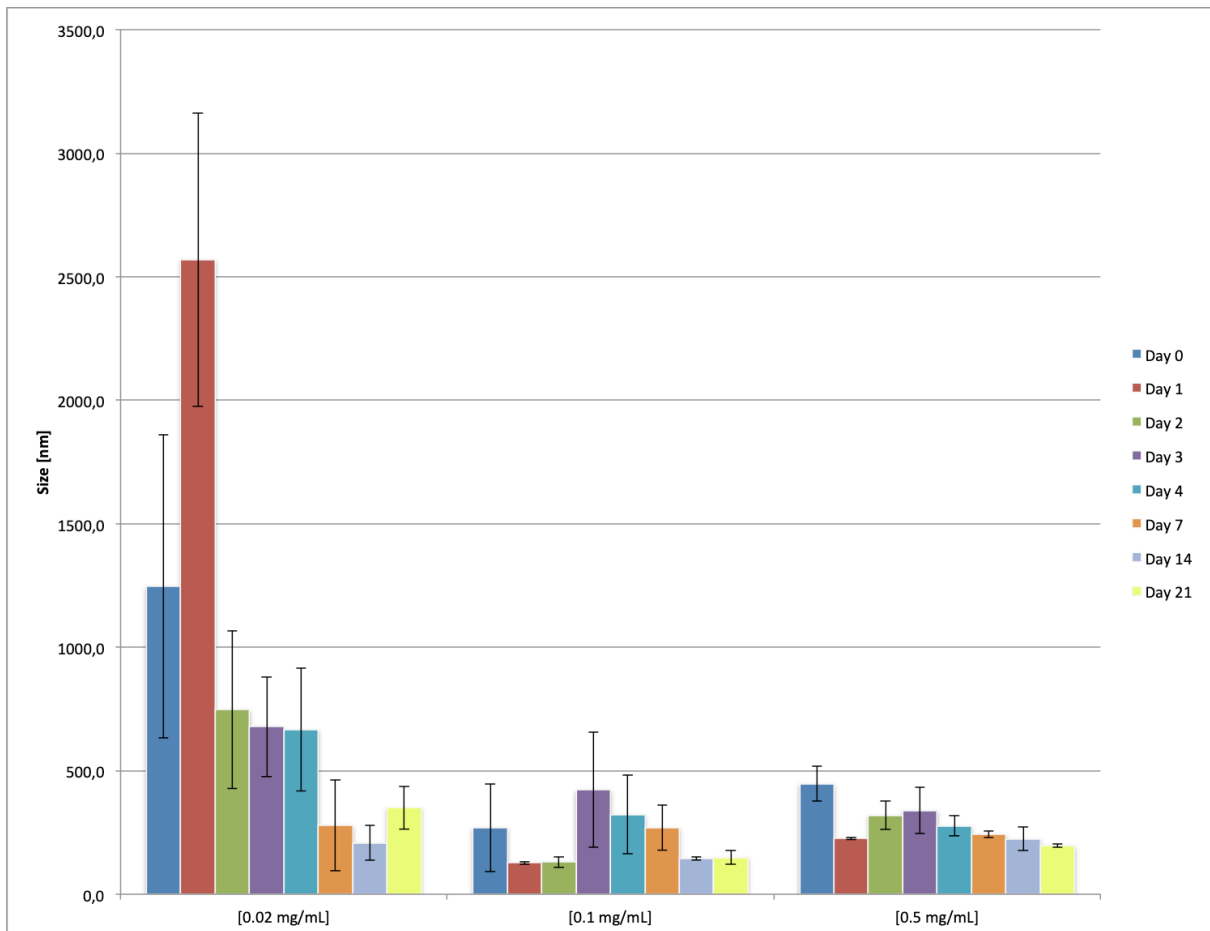


Fig. 44: Peak maxima of 10 nm core NP with 13000 PIPOx in different concentrations evaluated by volume-weighted size distribution. 10 μ L nonanoic acid was used as dispersed phase respective. Day 1 of 0.02 mg/mL shows a droplet diameter of 2500 nm; we hypothesized that the phase separation was not yet complete in this sample. Droplet diameters at a concentration of 0.5 mg/mL remained the most stable during the observation time. Each dataset showed multiple peaks, here only the maxima of the peaks with the largest area respectively are shown.

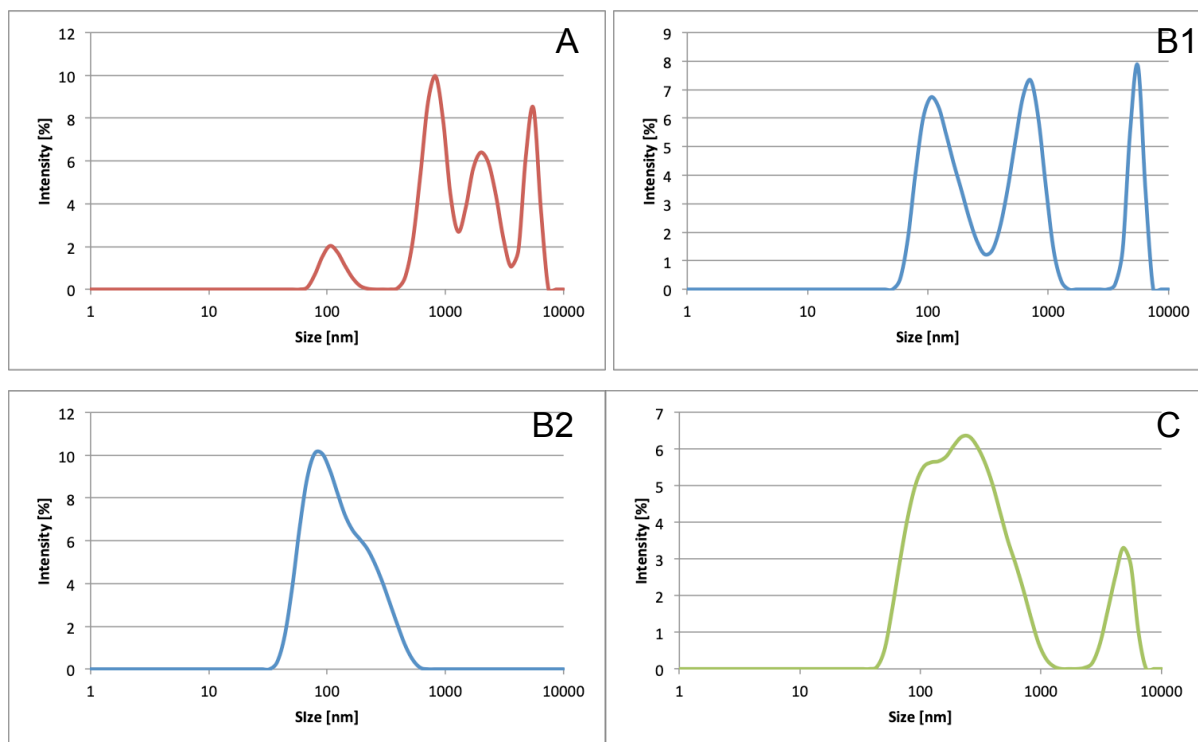


Fig. 45: Emulsions with 10 μ L nonanoic acid as dispersed phase. Volume-weighted size distributions are shown. 9.8 nm CSNP with 13000 DA PIPOx coating in different concentrations were used as stabilizers.

(A): 0.02 mg/mL NPs were too low a concentration to stabilize the emulsion. The example shown here was not reproducible.

(B): 0.1 mg/mL NPs 0 days (B1) and 14 days (B2) after preparation. The peaks signifying large droplet diameters in (B1) decreased over time until they were not detectable after 2 weeks (B2).

(C): 0.5 mg/mL NPs 3 days after preparation. The broad peak was visible over 3 weeks only shifting minimal in size.

Compared to the previous sample (10 nm cores, same polymer shell), the 5 nm core sample accomplished a stable emulsion with a NP concentration of 0.02 mg/mL (see Fig. 46). This is in sync with theory, since the amount of particles is higher in sample with smaller cores compared to the same weight concentration of larger core particles. This means less sample is needed to provide stable emulsification. The following results were evaluated by volume-weighted size distribution. The dataset showed two very well separated size peaks on the first day (see Fig. 47A). During the observation period, the two peaks became more similar in size until they finally merged on day 21 (droplet diameter 340 nm). For higher concentrations a similar behavior was observed. Multiple peaks were visible at the beginning, which converged over time and merged around day 14 with an average size of 220 nm (0.1 mg/mL, Fig. 47B) and 100 nm (0.5 mg/mL, Fig. 47C). This implies a rather long equilibration phase of around 1-2 weeks. However, literature gives examples of where the

Philipp Fabian - February 25, 2019

equilibrium droplet size was controllable via the amount of available particles.⁶⁰
 The droplet size increased at the beginning of week 3.

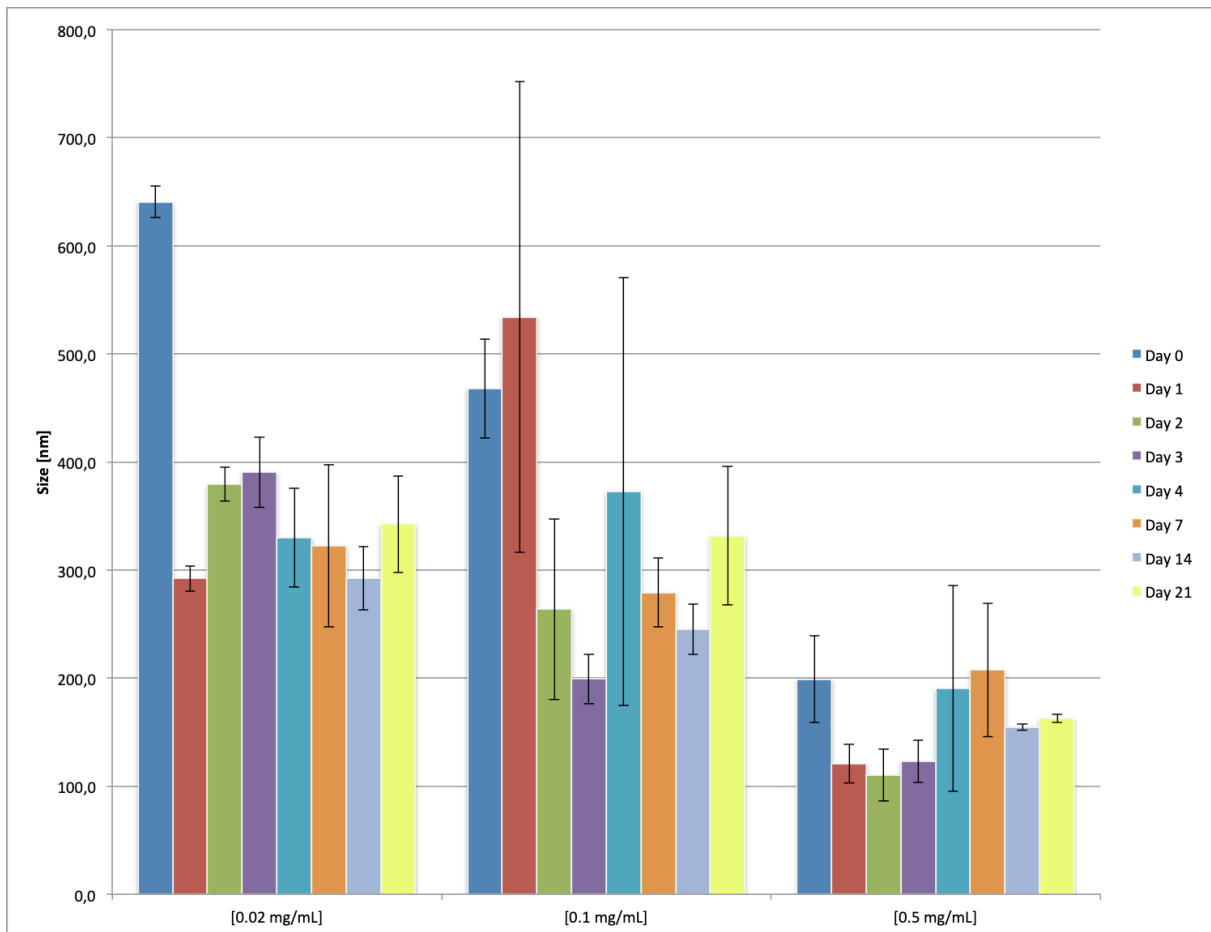
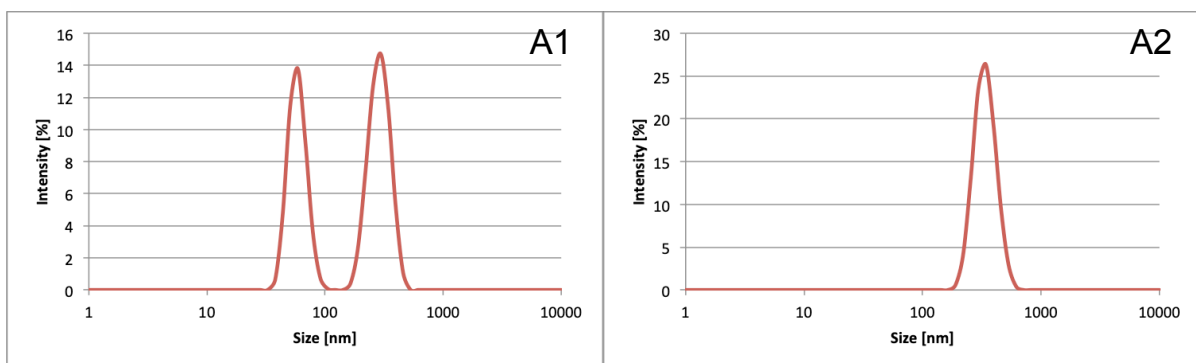


Fig. 46: Size of nonanoic acid based emulsions. 5 nm cores with 13000 Da PIPOx NP in different concentrations were used to stabilize the emulsions. Signals were calculated via volume-weighted size distribution. The droplet sizes varied strongly during the first week, after equilibration the droplet sizes thereafter remained relatively uniform.



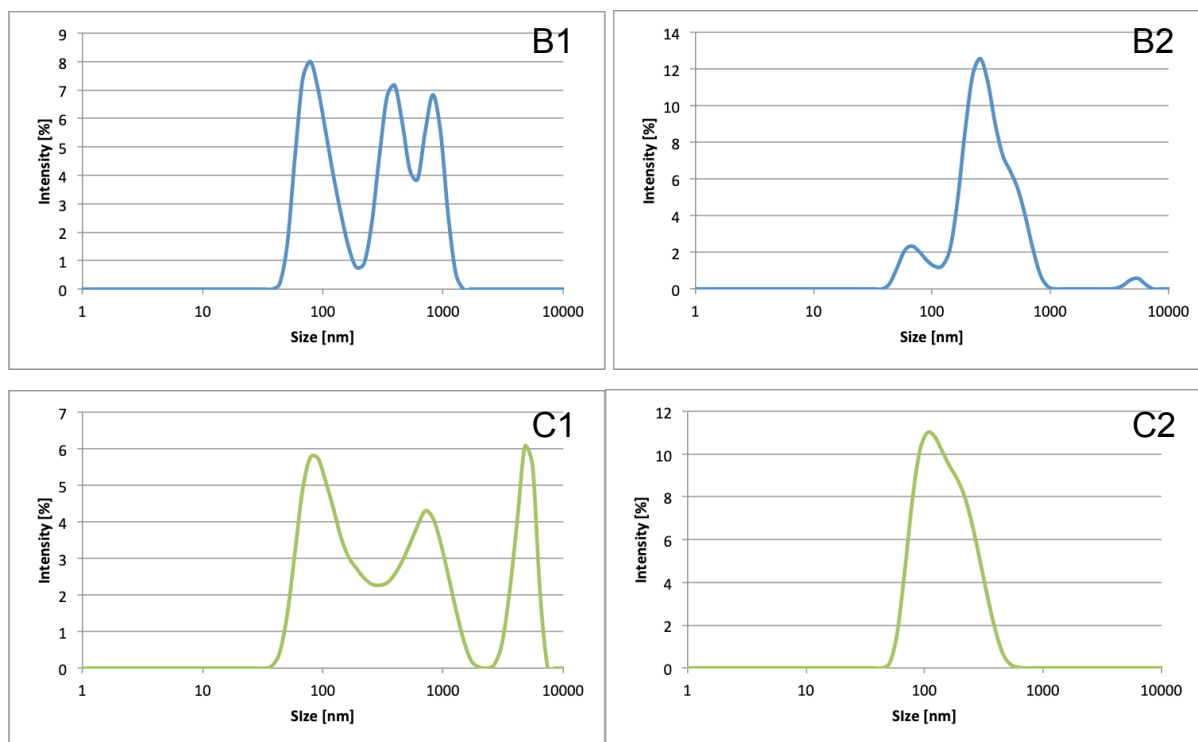


Fig. 47: Emulsions with 10 μL nonanoic acid as dispersed phase. Volume-weighted size distributions on day 1 (left) and days 21 (right) are shown. 9.8 nm CSNP with 13000 DA PIPOx coating in different concentrations were used as stabilizers. All samples shared a common behavior: multiple peaks were detectable between day of preparation and week 2, before finally merging on day 21.

(A): 0.02 mg/mL NP concentration yielded two separate peaks with 60 nm and 295 nm diameter respectively (A1), which merged together at day 21 (A2).

(B): 0.1 mg/mL NP concentration showed multiple peaks as well, however they were not as uniform as with 0.02 mg/mL NP concentration. The final peak shown signifies a droplet diameter of 255 nm.

(C): 0.5 mg/mL NP concentration also showed two peaks as (90 nm and 400 nm), as well as a third peak signifying large droplets over 1000 nm in diameter. This peak slowly decreased over time; all peaks merged together after 21 days (C2).

For nonanoic acid as dispersed phase, samples with 4.9 nm cores seemed to provide the most reliable CSNP emulsifier, as we could observe similar behaviors in droplet diameter transition between the different NP concentrations throughout our concentration range.

Unfortunately, we did not find this level of consistency in rapeseed oil based emulsions. The rapeseed oil based emulsions did not yield a trend in terms of droplet size as function of time. Objects of different size were detectable, but the objects, presumably droplets, varied significantly in size over the observation period. Thus, nonanoic acid was the better option for emulsification with uniform droplet size also for PIPOx-grafted NPs. Rapeseed oil is therefore unsuitable for controlling the droplet size of CSNP stabilized emulsions, a critical feat required as a drug delivery vehicle¹⁹.

5. Conclusion

Over the course of the thesis four different polymers were synthesized and two of them were successfully attached to FeOx-NPs at a reasonable grafting density of at least 0.7 chains per nm² surface. We successfully synthesized PNIPAM via ATRP and POX via ROP; low PDI values below 1.7 suggest the conditions for living polymerization were met. For ROP however we are still short on a certain explanation, why we needed significantly more initiator for the aimed chain lengths than theoretically required. Nevertheless, the obtained polymers possessed a desirable molecular weight (up to 40000 Da), as proven by GPC, and could be produced to a yield of up to 1.9 g. Additionally, the modified catechol derivate NDA was successfully synthesized (yield: 8.15 g) and all polymers were functionalized with this molecule, which was confirmed via ¹H-NMR. Usually we reached a grade of functionalization of 50% or more, yielding usually 1.2 g NDA-functionalized polymer. We managed to graft NDA-functionalized PNIPAM, PMOx, PEOx and PIPOx chains onto 4.9 nm and 9.8 nm Fe₃O₄ nanoparticles respectively, to assemble different polymer-functionalized, thermoresponsive CSNPs. A major drawback remained the often times lackluster grafting densities of most samples due to the grafting-to approach. Only for PNIPAM and PIPOx reasonable grafting densities above 0.7 chains/nm² were obtained.

We could verify the emulsion stabilizing abilities of polymer brush grafted FeOx-CSNP over a time span of at least three weeks. DLS measurements showed significant differences in colloid sizes between pure NP dispersions and oil containing samples. The change in sample turbidity was an important visual clue, supporting that emulsification was observed. Three different oils (Novec 7500™, nonanoic acid and rapeseed oil) were tested for CSNP-assisted emulsification. Emulsification was most successful using the two fatty acid based oils that have a low interfacial tension with water. Nonanoic acid, possibly due to its uniform composition and higher purity, produced the most monodisperse and stable oil-in-water emulsions with CSNPs. Rapeseed oil did

not yield the uniform droplet sizes we desired and was usually not as reproducible as nonanoic acid, while Novec 7500TM did not emulsify.

We also tested multiple Fe₃O₄ cores, 4.9 nm and 9.8 nm respectively, and found the smaller core to produce more reproducible emulsions regardless of polymer used for the grafting.

We have proven that droplet diameters were adjustable with varying NP concentration for both coatings, however droplet diameters using PNIPAM grafted NPs increased with NP concentration, while the hydrodynamic diameter recorded for PIPOx-CSNP stabilized emulsions decreased with increasing NP concentration. Average droplet diameters in PNIPAM grafted CSNP stabilized emulsion were between 80 nm and 150 nm, which are very small for emulsion droplets. PIPOx mediated emulsions underwent a stabilizing phase of 2-3 weeks before ending as droplets 100 nm to 300 nm in diameter, depending on the used NP concentration. Having observed a larger range of droplet diameters possible to tune, we find PIPOx mediated emulsions to be better tunable via shifts in particle concentration.

We recommend 0.1 to 0.5 mg/mL NP concentration with 1% dispersed oil phase for emulsification purposes, as we could form stable, size-tunable emulsions without an excess of dispersed leftover particles in this concentration range of core-shell nanoparticles. For polymer shell size we found an increase in droplet diameter with larger polymer shells. However, we only looked at two samples with different PNIPAM shells, so we cannot conclude on a solid basis over its influence on emulsion formation. A higher sample variety for this parameter is strongly recommended.

In terms of overall performance, we favored emulsions stabilized with PIPOx grafted nanoparticles, due to a better control over droplet diameter sizes, however the small sample size renders this recommendation uncertain.

6. Outlook

Altogether over 70 different emulsions have been observed via DLS over several weeks during this project, varying in CSNP composition and content, yet we can only hypothesize over the influence of most parameters that can be used to control the emulsification. To support our theories, we propose to examine our findings with additional analysis methods, including transmission electron microscopy, small angle x-ray scattering and contact angle measurements on particles on the interfacial area of emulsions. Another recommendation would be to investigate potential dissolution of dispersed phase during the observation period. We are still curious about the observed droplet growth with rising NP concentration in PNIPAM grafted NP stabilized emulsions, so further investigations into this behavior are recommended. Bridging of droplets by nanoparticles remains a possible explanation for this behavior; it was observed directly by French et al. via freeze-fracture scanning electron microscopy in silica particle based Pickering emulsions^{78,79}.

Even though we synthesized CSNPs with different core and shell sizes, as well as polymer compositions and dispersed (oil) phases in our samples, we addressed only a small spectrum of all possibilities. Firstly, we could add more variety in our investigated parameters, especially in shell thickness and composition. After all, the findings represented in this thesis on these subjects are not significant enough to draw definite conclusions; only trends could be suggested. On the other hand, we could expand on the already existing parameters to include new ones, for example changing the oil-to-water ratio of the emulsions. Last but not least, investigations in shell size and NP concentrations are also recommended for PMOx- and especially PEOx-CSNP stabilized emulsions.

7. References

1. Buzea C, Pacheco II, Robbie K. Nanomaterials and nanoparticles: Sources and toxicity. *Biointerphases*. 2007;2(4):MR17-MR71. doi:10.1116/1.2815690
2. Piella J, Bastús NG, Casals E, Puntès V. Characterizing Nanoparticles Reactivity: Structure-Photocatalytic Activity Relationship. *J Phys Conf Ser*. 2013;429:012040. doi:10.1088/1742-6596/429/1/012040
3. Viñes F, Gomes JRB, Illas F. Understanding the reactivity of metallic nanoparticles: beyond the extended surface model for catalysis. *Chem Soc Rev*. 2014;43(14):4922-4939. doi:10.1039/C3CS60421G
4. Khan I, Saeed K, Khan I. Nanoparticles: Properties, applications and toxicities. *Arab J Chem*. May 2017. doi:10.1016/J.ARABJC.2017.05.011
5. Valdiglesias V, Kiliç G, Costa C, et al. Effects of iron oxide nanoparticles: Cytotoxicity, genotoxicity, developmental toxicity, and neurotoxicity. *Environ Mol Mutagen*. 2015;56(2):125-148. doi:10.1002/em.21909
6. Strehl C, Maurizi L, Gaber T, et al. Modification of the surface of superparamagnetic iron oxide nanoparticles to enable their safe application in humans. *Int J Nanomedicine*. 2016;11:5883-5896. doi:10.2147/IJN.S110579
7. Kievit FM, Zhang M. Surface Engineering of Iron Oxide Nanoparticles for Targeted Cancer Therapy. *Acc Chem Res*. 2011;44(10):853-862. doi:10.1021/ar2000277
8. Santhosh PB, Ulrich NP. Multifunctional superparamagnetic iron oxide nanoparticles: Promising tools in cancer theranostics. *Cancer Lett*. 2013;336(1):8-17. doi:10.1016/j.canlet.2013.04.032
9. Heredia KL, Tolstyka ZP, Maynard HD. Aminoxy End-Functionalized Polymers Synthesized by ATRP for Chemoselective Conjugation to Proteins. *Macromolecules*. 2007;40(14):4772-4779. doi:10.1021/ma070432v
10. Caruso F. Nanoengineering of Particle Surfaces. *Adv Mater*. 2001;13(1):11-22. doi:10.1002/1521-4095(200101)13:1<11::AID-ADMA11>3.0.CO;2-N
11. Brittain WJ, Minko S, Brittain W. HIGHLIGHT A Structural Definition of Polymer Brushes. *J Polym Sci Part A Polym Chem*. 2007;45:3505-3512. doi:10.1002/pola.22180
12. Yang W, Zhou F. Polymer brushes for antibiofouling and lubrication. *Biosurface and Biotribology*. 2017;3(3):97-114. doi:10.1016/J.BSBT.2017.10.001
13. Ayres N. Polymer brushes: Applications in biomaterials and nanotechnology. *Polym*

- Chem.* 2010;1(6):769-777. doi:10.1039/B9PY00246D
14. Chen T, Amin I, Jordan R. Patterned polymer brushes. *Chem Soc Rev.* 2012;41(8):3280. doi:10.1039/c2cs15225h
 15. Ghosh Chaudhuri R, Paria S. Core/Shell Nanoparticles: Classes, Properties, Synthesis Mechanisms, Characterization, and Applications. *Chem Rev.* 2012;112(4):2373-2433. doi:10.1021/cr100449n
 16. Mahmoudi M, Sant S, Wang B, Laurent S, Sen T. Superparamagnetic iron oxide nanoparticles (SPIONs): Development, surface modification and applications in chemotherapy. *Adv Drug Deliv Rev.* 2011;63(1-2):24-46. doi:10.1016/j.addr.2010.05.006
 17. Reimhult E. Nanoparticle-triggered release from lipid membrane vesicles. *N Biotechnol.* 2015;32(6):665-672. doi:10.1016/j.nbt.2014.12.002
 18. Stark DD, Weissleder R, Elizondo G, et al. Superparamagnetic iron oxide: clinical application as a contrast agent for MR imaging of the liver. *Radiology.* 1988;168(2):297-301. doi:10.1148/radiology.168.2.3393649
 19. Veisoh O, Gunn JW, Zhang M. Design and fabrication of magnetic nanoparticles for targeted drug delivery and imaging. *Adv Drug Deliv Rev.* 2010;62(3):284-304. doi:10.1016/J.ADDR.2009.11.002
 20. Amstad E, Zurcher S, Mashaghi A, Wong JY, Textor M, Reimhult E. Surface Functionalization of Single Superparamagnetic Iron Oxide Nanoparticles for Targeted Magnetic Resonance Imaging. *Small.* 2009;5(11):1334-1342. doi:10.1002/smll.200801328
 21. Amstad E, Gillich T, Bilecka I, Textor M, Reimhult E. Ultrastable Iron Oxide Nanoparticle Colloidal Suspensions Using Dispersants with Catechol-Derived Anchor Groups. *Nano Lett.* 2009;9(12):4042-4048. doi:10.1021/nl902212q
 22. Bixner O, Lassenberger A, Baurecht D, Reimhult E. Complete Exchange of the Hydrophobic Dispersant Shell on Monodisperse Superparamagnetic Iron Oxide Nanoparticles. *Langmuir.* 2015;31(33):9198-9204. doi:10.1021/acs.langmuir.5b01833
 23. Roy I, Gupta MN. Smart Polymeric Materials: Emerging Biochemical Applications. *Chem Biol.* 2003;10(12):1161-1171. doi:10.1016/J.CHEMBIOL.2003.12.004
 24. Galaev IY, Mattiasson B. 'Smart' polymers and what they could do in biotechnology and medicine. *Trends Biotechnol.* 1999;17(8):335-340. doi:10.1016/S0167-7799(99)01345-1
 25. Kraynov A, Müller TE. *Concepts for the Stabilization of Metal Nanoparticles in Ionic Liquids.* www.intechopen.com. Accessed January 23, 2019.
 26. Kurzhals S, Gal N, Zirbs R, Reimhult E. *Aggregation of Thermoresponsive Core-Shell Nanoparticles: Influence of Particle Concentration, Dispersant Molecular Weight and*

- Grafting*. Vol 500. Elsevier Inc.; 2017. doi:10.1016/j.jcis.2017.04.007
27. Heskins M, Guillet JE. Solution Properties of Poly(N-isopropylacrylamide). *J Macromol Sci Part A - Chem*. 1968;2(8):1441-1455. doi:10.1080/10601326808051910
 28. Kunugi S, Tada T, Tanaka N, Yamamoto K, Akashi M. Microcalorimetric Study of Aqueous Solution of a Thermoresponsive Polymer, poly(N-vinylisobutyramide) (PNVIBA). *Polym J*. 2002;34(5):383-388. doi:10.1295/polymj.34.383
 29. Diab C, Akiyama Y, Kataoka K, Winnik FM. Microcalorimetric Study of the Temperature-Induced Phase Separation in Aqueous Solutions of Poly(2-isopropyl-2-oxazolines). *Macromolecules*. 2004;37(7):2556-2562. doi:10.1021/ma0358733
 30. Qiu X, Koga T, Tanaka F, Winnik FM. New insights into the effects of molecular weight and end group on the temperature-induced phase transition of poly(N-isopropylacrylamide) in water. *Sci China Chem*. 2013;56(1):56-64. doi:10.1007/s11426-012-4781-9
 31. Elloumi-Hannachi I, Yamato M, Okano T. Cell sheet engineering: a unique nanotechnology for scaffold-free tissue reconstruction with clinical applications in regenerative medicine. *J Intern Med*. 2010;267(1):54-70. doi:10.1111/j.1365-2796.2009.02185.x
 32. Cooperstein MA, Canavan HE. Assessment of cytotoxicity of (N-isopropyl acrylamide) and poly(N-isopropyl acrylamide)-coated surfaces. *Biointerphases*. 2013;8(1):19. doi:10.1186/1559-4106-8-19
 33. SZWARC M. 'Living' Polymers. *Nature*. 1956;178(4543):1168-1169. doi:10.1038/1781168a0
 34. Matyjaszewski K. Controlled radical polymerization. *Curr Opin Solid State Mater Sci*. 1996;1(6):769-776. doi:10.1016/S1359-0286(96)80101-X
 35. and KM, Xia J. Atom Transfer Radical Polymerization. 2001. doi:10.1021/CR940534G
 36. Matyjaszewski K, Jakubowski W, Min K, et al. Diminishing catalyst concentration in atom transfer radical polymerization with reducing agents. *Proc Natl Acad Sci U S A*. 2006;103(42):15309-15314. doi:10.1073/pnas.0602675103
 37. Kurzhals S, Gal N, Zirbs R, Reimhult E. *Controlled Aggregation and Cell Uptake of Thermoresponsive Polyoxazoline-Grafted Superparamagnetic Iron Oxide Nanoparticles*. Vol 9.; 2017. doi:10.1039/c6nr08654c
 38. Tomalia DA, Sheetz DP. Homopolymerization of 2-alkyl- and 2-aryl-2-oxazolines. *J Polym Sci Part A-1 Polym Chem*. 1966;4(9):2253-2265. doi:10.1002/pol.1966.150040919
 39. Seeliger W, Aufderhaar E, Diepers W, et al. Recent Syntheses and Reactions of Cyclic Imidic Esters. *Angew Chemie Int Ed English*. 1966;5(10):875-888. doi:10.1002/anie.196608751

40. Kagiya T, Narisawa S, Maeda T, Fukui K. Ring-opening polymerization of 2-substituted 2-oxazolines. *J Polym Sci Part B Polym Lett*. 1966;4(7):441-445. doi:10.1002/pol.1966.110040701
41. Bassiri TG, Levy A, Litt M. Polymerization of cyclic imino ethers. I. Oxazolines. *J Polym Sci Part B Polym Lett*. 1967;5(9):871-879. doi:10.1002/pol.1967.110050927
42. Saegusa T, Yamada A, Kobayashi S. Preparation of Poly(butadiene-g-N-acetyleneimine) and Its Hydrolysis to Poly(butadiene-g-ethyleneimine). *Polym J*. 1979;11(1):53-58. doi:10.1295/polymj.11.53
43. Kobayashi S, Mizutani T, Saegusa T. Polymer synthesis based on 2-(hydroxyphenyl)-2-oxazolines. *Die Makromol Chemie*. 1984;185(3):441-451. doi:10.1002/macp.1984.021850302
44. Sedlacek O, Monnery BD, Filippov SK, Hoogenboom R, Hruby M. Poly(2-Oxazoline)s - Are They More Advantageous for Biomedical Applications Than Other Polymers? *Macromol Rapid Commun*. 2012;33(19):1648-1662. doi:10.1002/marc.201200453
45. Weber C, Hoogenboom R, Schubert US. Temperature responsive bio-compatible polymers based on poly(ethylene oxide) and poly(2-oxazoline)s. *Prog Polym Sci*. 2012;37(5):686-714. doi:10.1016/J.PROGPOLYMSCI.2011.10.002
46. Schlaad H, Hoogenboom R. Poly(2-oxazoline)s and Related Pseudo-Polypeptides. *Macromol Rapid Commun*. 2012;33(19):1599-1599. doi:10.1002/marc.201200571
47. Frank Wiesbrock, Richard Hoogenboom, Mark A. M. Leenen, Michael A. R. Meier and, Schubert* US. Investigation of the Living Cationic Ring-Opening Polymerization of 2-Methyl-, 2-Ethyl-, 2-Nonyl-, and 2-Phenyl-2-oxazoline in a Single-Mode Microwave Reactor†. 2005. doi:10.1021/MA0474170
48. Hoogenboom R, Paulus RM, Fijten MWM, Schubert US. Concentration Effects in the Cationic Ring-Opening Polymerization of 2-Ethyl-2-Oxazoline in N,N-Dimethylacetamide. *J Polym Sci Part A Polym Chem*. 2005;43:1487-1497. doi:10.1002/pola.20603
49. Monnery BD, Shaunak S, Thanou M, Steinke JHG. Improved Synthesis of Linear Poly(ethylenimine) via Low-Temperature Polymerization of 2-Isopropyl-2-oxazoline in Chlorobenzene. *Macromolecules*. 2015;48(10):3197-3206. doi:10.1021/acs.macromol.5b00437
50. Einzmann M, Binder WH. *Novel Functional Initiators for Oxazoline Polymerization.*; 2001. <https://onlinelibrary.wiley.com/doi/pdf/10.1002/pola.1262>. Accessed August 17, 2018.
51. Ramsden W. Separation of Solids in the Surface-Layers of Solutions and "Suspensions" (Observations on Surface-Membranes, Bubbles, Emulsions, and Mechanical Coagulation). -- Preliminary Account. *Proc R Soc London*. 1903;72(477-

- 486):156-164. doi:10.1098/rspl.1903.0034
52. Pickering SU. CXCVI.—Emulsions. *J Chem Soc, Trans.* 1907;91(0):2001-2021. doi:10.1039/CT9079102001
 53. Pieranski P. Two-Dimensional Interfacial Colloidal Crystals. *Phys Rev Lett.* 1980;45(7):569-572. doi:10.1103/PhysRevLett.45.569
 54. Yang Y, Fang Z, Chen X, et al. An Overview of Pickering Emulsions: Solid-Particle Materials, Classification, Morphology, and Applications. *Front Pharmacol.* 2017;8:287. doi:10.3389/fphar.2017.00287
 55. and BPB, Lumsdon SO. Influence of Particle Wettability on the Type and Stability of Surfactant-Free Emulsions†. 2000. doi:10.1021/LA000189S
 56. Chevalier Y, Bolzinger MA. *Emulsions Stabilized with Solid Nanoparticles: Pickering Emulsions.* Vol 439. Elsevier B.V.; 2013. doi:10.1016/j.colsurfa.2013.02.054
 57. Popp N, Kutuzov S, Böker A. Various Aspects of the Interfacial Self-Assembly of Nanoparticles. In: Springer, Berlin, Heidelberg; 2010:39-58. doi:10.1007/12_2010_52
 58. Kaiser A, Liu T, Richtering W, Schmidt AM. *Magnetic Capsules and Pickering Emulsions Stabilized by Core - Shell Particles.* Vol 25.; 2009. doi:10.1021/la900401f
 59. Zhou J, Wang L, Qiao X, Binks BP, Sun K. *Pickering Emulsions Stabilized by Surface-Modified Fe₃O₄nanoparticles.* Vol 367. Elsevier Inc.; 2012. doi:10.1016/j.jcis.2011.11.001
 60. Arditty S, Schmitt V, Giermanska-Kahn J, Leal-Calderon F. Materials based on solid-stabilized emulsions. *J Colloid Interface Sci.* 2004;275(2):659-664. doi:10.1016/J.JCIS.2004.03.001
 61. and EV, Piazza* R, Lockhart TP. Pickering Emulsions: Interfacial Tension, Colloidal Layer Morphology, and Trapped-Particle Motion. 2003. doi:10.1021/LA034264L
 62. Horozov TS, Binks BP. Particle-Stabilized Emulsions: A Bilayer or a Bridging Monolayer? *Angew Chemie Int Ed.* 2006;45(5):773-776. doi:10.1002/anie.200503131
 63. Aveyard R, Binks BP, Clint JH. Emulsions stabilised solely by colloidal particles. *Adv Colloid Interface Sci.* 2003;100-102:503-546. doi:10.1016/S0001-8686(02)00069-6
 64. Thieme J, Abend S, Lagaly G. Aggregation in Pickering emulsions. *Colloid Polym Sci.* 1999;277(2-3):257-260. doi:10.1007/PL00013752
 65. Yameen B, Choi W II, Vilos C, Swami A, Shi J, Farokhzad OC. Insight into nanoparticle cellular uptake and intracellular targeting. *J Control Release.* 2014;190:485-499. doi:10.1016/j.jconrel.2014.06.038
 66. Soppimath KS, Aminabhavi TM, Kulkarni AR, Rudzinski WE. Biodegradable polymeric nanoparticles as drug delivery devices. *J Control Release.* 2001;70(1-2):1-20. doi:10.1016/S0168-3659(00)00339-4
 67. Zhang J, Misra RDK. Magnetic drug-targeting carrier encapsulated with

- thermosensitive smart polymer: Core-shell nanoparticle carrier and drug release response. *Acta Biomater.* 2007;3(6):838-850. doi:10.1016/J.ACTBIO.2007.05.011
68. Gelperina S, Kisich K, Iseman MD, Heifets L. The potential advantages of nanoparticle drug delivery systems in chemotherapy of tuberculosis. *Am J Respir Crit Care Med.* 2005;172(12):1487-1490. doi:10.1164/rccm.200504-613PP
69. Zhao J, Castranova V. Toxicology of Nanomaterials Used in Nanomedicine. *J Toxicol Environ Heal Part B.* 2011;14(8):593-632. doi:10.1080/10937404.2011.615113
70. Wilczewska AZ, Niemirowicz K, Markiewicz KH. *Review Nanoparticlessassdrugdeliverysystems.*; 2012. http://www.if-pan.krakow.pl/pjp/pdf/2012/5_1020.pdf. Accessed January 23, 2019.
71. Zirbs R, Lassenberger A, Vonderhaid I, Kurzhals S, Reimhult E. Melt-grafting for the synthesis of core-shell nanoparticles with ultra-high dispersant density. *Nanoscale.* 2015;7(25):11216-11225. doi:10.1039/c5nr02313k
72. Kurzhals S, Zirbs R, Reimhult E. *Synthesis and Magneto-Thermal Actuation of Iron Oxide Core-PNIPAM Shell Nanoparticles.* Vol 7.; 2015. doi:10.1021/acsami.5b05459
73. Witte H, Seeliger W. Simple Synthesis of 2-Substituted 2-Oxazolines and 5,6-Dihydro-4H-1,3-oxazines. *Angew Chemie Int Ed English.* 1972;11(4):287-288. doi:10.1002/anie.197202871
74. Witte H, Seeliger W. Cyclische Imidsäureester aus Nitrilen und Aminoalkoholen. *Justus Liebigs Ann Chem.* 1974;1974(6):996-1009. doi:10.1002/jlac.197419740615
75. Napolitano A, d'Ischia M, Costantini C, Prota G. A new oxidation pathway of the neurotoxin 6-aminodopamine. Isolation and characterisation of a dimer with a tetrahydro[3,4a]iminoethanophenoxazine ring system. *Tetrahedron.* 1992;48(39):8515-8522. doi:10.1016/S0040-4020(01)86599-6
76. Glassner M, D'hooge DR, Young Park J, et al. Systematic investigation of alkyl sulfonate initiators for the cationic ring-opening polymerization of 2-oxazolines revealing optimal combinations of monomers and initiators. *Eur Polym J.* 2015;65:298-304. doi:10.1016/J.EURPOLYMJ.2015.01.019
77. Kraft DJ, Luigjes B, De Folter JWJ, Philipse AP, Kegel WK. *Evolution of Equilibrium Pickering Emulsions-a Matter of Time Scales.* Vol 114.; 2010. doi:10.1021/jp104662g
78. French DJ, Taylor P, Fowler J, Clegg PS. Making and breaking bridges in a Pickering emulsion. *J Colloid Interface Sci.* 2015;441:30-38. doi:10.1016/J.JCIS.2014.11.032
79. French DJ, Brown AT, Schofield AB, Fowler J, Taylor P, Clegg PS. The secret life of Pickering emulsions: particle exchange revealed using two colours of particle. *Sci Rep.* 2016;6(1):31401. doi:10.1038/srep31401

8. Abbreviations

ATRP	atom transfer radical polymerization
COMU	[(1-cyano-2-ethoxy-2-oxoethylideneaminoxy) dimethylamino morpholino carbenium hexafluorophosphate]
CRP	controlled/living free-radical polymer synthesis
CSNP	core-shell nanoparticle
DCM	dichloromethane
DIPEA	N,N-diisopropylethylamine)
DLS	dynamic light scattering
DMA	dimethylacetamide
DMAP	4-dimethylaminopyridine
DMF	dimethyl formamide
DMSO-d6	dimethyl sulfoxide-d6
Et ₂ O	diethyl ether
GD	grafting density
GPC	gel permeation chromatography
IPOX	2-Isopropyl-2-oxazoline
LCST	lower critical solution temperature
Me ₆ Tren	tris[2-(dimethylamino)ethyl]amine
MeOD	methanol-d6
MetTos	methyl tosylate
Mn	number average molecular weight
Mw	weight average molecular weight

NDA	nitrodopamine
NIPAM	N-isopropylacrylamide
NMR	nuclear magnetic resonance spectroscopy
NP	nanoparticle
PDI	polydispersity Index
PEG	polyethylene glycol
PEOx	poly-2-ethyl-2-oxazoline
PIPOx	poly-2-isopropyl-2-oxazoline
PMOx	poly-2-methyl-2-oxazoline
PNIPAM	poly-(N-isopropyl-acrylamide)
POX	2-poly-2-oxazoline
SPION	superparamagnetic iron oxide nanoparticle
TGA	thermogravimetric analysis